Fluid Dynamics in Sartobind® Membrane Adsorber Systems

Von der Naturwissenschaftlichen Fakultät
der Gottfried Wilhelm Leibniz Universität Hannover

zur Erlangung des Grades
Doktor der Naturwissenschaften
Dr. rer. nat.
genehmigte Dissertation
von

Dipl-Ing. (FH) Stéphan Barbe
geboren am 11.11.1976 in Dieuze (Frankreich)

2009

Referent: Prof. Dr. Thomas Scheper
Institut für Technische Chemie
Gottfried Wilhelm Leibniz Universität Hannover

Korreferent: Prof. Dr. Bernd Hitzmann
Institut für Technische Chemie
Gottfried Wilhelm Leibniz Universität Hannover

Tag der Promotion: 13.10.2009

Erklärung

Ich versichere, dass ich diese Dissertation selbstständig und nur unter Verwendung der angegebenen Hilfsmittel und Quellen durchgeführt habe. Diese Arbeit wurde nicht als Diplomarbeit oder ähnliche Prüfungsarbeit verwendet.

Hannover, im Oktober 2009

Acknowledgements

This work was conducted at the R&D Department at Sartorius-Stedim Biotech GmbH in Göttingen (Germany). I would like to express my gratitude to Professor Dr. Thomas Scheper and to Dr. Dieter Melzner for providing me this position and this really interesting subject. Particular thanks go to Prof. Dr. Hitzmann and Prof. Dr. Caro for accepting to be co-supervisor of this thesis. I also would like to thank my colleagues and friends who helped me during this work.

Kurzfassung

Die vorliegende Arbeit berichtet sowohl über die theoretischen Entwicklungen als auch die innovativen experimentellen und numerischen Methoden, die für die Vorhersage von Verweilzeitverteilungen, Strömungs- und Druckfeldern in Q-Sartobind® Membrane Adsorber Systems mittels Computational Fluid Dynamics (CFD) notwendig sind.

Es wird gezeigt, wie durch den Einsatz von Rasterelektronmikroskopie und Röntgenstrahlungsmikrotomographie wichtige Hinweise über den Transport und die Adsorption von gelösten Stoffen innerhalb der porösen Struktur von Q-Sartobind® Membranen gewonnen werden können. Mit Hilfe dieser strukturellen Untersuchung wurden geeignete und implementierbare makroskopische Modelle (CDE- und dual porosity Modell) ausgewählt. Weiterhin wurde eine experimentelle Einrichtung entwickelt, die die einfache Messung von eindimensionalen Verweilzeitverteilungen ermöglicht. Die resultierenden Kurven wurden mit der eindimensionalen analytischen Lösung der oben erwähnten Modelle gefittet. Dabei wurde eine Optimierungsmethode implementiert, die gleichzeitig nicht Membran gebunden Dispersionseffekte entfernt und die entsprechenden Transportparameter für adsorptive und nicht-adsorptive Stoffe schätzt.

Anschließend wurden die dreidimensionalen Formulierungen der ausgewählten Modelle hergeleitet und in dem open-source CFD-Code Code_Saturne implementiert. Die entsprechenden CFD Simulationen haben die erfolgreichen Vorhersagen von Verweilzeitverteilungen von niedermolekularen Stoffen (Aceton) mit Hilfe des dual porosity Modells und von hochmolekularen Stoffen (Rinderserumalbumin) mit Hilfe des CDE-Modells ermöglicht. Die Implementierung des Transportmodells wurde durch die Einführung eines Adsorptionsterms erweitert und Verweilzeitverteilungen von Benzoesäure unter bindenden Bedingungen wurden vorhergesagt. Die Vorhersage von Strömungs- und Druckfeldern haben die Detektion und die Lokalisierung von nicht strömungsoptimierten Strömungsumlenkungen und Totvolumina ermöglicht.

Schlagworte: Membranadsorber, Chromatographie, Fluiddynamik

Abstract

The present work reports the theoretical developments as well as the innovative experimental and numerical methods necessary for the prediction of flow fields, pressure fields, residence time distributions (RTD) of adsorptive and non adsorptive solutes (proteins and metabolites) in Q-Sartobind® Membrane Adsorber Systems using Computational Fluid Dynamics (CFD).

It first demonstrates how Scanning Electron Microscopy and X-ray microtomography may be used to understand the transport and the eventual adsorption of solute within the porous structure of Q-Sartobind® membranes. According to this structural analysis, appropriate and implementable averaged macroscopic transport models (CDE and dual porosity models) have been selected. Furthermore, an experimental setup, which enables the easy measurement of one dimensional RTD's, was developed and the measured curves were fitted using the one dimensional analytical solutions of the above mentioned transport models. In this regard, an optimization method, which simultaneously removes extra membrane dispersion effects and estimates the corresponding transport parameters for adsorptive and non adsorptive solutes, has been implemented.

Finally, the three dimensional forms of the selected transport models have been formulated and implemented in the open source CFD code Code_Saturne using the estimated transport parameters. The corresponding CFD simulations enabled successful predictions of residence time distributions of the low molecular weight compound acetone using the dual porosity model and the high molecular weight compound Bovine Serum Albumin using the CDE model. Furthermore, the implementation of the transport models has been extended by adding an adsorption term and RTD's of benzoic acid under adsorptive conditions have been predicted. Additionally, the prediction of flow fields allowed the detection and localization of imperfect flow distributions.

Keywords: membrane adsorber, chromatography, fluid dynamics

Acknowledgements I

Kurzfassung II

Abstract III

List of Symbols VIII

List of abbreviations X

1 Introduction 1

2 Chromatographic performances of Q-Sartobind® Membrane Adsorber Systems 3

2.1 Objectives 3

2.2 Theoretical Background 3

2.2.1 Height of Theoretical Plate (HETP) 3

2.2.2 Resolution of two components 6

2.2.3 Protein chromatography with Membrane Adsorbers 6

2.2.4 Sartobind® Membrane Adsorber Systems 8

2.3 Materials and methods 9

2.3.1 Chemicals 9

2.3.2 Sartobind® Membrane Adsorber Systems 9

2.3.3 Experimental setup for RTD's and retention measurements 11

2.3.4 Determination of HETP values 11

2.3.5 Determination of Peak resolution 12

2.3.6 Injection of tracer pulses 13

2.4 Results and discussion 16

2.4.1 Height of Theoretical Plates (HETP) 16

2.4.2 Peak Resolution 21

2.5 Conclusion 22

2.6 References 24

3 Investigation of structure and adsorption behaviour of Q-Sartobind® membranes 26

3.1 Objectives 26

3.2 Theoretical background 26

3.2.1 Scanning Electron Microscopy (SEM) 26

3.2.2 X-ray microtomography 27

3.2.3 Langmuir adsorption model and chromatographic retention 28

3.3 Materials and methods 29

3.3.1 Scanning Electron Microscopy 29

3.3.2 Adsorption of monoclonal conjugates 29

3.3.3 Investigation of saturated samples using X-ray microtomography 30

3.3.4 Measurement of adsorption isotherms 30

3.4 Results and discussion 31

3.4.1 Structural characterization of Sartobind® membranes 31

3.4.2 Investigation of membrane swelling 37

3.4.3 Adsorption behavior of Q-Sartobind® membranes 38

3.5 Conclusions 42

3.6 References 43

4 Analysis of tracer transport in Q-Sartobind® membranes 45

4.1 Objectives 45

4.2 Theoretical background 46

4.2.1 Convection Dispersion Equation (CDE) 46

4.2.2 Dual porosity model 47

4.3 Materials and methods 48

4.3.1 Chemicals 48

4.3.2 Sample preparation 48

4.3.3 Dispersion measurement 50

4.3.4 Estimation of strictly membrane related dispersion parameters 50

4.4 Results and discussion 53

4.4.1 Assumptions 53

4.4.2 Dispersion of non adsorptive tracers 54

4.4.3 Dispersion of adsorptive tracer 61

4.5 Conclusions 64

4.6 References 66

5 Fluid dynamics in Q-Sartobind® Membrane Adsorber Systems using CFD 68

5.1 Objectives 68

5.2 Theoretical Background 68

5.2.1 Computational Fluid Dynamics (CFD) 68

5.2.2 Code_Saturne® 69

5.3 Case setup and model implementation 70

5.3.1 Geometry and meshing 70

5.3.2 Calculation of flow field and pressure field 71

5.3.3 Calculation of residence time distributions 72

5.3.4 Implementation of the CDE model 72

5.3.5 Implementation of the dual porosity model 73

5.4 Results and discussion 75

5.4.1 Comparison between model predictions and measurements 75

5.4.2 Pressure and flow fields 78

5.4.3 Concentration field 80

5.5 Conclusions 82

5.6 References 83

6 Summary and perspectives 84

List of publications 85

Curriculum vitae 89

List of Symbols

Uppercase symbols

A	Eddy diffusion [-]
B	Longitudinal diffusion [-]
C	Resistance to mass transfer [-]
C_f	Dimensionless flux averaged concentration [-]
D	Dispersion coefficient [m²/s]
D_{diff}	Diffusion coefficient [m²/s]
D_m	Dispersion coefficient of the mobile phase [m²/s]
H_1	Auxiliary function with Bessel functions for non equilibrium transport [-]
I_1	Modified first order Bessel function [-]
K_d	Distribution coefficient for linear adsorption distribution [m³/kg]
K_{lang}	Langmuir constant [-]
L	Column length [m]
N_p	theoretical plate number [-]
Pe	Peclet number [-]
Q	Number of occupied adsorption sites [-]
Q_{max}	Maximum number of adsorption sites [-]
R	Retardation factor [-]
R_S	Peak resolution [-]
T	Dimensionless time [-]
V_{cell}	Cell volume [m³]
V_m	Volume of mobile region in a finite volume [m³]
W	Width of elution curve at the base line [s]
Z	Dimensionless distance [-]

Lowercase symbols

c_{im} Solute concentration in the immobile region [kg/L]

c_m Concentration in the mobile region [kg/L]

c_r resident concentration [kg/kg]

f Fraction of adsorption sites that equilibrates with the mobile liquid region [-]

k_a Adsorption constant [s^{-1}]

k_d Desorption constant [s^{-1}]

s Solute concentration on the solid phase [kg/kg]

t Time [s]

$t_{,R}$ Peak position [s]

u Linear velocity [cm/min]

v Superficial velocity [cm/s]

x Distance [m]

Greek symbols

α First-order kinetic rate coefficient [s^{-1}]

β Dimensionless variable for partitioning in non equilibrium transport models [-]

Γ_1 Auxiliary function for non equilibrium transport [-]

θ Porosity [-]

θ_m Porosity of the mobile liquid phase [-]

θ_{im} Porosity of the immobile liquid phase [-]

μ_1 First moment of residence time distribution [s]

μ_2 Second moment of residence time distribution [s^2]

ρ_b Bulk density [kg/m^3]

τ time [s]

ω Dimensionless mass transfer coefficient [-]

List of abbreviations

BSA	Bovine Serum Albumin
CDE	Convection Dispersion Equation
CFD	Computational Fluid Dynamics
EDF	Electricité de France
ETD	Everhart-Thornley Detector
ESEM	Environmental Scanning Electron Microscopy
HETP	Height of Theoretical Plate
LFD	Large Field Detector
MA	Membrane Adsorber
RTD	Residemce Time Distribution
SEM	Scanning Electron Microscopy

1 Introduction

Downstreaming in biotechnology involves a series of separation steps with the final goal of attaining the highest purity of the product at a maximum rate of recovery. Most of these separation steps are chromatographic processes using physical interactions (ion exchange, hydrophobic interactions and reverse phase), stereochemical recognition (affinity chromatography) and size exclusion (gel filtration). The scale-up of biotechnological processes is an important key step for the industrial production of biological molecules and membrane chromatography represents a suitable technology for the transfer of bench scale purification protocols to the production scale. This considerable advantage leads to the increasing role of chromatographic membranes for large scale isolations and purifications of biomolecules (monoclonal antibodies, food proteins, viruses …).

Millipore (USA), Pall (USA) and Sartorius-Stedim Biotech GmbH (Germany) are the main providers of chromatographic devices based on adsorptive membranes. The present work exclusively investigates Q-Sartobind® Membrane Adsorber Systems. These are the anion-exchange chromatographic devices developed by Sartorius-Stedim Biotech GmbH. Furthermore, the terms “adsorption” and “binding”, frequently used in this thesis, always refer to the reversible and specific adsorption of anions from a liquid mobile phase on a positive charged stationary phase via electrostatic interactions.

The first Q-Sartobind® Membrane Adsorber Systems were derived from filtration systems and therefore not optimized for chromatographic purposes. During the last decade, experimental prototyping has been intensively used for the improvement of Sartobind® Membrane Adsorber Systems in order to reduce dead zones and achieve a plug flow. The limits of experimental prototyping, in terms of product design and flow optimization, are almost reached and there is a real need for more precise development techniques. Due to considerable developments in the last two decades, modern CFD (Computational Fluid Dynamics) methods are now able to solve problems in very complex geometries and have been proposed as a new technique for the further optimization of such chromatographic devices.

The main object of the present work was the development of a CFD model enabling the prediction of residence time distributions (RTD’s) of adsorptive and non-adsorptive

compounds in Q-Sartobind® Membrane Adsorber Systems. This project has been divided into the four following objectives:

1) The chromatographic performances of Q-Sartobind® Membrane Adsorber Systems were characterized in terms of heights of theoretical plates (HETP) and peak resolution. Simultaneously, a set of experimental data was generated, which was necessary for the "validation" of the future CFD model.

2) A structural characterization of the corresponding membrane was performed using scanning electron microscopy (SEM) and X-ray microtomography. Additionally, adsorption isotherms have been measured and fitted with the Langmuir adsorption model. The severest limitation for the successful achievement of accurate CFD predictions was the mathematical description of the transport phenomena occurring in Q-Sartobind® membranes.

3) On the basis of the results obtained from the second step, the third milestone aimed to find out appropriate mathematical models for the description of the transport phenomena occurring in Q-Sartobind® membranes. Because CFD is based on continuum mechanics, only macroscopic transport models came into consideration. The convection-dispersion equation (CDE) and the dual porosity model have been found to fulfil these requirements and their capability to fit measured RTD's under adsorptive and non-adsorptive conditions for high and low molecular weight compounds was evaluated.

4) The three dimensional geometry of a Q-Sartobind® Membrane Adsorber System has been then created and meshed. Using the transport parameters estimated in the frame of previous milestone, CDE and dual porosity models for adsorptive and non adsorptive compounds were implemented in the open source CFD code Code_Saturne. Finally, predicted and measured RTD's were compared, which enabled to find out transport models for low and high molecular weight non-adsorptive compounds.

2 Chromatographic performances of Q-Sartobind® Membrane Adsorber Systems

2.1 Objectives

This first part is dedicated to the systematic characterization of Sartobind® Membrane Adsorber Systems in terms of chromatographic performances. Such a study has not been yet reported in the literature and the present contribution aims to partially compensate this deficiency. In this regard, an apparatus, that enables automatic injections of tracer pulses through Membrane Adsorber Systems and their monitoring, has been developed. The influences of bed thickness, bed height and linear flow velocity on the following chromatographically relevant parameters have been investigated:

- Heights of Theoretical Plate (HETP) have been determined for adsorptive and non adsorptive tracers. This determination was performed from measured residence time distributions (RTD).
- Separation resolution of adjacent peaks during the isocratic separation of BSA and benzoic acid.

The chromatographic performances of Membrane Adsorber Systems and column chromatography have been then compared. Beside this characterization, the second objective of this chapter was the generation of a set of experimental data, which has been used for the evaluation of the accuracy of CFD simulations.

2.2 Theoretical Background

2.2.1 Height of Theoretical Plate (HETP)

The concept of theoretical plates is commonly used to describe chromatographic performance. It assumes that the solute, during its passage through the column, is always in equilibrium with the mobile and stationary phases. However, as the solute is continuously passing from one phase to the other, equilibrium between the phases never occurs. In order to accommodate this non-equilibrium condition, a technique was introduced, which considers the column to be

divided into a finite number of plates. The plates have a specific length and the solute will spend a finite time on each plate. The plate is chosen to be of such size as to give the solute sufficient residence time to establish equilibrium with the two phases. Consequently, the smaller the plate is found to be, the faster will equilibrium be achieved and the more plates will be in the column.

The theoretical plate concept is widely used to characterize the performance of a chromatographic column. All peaks in a chromatogram show roughly the same plate number and this number can be consequently considered as an inherent characteristic of the column used.

The definition of the "theoretical plate number" is based on the statistical theory:

$$N_P = \frac{\mu_1^{\,2}}{\mu_2},$$

where μ_1 and μ_2 are the mean and variance, so called first absolute and second central moments of the RTD.

As the plate number is approximately proportional to the column length L, column quality can also be expressed in terms of theoretical plates per meter column or HETP which is defined by

$$HETP = \frac{L}{N_P},$$

where L is the column length and N_p is the Number of theoretical plates.

According to the theory originally developed by van Deemter et al., the plate height (HETP) for column is equal to the sum of three independent contributions according to the following equation:

$$HETP = A + \frac{B}{u} + C \cdot u,$$

where A is the Eddy diffusion (describes peak broadening resulted from the packed column geometry), B – longitudinal diffusion, C – resistance to mass transfer and u – linear velocity. A plot of the van Deemter equation shows a minimum at certain flow rate (Fig. 2.1).

There is an "optimal" flow rate at which a minimal HETP value is achieved and, consequently, maximal plate number is obtained. In conventional chromatography of macromolecules, the optimal flow rate is often impractically low. This is due to the third component of the equation (Cu), which dramatically affects the HETP minimum and depends on various kinetic parameters such as the slow transfer of the molecules into and out of the pores within the stationary phase.

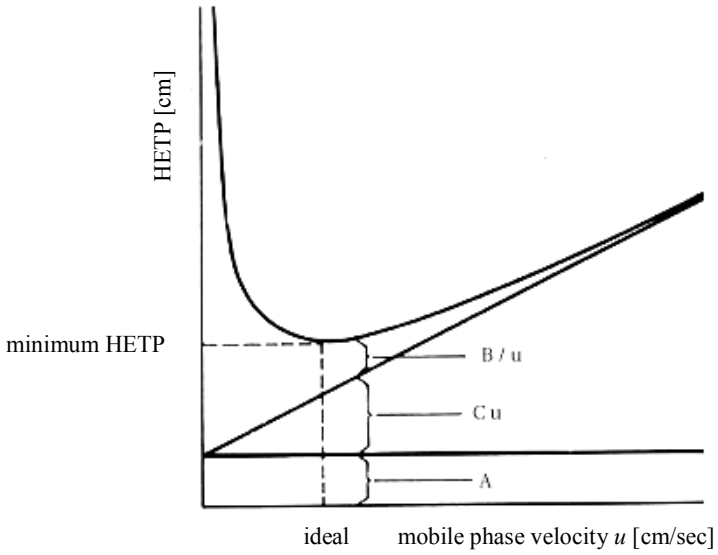

Fig. 2.1 Plot of the three terms in the Van Deemter equation and their sum

2.2.2 Resolution of two components

The resolution R_S is a measure of the degree of separation efficiency of two adjacent peaks. It is frequently employed and defined by

$$R_S = \frac{t_{R,2} - t_{R,1}}{(W_1 + W_2)/2}$$

where t_R = peak position an W = width of the elution curve at the baseline. The subscripts 1 and 2 refer to components 1 and 2, respectively.

2.2.3 Protein chromatography with Membrane Adsorbers

Conventional chromatographic supports are made from porous beads packed into a column, making chromatographic process very dependent on the molecular diffusion into the pores inside of the beads, the preferential solute flows and the pressure drop. To circumvent these difficulties, a variety of novel chromatographic processes have been considered. That is for example monolithic stationary phase columns (Zhou et al., 2002), non-porous beads (Lee, 1988) or perfusion chromatography packings (Afeyan et al., 1991). However, these media are generally expensive and the solute binding capacity is greatly reduced, since binding can now only take place on the external surfaces. Moreover, the problem of high pressure drop still persists.

In contrast to conventional columns, membrane adsorbers are supposed to reduce diffusion problems, because solutes should theoretically access the total inner surface area of the macroporous structure by convection (Fig. 2.2).

The binding efficiency of membrane adsorbers is generally independent of the feed flow-rate over a wide range and therefore very high flow-rates may be used. Moreover, the pressure drop is significantly lower than with packed beds. Membrane adsorbers can be used until the desirable properties (i.e. hydraulic permeability, binding capacity, selectivity and resolving power) are maintained and then disposed, that eliminates the requirement for cleaning and equipment revalidation.

As with conventional resins, all kind of ligands (ion exchange, bioaffinity) can be coupled to the membranes inner surface leading to an adsorption of the target protein at the pore wall (Roper and Lightfoot, 1995; Thömmes and Kula, 1995; Kökpinar O et al., 2006). The main advantage of the membrane chromatography mentioned in the literature is the fact, that the interaction between a solute (protein) and a matrix (immobilized ligand) does not take place in the dead-end pores of particle, but mainly in the throughout pores of a membrane (Fig. 2.2).

Despite of several obvious advantages of membrane adsorbers compared to the conventional chromatography, there are still some challenges to overcome. The most important ones are distorted or poor inlet flow distribution (Roper and Lightfoot, 1995), non-identical (Frey et al., 1992) membrane pore size distribution, uneven membrane thickness and scale up (Ghosh, 2002). If a flow distribution problem is not unique to membrane adsorbers alone and appears to be a property of chromatographic process in general (Yuan et al., 1999) and can affect most likely only pulse chromatography, pore size distribution can seriously reduce the efficiency of adsorbent utilization.

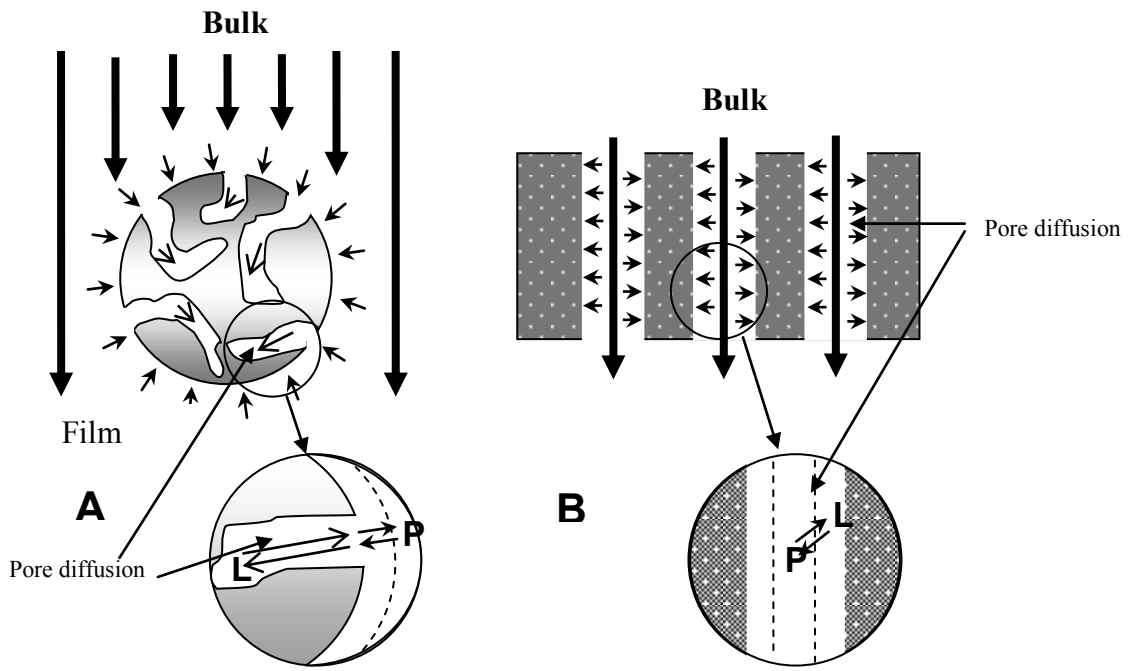

Fig. 2.2 Simplified schematic representation of solute transport in packed bed chromatography (A) and membrane adsorber (B). P – protein, L - ligand

2.2.4 Sartobind® Membrane Adsorber Systems

Sartobind® membranes (Sartorius-Stedim Biotech GmbH, Göttingen), appeared on the market in the beginning of the last decade and are one of the major representatives of the membrane adsorbers at the present time. Initially dedicated to laboratory applications, they were flat sheet membranes with a methacrylic polymer grafted onto a macroporous support and bearing different ionic groups. In the first generation of Sartobind® membranes synthetic nylon support with 0.45 µm nominal pore size was used. This matrix was later replaced by high chemically and enzymatically stable polysaccharide (regenerated cross linked cellulose) support of 3 µm nominal pore size with very low non-specific adsorption.

However, the capacity of single adsorptive membranes for preparative recovery was limited. To achieve the adsorptive capacities necessary for preparative biological recovery, multiple thin sheet disk membranes were stacked and housed in a rigid cylindrical shell, so that surface membrane area achieved up to 0.5 m^2. For the further scale-up a cylindrical module geometry was developed, which makes the design of large scale plants with membrane areas up to 100 m^2 feasible.

Sartobind® Membrane Adsorber Systems consists of a membrane (Fig. 2.3), reeled to form a hollow cylinder, with screens of stainless steel on the inner and outer sides, which are embedded in plastic caps on both ends. Modules have different heights – 3, 6, 12, 25 and 50 cm and different bed thicknesses -15, 30 and 60 membrane layers (2, 4 and 8 m^2 nominal membrane area, respectively). They all have the same outer diameter and fit into the same housings.

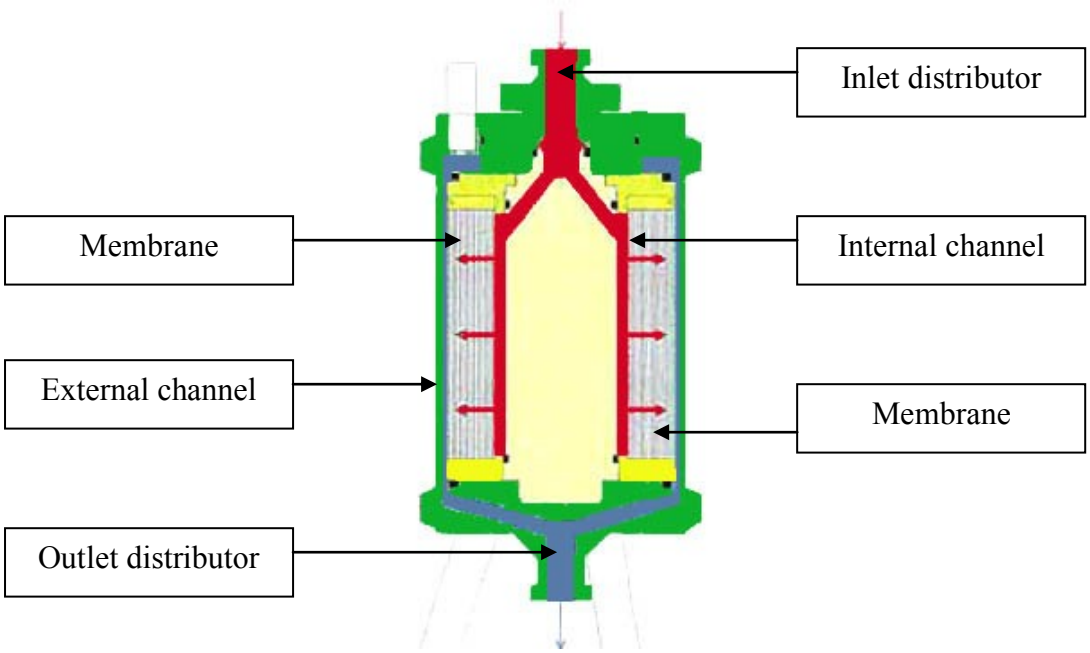

Fig. 2.3 Cross sectional drawing of a Sartobind® Membrane Adsorber System.

Despite of the clear advantages of membrane chromatography and, namely, Membrane Adsorber Systems for large-scale protein purification, existing limitations are still to be solved. The proper understanding of the transport phenomena as well as strict control of homogeneity of the microstructure can rationalize the design of the membrane chromatographic process and consequently improve the process efficiency.

2.3 Materials and methods

2.3.1 Chemicals

If not indicated otherwise all chemical reagents were obtained from Merck (Darmstadt, Germany).

2.3.2 Sartobind® Membrane Adsorber Systems

Sartobind® Membrane Adsorber Systems used in this work have been directly provided by Sartorius-Stedim Biotech GmbH (Göttingen, Germany). In all Membrane Adsorber Systems (Tab. 2.1), stabilized regenerated cellulose membrane with an average thickness of 275 µm and a nominal pore size higher than 3µm, coupled with a strong basic anion exchanger (quaternary ammonium Q) has been used. All membranes were taken from one production

charge (Membrane charge number 19-00861354). Housings and cores were made out of polyoxymethylene or stainless steel.

Tab. 2.1 Properties of Sartobind® Membrane Adsorber Systems used in this work

Module reference	Bed height [mm]	#Number membrane layers	Bed thickness [mm]	Bed volume [ml]	Nominal membrane area [cm²]	Abbreviation
91-Q-05K-15-12	120	15	4	140	0.5	12_15
91-Q-05K-30-12	120	30	8	288	1.0	12_30
91-Q-05K-60-12	120	60	16	533	2.0	12_60
91-Q-01K-15-03	30	15	4	35	0.1	03_15
91-Q-02K-15-06	60	15	4	70	0.2	06_15
91-Q-10K-15-25	250	15	4	280	1.0	25_15

2.3.3 Experimental setup for RTD's and retention measurements

For RTD's and retention measurements, an apparatus, that enables automatic injections of tracer pulses through Membrane Adsorber Systems and their monitoring, has been developed and calibrated. Tab. 2.2 shows the instrumentation used and a flow diagram (Fig. 2.4) illustrates the interconnection of process equipment and the instrumentation used for process monitoring. The filling of the injection loop has been performed using hydrostatic pressure drop.

In this work, measurements have been performed by injecting a pulse of adsorptive or non adsorptive tracer through different Membrane Adsorber Systems. These measurements have been performed by Antonina Lavrentieva in the frame of her Master thesis (Lavrentieva 2008). Resulting Input and Output signals have been monitored photometrically at 280 nm and recorded with a time step of 0.2 s. The volume of the used injection loops has been set to 7 % of the corresponding bed volumes.

2.3.4 Determination of HETP values

As tracers, a 5% (w/w) acetone solution in 30 mM sodium acetate buffer (pH 5.2, IS 50 mM) or 20 mM potassium phosphate buffer (PPi) (pH 7.2, IS 175 mM) and a BSA (10 g/L, Kraeber GmbH & Co, Ellerbeck, Germany) solution in 30 mM sodium acetate buffer (pH 5.2, IS 50 mM) or 20 mM PPi buffer (pH 7.2, IS 175 mM) have been used. RTD's have been measured at three different linear velocities and the corresponding HETP values have been determined by calculating first and second moments of these RTD's. HETP values shown in the present thesis have been averaged from three runs.

Tab. 2.2 Equipment used for the experimental setup

Equipment	**Model and Manufacturer**
Flowmeter	MAGFLO® Flowmeter Type MAG 3000 (Danfoss, Danemark)
UV Detector	AF44VEQHNT1C4-C(Wedgewood technology inc., USA)
Manometers	Sartorius-Stedim Biotech GmbH (Göttingen, Germany)
Pump	Sartorius®Sartojet (Göttingen, Germany)
Valves	0330 C 4,0 FKM VA (Burkert, Germany)
Sartobind® Membrane Adsorber Systems	Sartobind®Q (Sartorius-Stedim Biotech GmbH, Göttingen, Germany)

2.3.5 Determination of Peak resolution

Peak resolution of the isocratic separation of a mixture of BSA (10g/L, Kraeber GmbH & Co, Ellerbeck, Germany) and benzoic acid (3.2 g/L) in 200 mM sodium acetate buffer (IS 82 mM, pH 4.5) has been estimated. Resolution of adjacent peaks (*Rs*) has been calculated with the help of the “ACD SpecManager” software (Advanced Chemistry Development, Inc., Canada). Resolution values shown in the present thesis have been averaged from three runs.

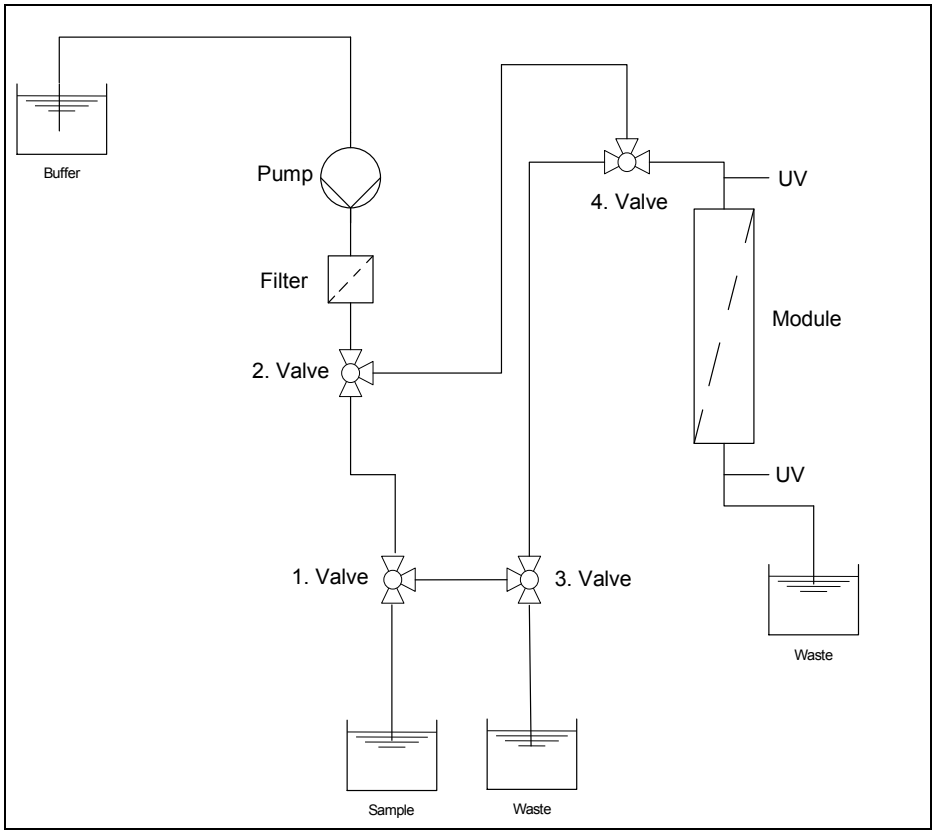

Fig. 2.4 Piping and instrumentation diagram of the dispersion measurement system

2.3.6 Injection of tracer pulses

For the injection of tracer pulses through Membrane Adsorber Systems, four 3-way automatic valves have been used. In order to achieve a proper pulse injection, an injection procedure consisting of the four following steps has been developed using Labview:

"Loading + Bypass". 5 sec. During this step, the injection loop was filled with the sample solution (driving force in this case was the gravity) (red line), the main buffer stream flowed via the bypass (blue line)

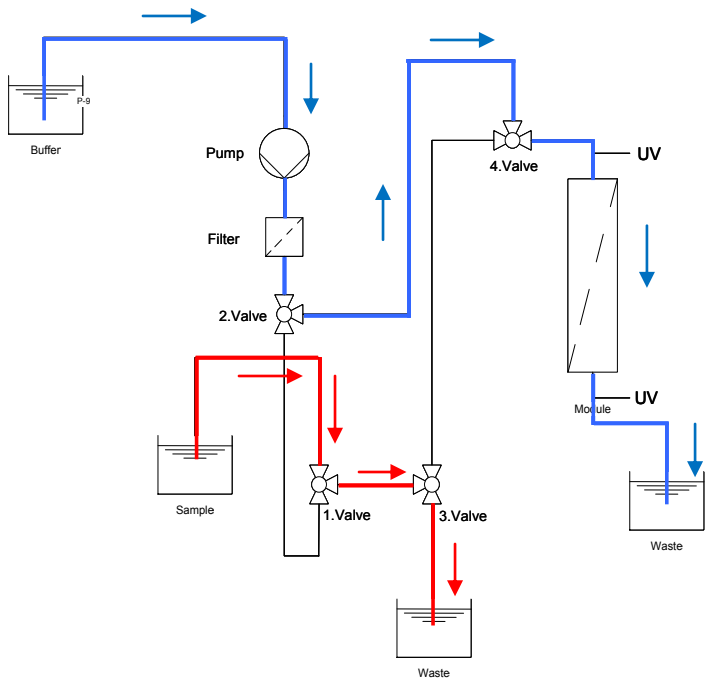

"End of Loading + Bypass". 5 Sec. At this step, loading was finished (red line), the main buffer stream still flowed via the bypass (blue line)

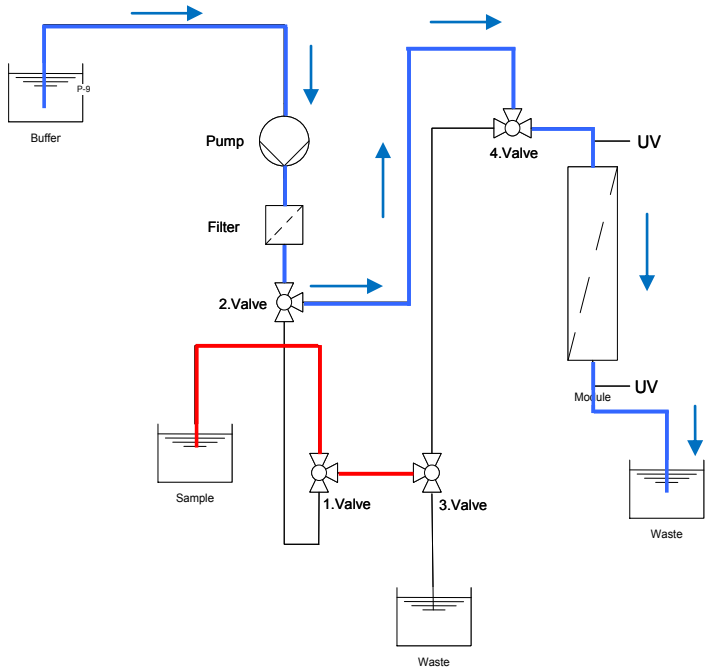

"Injection". 45 Sec. During this step, the loaded loop was connected with the main buffer stream and the sample passed through the Membrane Adsorber System.

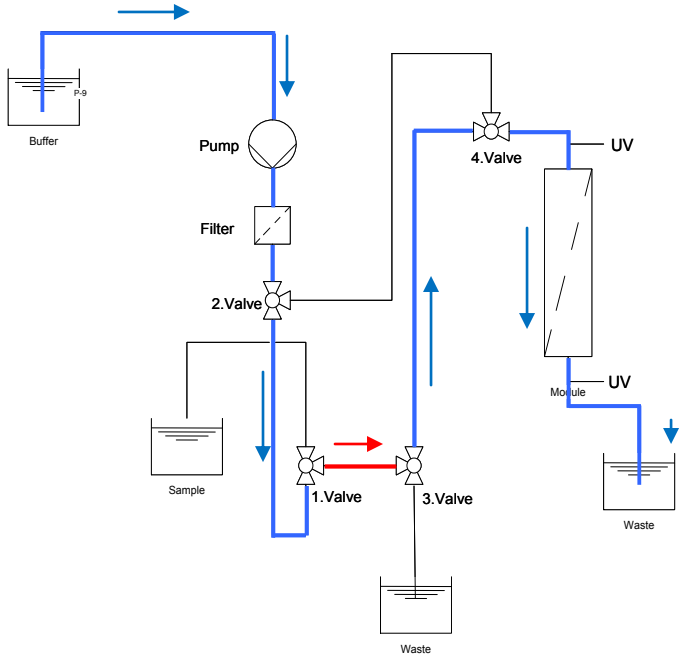

"Bypass". 5 Sec. At this step, the main buffer stream went again via the bypass in order to rinse the system module (blue line).

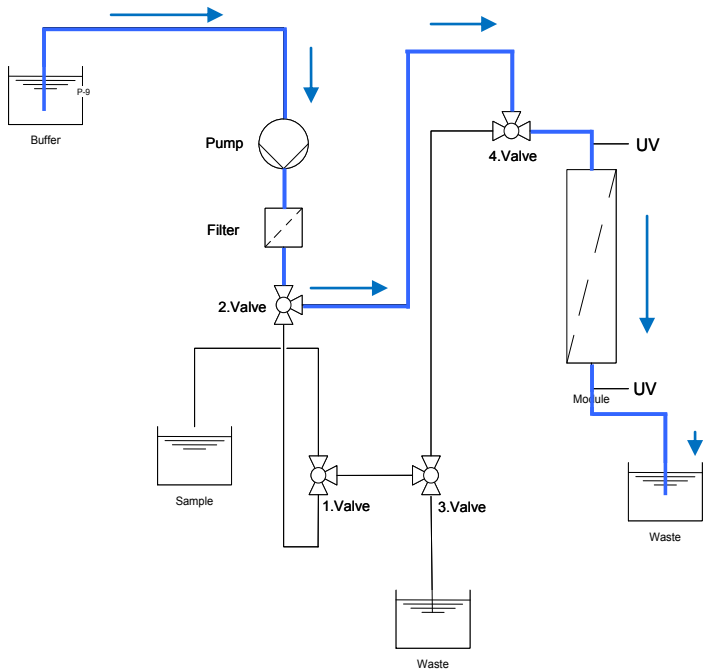

2.4 Results and discussion

2.4.1 Height of Theoretical Plates (HETP)

In the frame of these investigations, two different tracers have been used:

- Acetone was used as a non-adsorptive tracer in order to reflect dispersion effects strictly due to hydrodynamic processes occurring in the distributors, the channels and in the membrane pores.
- Bovine Serum Albumine (BSA, pI = 4.9) was used as an adsorptive tracer under two different binding conditions. At pH 7.2 (20 mM PPi, IS 175 mM), the surface of BSA is mostly deprotonated and consequently negatively charged. So binding under these conditions mostly took place due to a 'pH effect'. At pH 5.2 (30 mM sodium acetate, IS 50 mM), the surface of BSA was not fully deprotonated and still exhibited positive charges and was slightly negatively charged. Under these conditions, binding occurred via an 'ionic strength effect'.

2.4.1.1 Influence of bed thickness

Three modules with a bed height of 120 mm and bed thicknesses of 4, 8 and 16 mm have been investigated at 3 different linear flow velocities. The corresponding results are shown in Fig. 2.5 and Fig. 2.6. Bed height and bed thickness are shown in Fig. 2.9.

Janson and Jönsson (1998) performed HETP measurements on chromatographic columns and reported that the HETP value was proportional to the column length. Indeed, for a given linear velocity the solute spends more time in the porous medium and is longer subject to dispersion effects when the column length is increased.

In this study, the column length was represented by the bed thickness and it was consequently expected that the HETP value increases with bed thickness. This expectation has only been fulfilled when an adsorptive tracer was injected. The discrepancies obtained by injecting a non adsorptive tracer may only be explained by more disordered hydrodynamic processes occurring in the membrane stack of the module with 30 layers. This may be related to stronger

structural fluctuations in this membrane stack than in the other ones. These structural discrepancies seemed to be compensated when adsorption equilibrium was present.

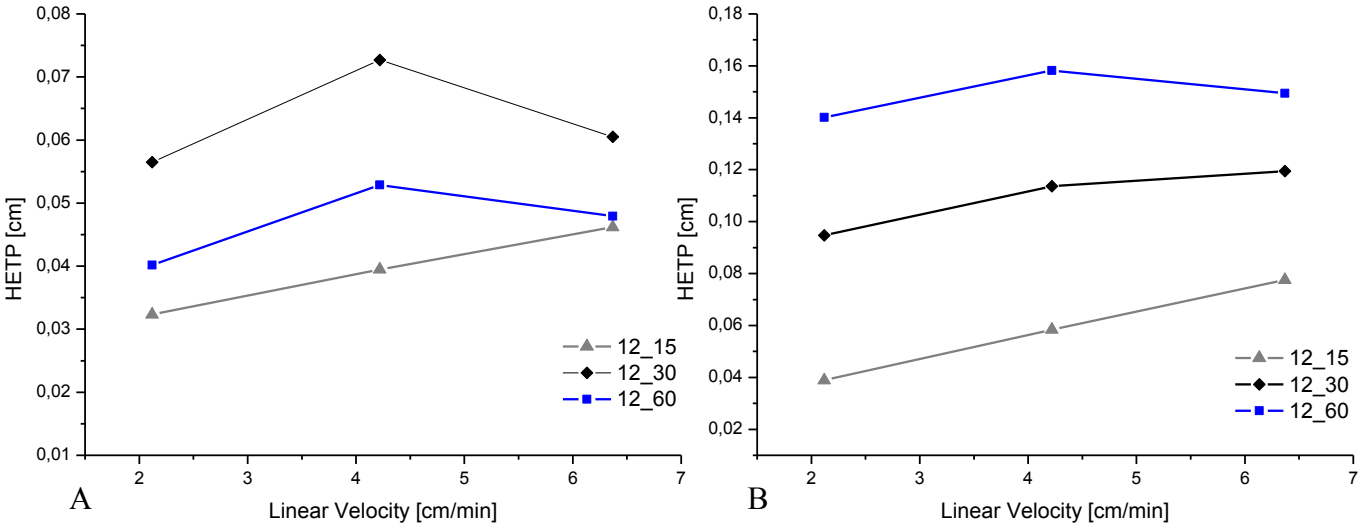

Fig. 2.5 Height of Theoretical Plate (HETP) values (Q- Sartobind® Membrane Adsorber Systems) as a function of the linear flow velocity for three different bed thicknesses: 4 mm (12_15), 8 mm (12_30) and 16 mm (12_60). Bed height was 120 mm. (A) – acetone as a non adsorptive tracer and (B) –Bovine Serum Albumin as an adsorptive tracer. 20 mM PPi buffer (pH 7.2, IS 175 mM).

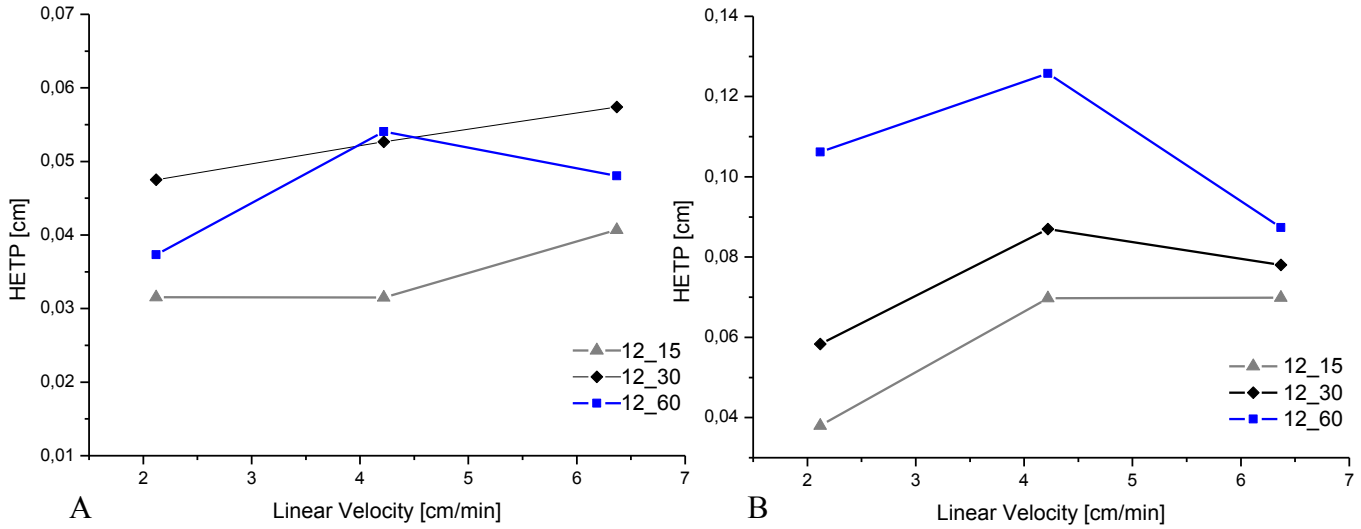

Fig. 2.6 Height of Theoretical Plate (HETP) values (Q- Sartobind® Membrane Adsorber Systems) as a function of the linear flow velocity for three different bed thicknesses: 4 mm (12_15), 8 mm (12_30) and 16 mm (12_60). Bed height was 120 mm. (A) – acetone as a non adsorptive tracer and (B) –Bovine Serum Albumin as an adsorptive tracer. 30 mM sodium acetate buffer (pH 5.2, IS 50 mM).

Additionally to hydrodynamic processes, BSA, as an adsorptive tracer, also reflected dispersion effects due to the adsorption equilibrium taking place in the membrane. The magnitude of HETP values estimated by injecting BSA were therefore about twice higher than the magnitude of HETP values obtained by injecting a non adsorptive tracer. No differences in HETP values have been observed by comparing the different binding effects of BSA.

2.4.1.2 Influence of bed height

Three modules with a bed thickness of 4 mm and bed heights of 30, 60 and 120 mm have been investigated at 3 different linear flow velocities. The corresponding results are shown in Fig. 2.7 and Fig. 2.8.

The magnitude of HETP values estimated under binding and non-binding conditions were unexpectedly similar. According to this observation, hydrodynamic processes present in these modules had the major contribution to the total dispersion and dispersion effects related to the adsorption equilibrium appeared to be negligible.

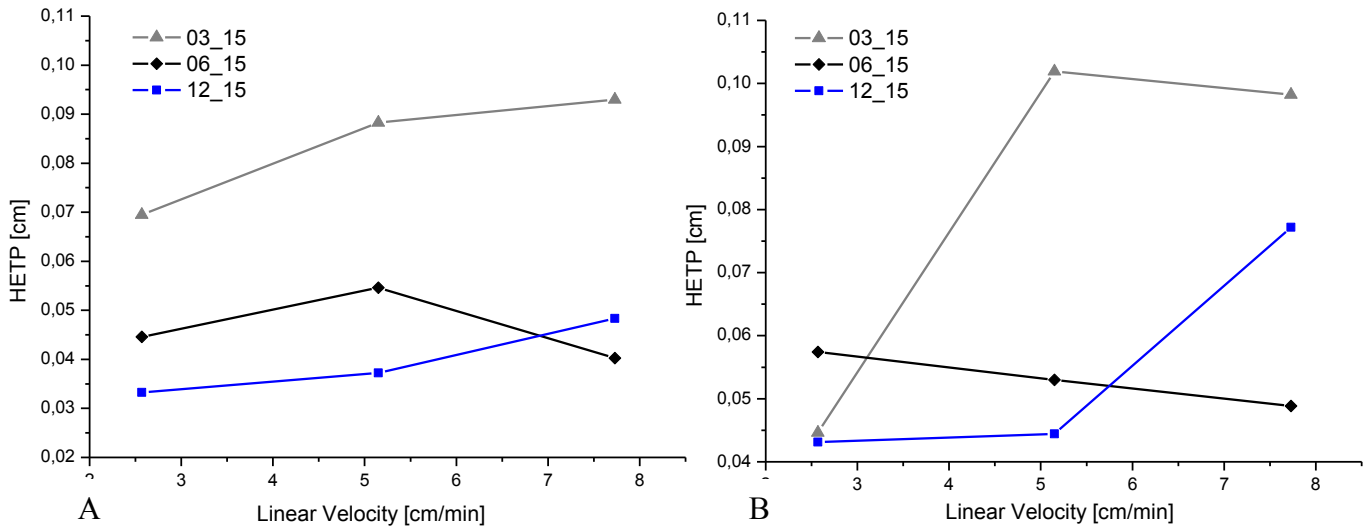

Fig. 2.7 Height of Theoretical Plate (HETP) values (Q- Sartobind® Membrane Adsorber Systems) as a function of the linear flow velocity for three different bed heights: 30 mm (03_15), 60 mm (06_15) and 120 mm (12_15). Bed thickness was 4 mm. (A) – acetone as a non adsorptive tracer and (B) –Bovine Serum Albumin as an adsorptive tracer. 20 mM PPi buffer (pH 7.2, IS 175 mM).

Furthermore, HETP values were found to decrease with the bed height and therefore with the flow area. By increasing this flow area, the contribution of dispersive effects due to structural heterogeneities of the membrane should increase and more strongly affect the total dispersion. The reverse trend was therefore expected and the observed relationship may not be exclusively explained by membrane related dispersion effects.

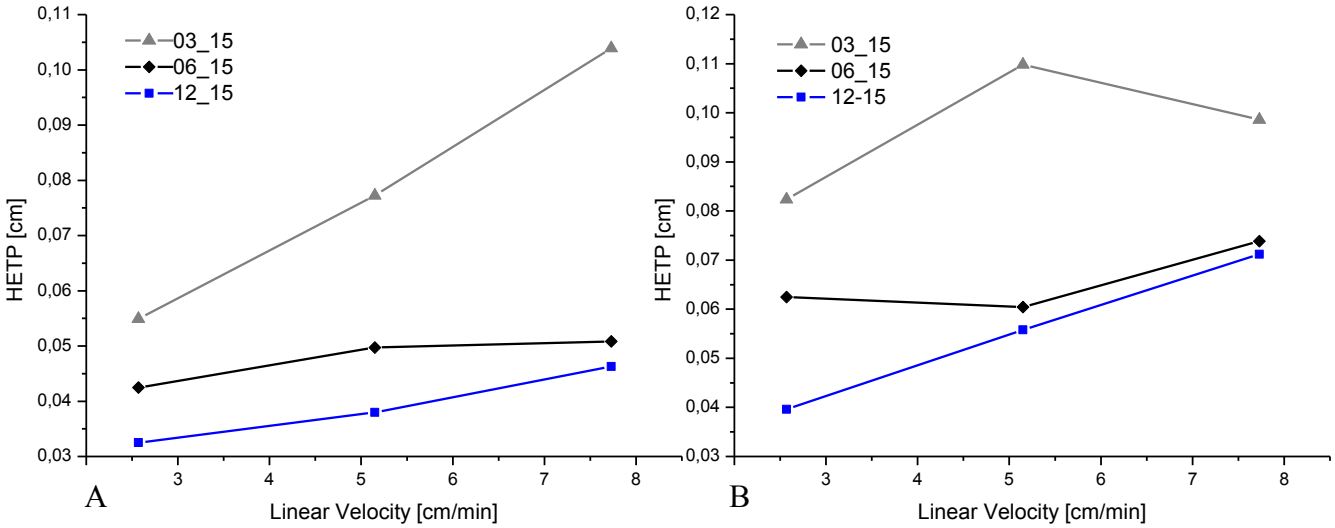

Fig. 2.8 Height of Theoretical Plate (HETP) values (Q- Sartobind® Membrane Adsorber Systems) as a function of the linear flow velocity for three different bed heights: 30 mm (03_15), 60mm (12_15) and 120 mm (12_15). Bed thickness was 4 mm. (A) – acetone as a non adsorptive tracer and (B) –Bovine Serum Albumin as an adsorptive tracer. 30 mM sodium acetate buffer (pH 5.2, IS 50 mM).

Fig. 2.9 (B) is a photograph of the cores used in the frame of this investigation. The upper part of these cores corresponds to the inlet distributor, which was similar and therefore created the same mixing zone for all 4 mm thick modules. After having been subject to this mixing zone, solutes were further transported into the internal channel, where the mixing intensity strongly decreased.

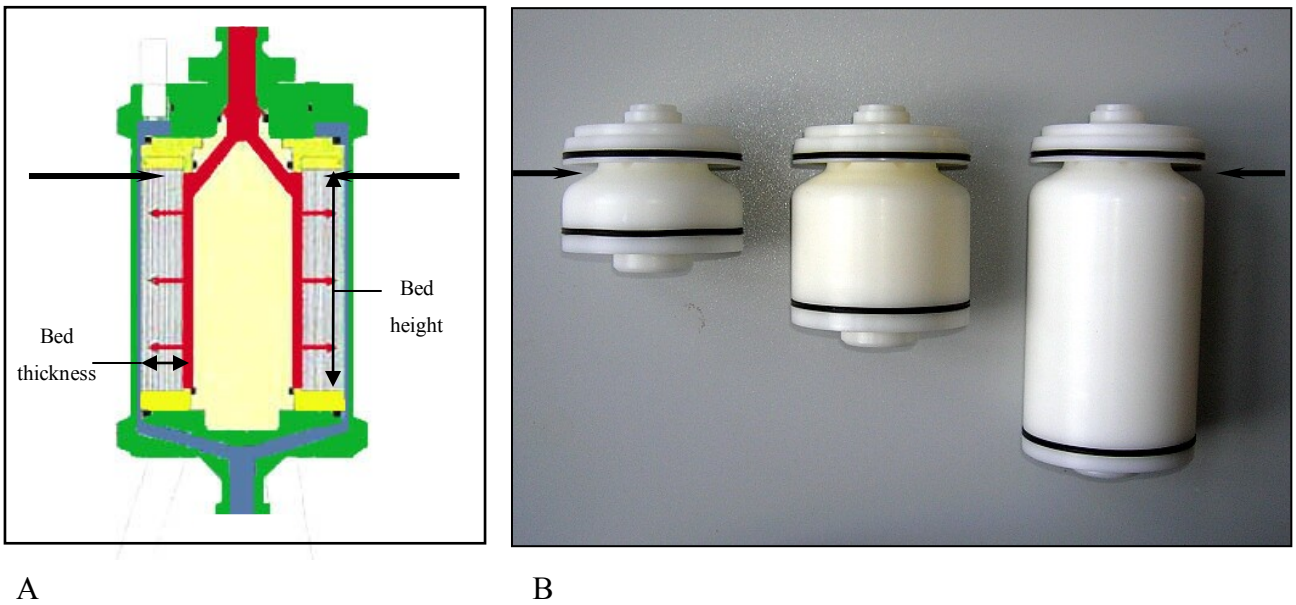

Fig. 2.9 Schematic representation of a Sartobind® Membrane Adsorber System (A) and photograph of the cores of the Membranes Adsorber Systems, used in the experiment: 30 mm, 60 mm and 120 mm long (B). Upper part of the cores is the inlet distributor which creates a mixing zone and is indicated with black arrows.

In the shortest modules, most of the membrane surface area was exposed to the above mentioned mixing zone so that total dispersion was dramatically affected by the relative contribution of the inlet distributor. In contrast to short modules, the membrane surface area in higher modules was only partially exposed to this mixing zone and its relative contribution to total dispersion became weaker leading to lower HETP values.

2.4.1.3 Influence of linear flow velocity

In most of the measurements, HETP values have been found to increase with the linear flow velocity. According to the HETP theory, the third term of the van Deemter equaton is defined as the product of the linear flow velocity by the resistance to mass transfer between stationary and mobile phase. This term reflects the dependency of HETP values on the linear flow velocity. In column chromatography, because of the necessary diffusion into porous beads via film diffusion, a certain resistance to mass transfer is always present even under non binding conditions and HETP values mostly increase with the linear flow velocity as shown in Fig. 2.10.

Solute transport in Membrane Adsorber Systems is theoretically characterized by the absence of film diffusion in dead end pores, so that a resistance to mass transfer may only exist under binding conditions. This inconsistency may be related to the existence of dead end pores inside of Q-Sartobind® Membranes. This would explain the observed dependency of HETP values on the linear flow velocity under non binding conditions.

2.4.1.4 Comparison with Column Chromatography

According to Fig. 2.10, the magnitude of the measured HETP values is very similar to the values measured with various chromatographic columns (Gel filtration and ion-exchanger under non binding conditions). The major difference resides in the achieved linear flow velocities, which are much higher when working with Membrane Adsorber Systems.

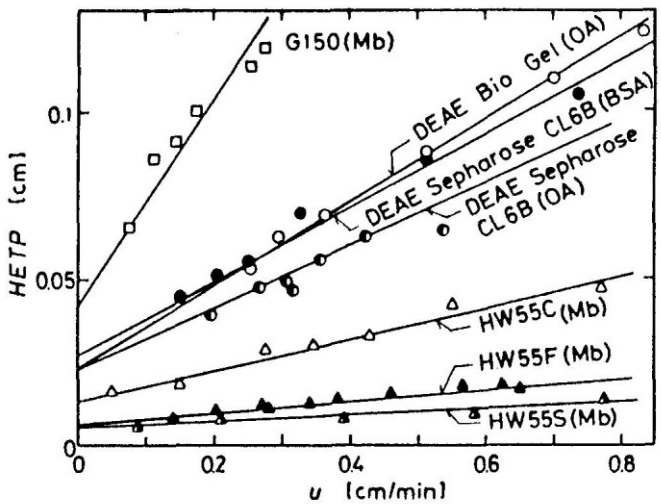

Fig. 2.10 HETP versus linear mobile phase velocity u for various gel filtration columns and for ion-exchange gel columns at high ionic strength where the ion-exchange gels act as gel filtration chromatographic media (from Yamamoto et al. (1988)): Mb, OA, and BSA, Myoglobin, Ovalbumin, and bovine serum albumin respectively.

2.4.2 Peak Resolution

Peak resolution of the isocratic separation of BSA and benzoic acid has been measured. Under the chosen elution conditions, BSA acted as non adsorptive tracer and benzoic acid as an adsorptive tracer.

As expected, peak resolution (Fig. 2.11) increased with bed thickness (at constant bed height), e.g. increasing the bed thickness by four times resulted in approximately three time higher

resolution. It is conceivable that an increase of bed thickness statistically compensates the structural heterogeneities from membrane layer to membrane layer and leads to a structurally more homogeneous membrane stack and fully developed laminar flow. Consequently, a sharper separation has been achieved. For the above mentioned reasons (see section 2.5.1.3), peak resolution has been found to increase unexpectedly with bed height.

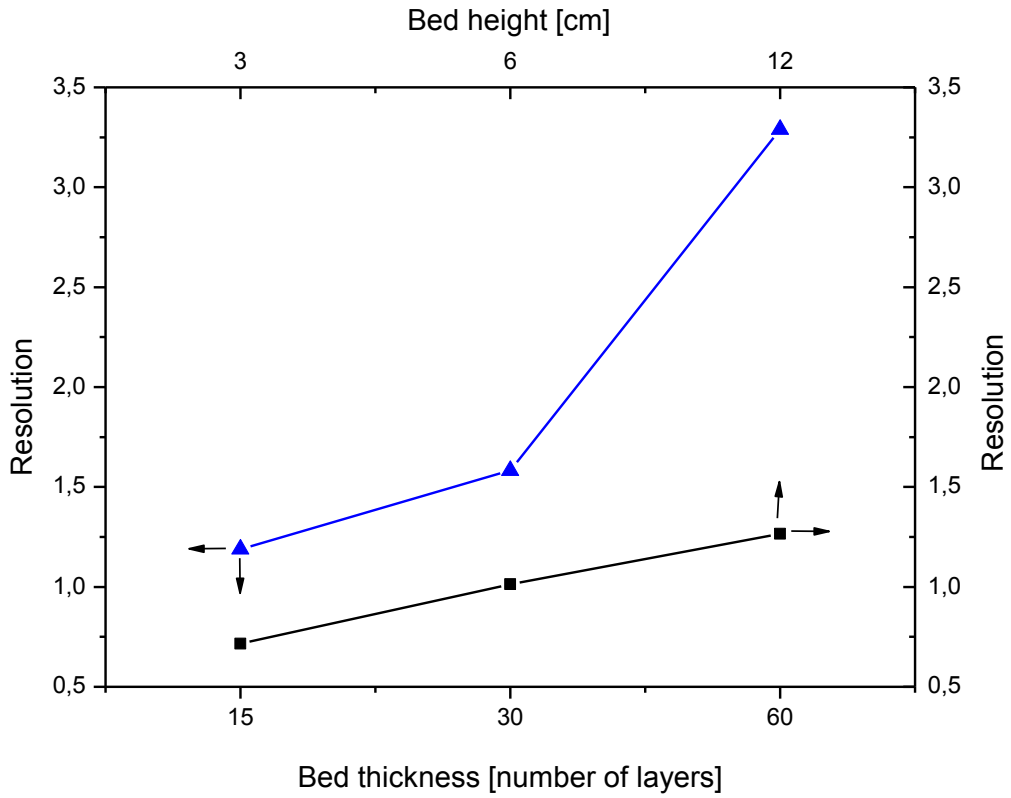

Fig. 2.11 Resolution of the isocratic separation of BSA (10g/L) and benzoic acid (3.2 g/l) in 200 mM sodium acetate buffer (pH4.5, IS 82 mM) versus linear flow velocity for different Q- Sartobind® Membrane Adsorber Systems. Investigation of bed thickness: linear flow velocity: 4.2 cm/min and bed height: 120 mm. Investigation of bed height: linear flow velocity: 5.1 cm/min and bed thickness was 4 mm (15 layers).

2.5 Conclusion

The investigation of Sartobind® Membrane Adsorber Systems in terms of HETP values and resolution revealed new issues about the technical design of inlet distributors and especially about the membrane structure by suggesting the existence of dead end pores inside of Q-Sartobind® membranes.

Fig. 2.12 shows the RTD measured with a Sartobind® Membrane Adsorber System by injecting a non adsorptive tracer (acetone). This RTD is characterized by a very strong asymmetry with a steep increase and a peak tailing. This shape may be due to a heterogeneous flow distribution in channels and distributors as well as a more complex transport phenomena occurring in the porous membrane e.g. enclosing dead end pores.

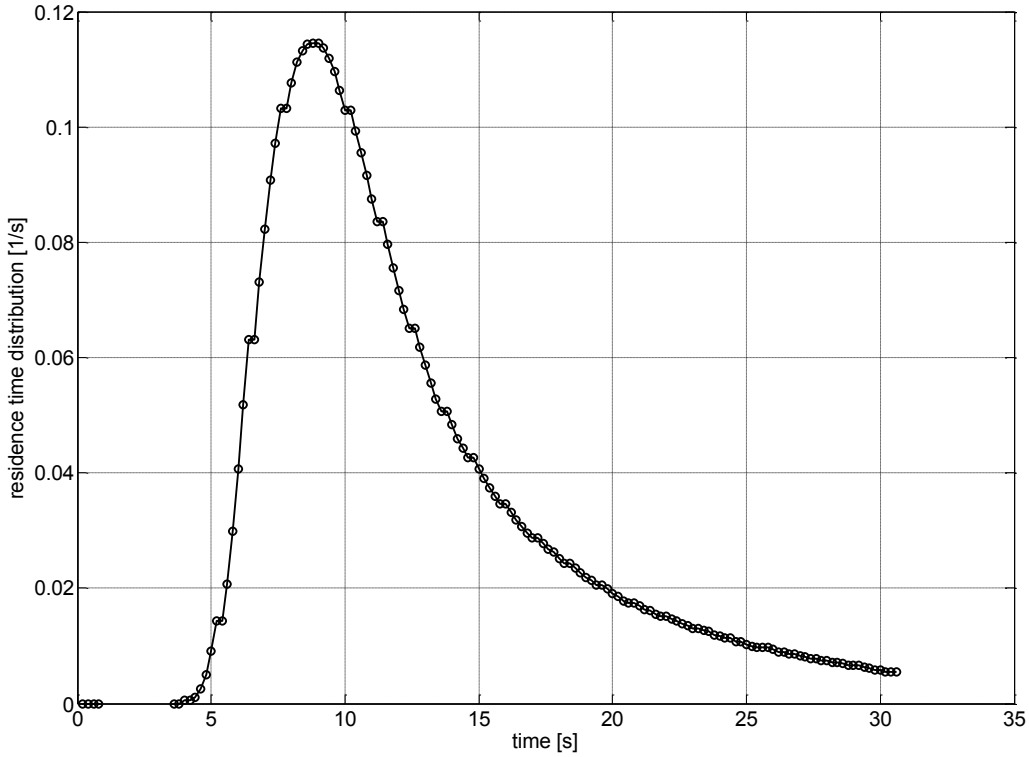

Fig. 2.12 Residence time distribution of acetone in a Q-Sartobind® Membrane Adsorber System (bed height 3cm, bed thickness 4 mm). Buffer was 30 mM sodium acetate (IS 50 mM, pH 5.2) and flow rate was set to 0.68 L/min (linear velocity 7.75 cm min^{-1}).

The future CFD model should not only predict the flow distribution in Membrane Adsorber Systems but also solute transport phenomena occurring in these devices. Predictions of solute transport in distributors and channels may be easily performed by solving the convection-diffusion equation in the considered mesh of finite volumes. The severest problem is to find an appropriate transport model, which enables an accurate description of solute transport in Sartobind® membranes. This problem was the object of the third chapter of the present thesis.

2.6 References

Afeyan NB, Fulton SP, Regnier FE. 1991. Perfusion chromatography packing materials for proteins and peptides. J. Chromatogr. 544: p. 267-279

Asenjo JA, Parrado J, Andrews BA. 1991. Rational Design of Purification Processes for Recombinant Proteins Annals of the New York Academy of Sciences 646 (1): 334–356.

Barbe S, Nussbaumer D, Demmer W, Faber R, Scheper T. 2006. Presentation of a tandem-Sartobind pilot plant as an approach for large scale membrane chromatography. Desalination 200: 480-482.

Barbe S. 2006. Design of membrane chromatography systems for large scale applications. Network Young Membrains 2006 (NYM8), 21-23.09.2006, Institute for Membrane Technology (ITM) Rende (Italy)

Demmer W, Nussbaumer D. 1999. Large-scale membrane adsorbers. J. Chromatogr. A 852: 73-81.

Demmer W, Nussbaumer D, Weiss A. 1999. Tandem system, US-Patent 6,287,461

Frey DD, Van de Water R, Zhang B. 1992. Dispersion in stacked-membrane chromatography. J. Chromatogr. A 603: 43-47.

Ghosh R. 2002. Protein separation using membrane chromatography: opportunities and challenges. Journal of Chromatogr. A 952:13-26.

Janson JC, Jönsson JA. 1998. Introduction to chromatography. In: “Protein purification: principles, high resolution methods and applications”. Wiley-Liss. 43-78.

Kökpinar O, Harkensee D, Kasper C, Scheper T, Zeidler R, Reif OW, Ulber R. 2006. Innovative modular membrane adsorber system for high-throughput downstream screening for protein purification. Biotechnol Prog, 22(4): 1215-1219.

Lavrentieva A. 2008. Dispersion characterization in membrane adsorber systems. Master thesis, Institute of technical chemistry, University Hannover.

Roper DK, Lightfoot EN. 1995. Separation of biomolecules using adsorptive membranes. J. Chromatogr. A 702: 3–26.

Thömmes J, Kula MR. 1995. Membrane chromatography—An integrative concept in the downstream processing of proteins. Biotechnol. Progr. 11: 357–367.

Van Deemter JJ, Zuiderweg FJ, Klinkenberg A. 1956. Longitudinal diffusion and resistance to mass transfer as causes of nonideality in chromatography. Chem. Eng. Sci. 5: 271-89

Yamamoto S, Nakanishi K, Matsuno R. 1988. Ion-Exchange chromatography of proteins. Chromatographic science, v. 43. Mercel Dekker. New York.

Yuan QS, Rosenfeld A, Root TW, Klingenberg DJ, Lightfoot EN. 1999. Flow distribution in chromatographic columns. J. Chromatogr. A 831: 149-165.

Zou H, Huang X, Ye M, Luo Q. 2002. Monolithic stationary phases for liquid chromatography and capillary electrochromatography. Journal of Chromatogr. A 954(1-2): 5-32

3 Investigation of structure and adsorption behaviour of Q-Sartobind® membranes

3.1 Objectives

As mentioned in the previous chapter, the limitation for the successful prediction of RTD's using CFD was the choice of an appropriate transport model, which could predict the transport phenomena occurring Q-Sartobind® membranes.

Therefore, information about the macroporous structure of the Q-Sartobind® membrane and its adsorption behaviour had to be obtained. Following this aim, different techniques and methods have been applied:

- Scanning Electron Microscopy (SEM)
- X-ray microtomography
- Measurement of adsorption isotherms

3.2 Theoretical background

3.2.1 Scanning Electron Microscopy (SEM)

In this form of microscopy, a focused electron beam scans across the sample. The incident beam interacts with the surface of the sample emitting different types of electrons. These can be primary, secondary, auger, and back scattered electrons which are then collected and focused to be viewed as an image by using an appropriate detector.

3.2.1.1 Detection of secondary electrons (Everhart-Thornley Detector ETD)

Special requirements on the sample are needed when working with this kind of detector. Sample must be electrically conductive, at least at the surface, and electrically grounded to prevent the accumulation of electrostatic charge at the surface. They are therefore coated with an ultrathin coating of electrically-conducting material, commonly gold, deposited on the sample by low vacuum sputter coating.

3.2.1.2 Environmental Scanning Electron Microscopy (ESEM)

This method allows the observation of samples in low pressure environments with high relative humidity and sputter coating is not necessary. This method is especially useful for the observation of non-metallic and biological materials. Despite recent developments, the degree of resolution obtained with sputter coating and ETD detectors has not been yet achieved with ESEM methods.

3.2.2 X-ray microtomography

X-ray microtomography is a well known method for the investigation of materials. During the scanning procedure, the sample rotates around an axis that is perpendicular to the beam and a series of radiographs (typically in the order of 1000) is recorded for different angular positions. Despite the existence of commercial laboratory microtomographs, the best images, in terms of spatial resolution, signal-to-noise ratio and quantitative exploitation, are obtained using synchrotron radiations which result from a high intensity and parallel incoming beam.

The particularity of this imaging method is the absence of a magnification step. It means that the spatial resolution mostly results from the effective pixel size of the detector. The range of pixel sizes available at the European Synchrotron Radiation Facility (ESRF in Grenoble, France) is from 0.3 µm to 30 µm. Actions are currently taken to enhance the spatial resolution to 100 nm range. The total acquisition time is in the few seconds ('fast tomography') to 1 hour range, and the recorded data is often several Gigabytes. Microtomography may be coupled with phase contrast imaging, either in a qualitative way ('edge enhancement') or, more quantitatively, including phase retrieval ('holotomography'). After the scanning procedure, reconstruction algorithms enable the observation of the tridimensional image in form of a set of cross sectional radiographs.

X-ray microtomography is also a well established method for the characterization of porous media and for the visualization of the flow in porous media (Wildenschild et al. 2002, Culligan et al. 2004). Wildenschild et al. (2005) has used X-ray microtomography for the visualization of water flow in a sample of porous material (sand).

3.2.3 Langmuir adsorption model and chromatographic retention

Several models have been suggested for the description of the distribution of sample components between the stationary and the mobile phases. The most common and the simplest nonlinear isotherm model is the two-parameter Langmuir model (Langmuir, 1918). The main assumptions of this model are:

- One molecule adsorbs on one site and the number of sites is limited
- The adsorption is reversible
- There are no lateral interactions between adsorbed molecules
- Molecules adsorb by building a monolayer

Langmuir isotherm describes the adsorption by equating adsorption and desorption rates:

$$\frac{dQ}{dt} = k_a C(Q_{\max} - Q) - k_d Q ,$$

where C is the concentration of compound in the mobile phase, k_a is an adsorption equilibrium constant, k_d a desorption constant, $Q_{\max}$ is the maximal number of bounding sites, Q is the number of occupied bounding sites and ($Q_{\max} - Q$) is the number of free bounding sites on the surface.

Assuming steady state, the following relationship between adsorbed and bulk concentrations can be used for the prediction of adsorption isotherms:

$$Q = Q_{\max} \frac{C}{K_{lang} + C} ,$$

where K_{lang} is the Langmuir constant and represents a measure for the affinity of the sorbent to the stationary phase. Despite the fact that the assumptions involved in Langmuir isotherms are seldom satisfied in the case of protein adsorption (Norde, 1986), it provides fittings in good agreement with many systems.

3.3 Materials and methods

3.3.1 Scanning Electron Microscopy

SEM imaging has been performed using FEI Quanta 200F FEG-SEM scanning electron microscope (FEI, Hilsboro, Oregon, USA).

3.3.1.1 Sample preparation

Membrane samples have been washed with deionised water and dried for 30 min at 30°C. Perpendicular and tangential cuts have been performed using a freezing microtome (Leica CM30505 cryostat and Leica CE/CN knife holder, Leica Microsystems Nussloch GmbH).

For investigations using ETD detector, Sputter coating (K550 Sputter Coater, Emitech Ltd.) has been performed with gold (approx. 150 Angstroms thin layer) at 35 mA during 3 min under vacuum (0.01 mbar).

3.3.1.2 Investigation of membrane swelling

This investigation has been performed in ESEM mode. Peltier elements have been used in order to cool down the samples at 2°C. A pressure range between 130 and 2600 Pa has been used (1-30 Torr). The sample humidity has been controlled by changing the partial pressure inside of the chamber.

3.3.2 Adsorption of monoclonal conjugates

Membrane samples have been loaded with monoclonal anti-hCG gold conjugates (BBInternational, Cardiff, UK). These gold conjugates are protein-coated gold nanoparticles (40nm). Nanoparticles were coated with monoclonal antibodies (Monoclonal anti Beta HCG CGC clone 1). For sample preparation, the following procedure has been applied:

1:100 dilution of stock suspension in 20mM Tris buffer pH 9.0 was prepared. Membrane samples were incubated in 5ml of the diluted suspension for 1 hour under stirring. After loading, the membrane samples were washed in 5ml of 20mM Tris buffer pH 9.0 under stirring for 30 s. Imaging has been performed using large field detection (LFD) in a pressure range of 10-200 Pa.

3.3.3 Investigation of saturated samples using X-ray microtomography

The experiments were carried out on the ID 19 beamline at the ESRF (European Synchrotron Radiation Facility in Grenoble, France). An appropriate method for the analysis of saturated Q-Sartobind® membrane samples has been developed in collaboration with the ESRF.

Membrane samples were saturated with deionized water. Samples have been then deposed on top of a capillary and short acquisition times were used to avoid light-matter interactions. Membrane samples were squares with a surface area of approx. 1 mm². At such high resolution (pixel size of 0.56 micron), the camera field of view is only 600 x 600 µm² and local X-ray microtomography was so necessary. It means that the size of the samples were larger than the camera field of view. The following parameters were set on the ID19 beamline:

- X-ray energy: 15 keV
- A set of 600 projection images was taken over 180° at 0.1s exposure time per image
- Pixel size: 0.56µm
- Distance between sample and detector: 50mm
- Total scan time: 3minutes

3.3.4 Measurement of adsorption isotherms

Circular pieces of membrane with a total surface area of 0.5 cm^2 were used. Adsorption isotherms of Bovine Serum albumin (BSA) and Benzoic acid on Q-Sartobind® membranes were measured (Tab. 3.1).

One membrane piece was immersed in 1.8 mL of Sample solution. Incubation was performed at 20°C under stirring for 10 hours.

Tab. 3.1 Buffers and tracers concentrations, used for the adsorption isotherm measurement

Buffer	Tracer, Concentrations [mg/mL]
20 mM potassium phosphate, IS 175 mM, pH 7.2	BSA; 0, 1.0, 2.0, 4.0, 8.0, 16.0, 32.0
30 mM sodium acetate, IS 50 mM, pH 5.2	BSA; 0, 1.0, 2.0, 4.0, 8.0, 16.0, 32.0
200 mM sodium acetate, IS 82 mM, pH 4.5	Benzoic acid; 0, 0.2, 0.4, 0.8, 1.56, 3.2, 6.4

After incubation, BSA or Benzoic acid concentrations were measured photometrically at 280nm.

3.4 Results and discussion

3.4.1 Structural characterization of Sartobind® membranes

3.4.1.1 Investigation using Scanning Electron microscopy coupled with ETD detection

Sartobind® membranes are made of reinforced cross linked cellulose and manufactured by evaporative casting. For reinforcement purposes, a polyester fleece (Fig. 3.1) with a coarse structure (average pore diameter of approx. 100-200 µm) assures the mechanical membrane stability. At process begin, the polyester fleece is layered with a colloidal cellulose casting solution and then transported on a conveyor through the casting machine. A certain amount of polar solvents present in this solution assures the solubility of cellulose.

During evaporative casting, due to a conditioned gaseous phase and a controlled conveyor temperature, solvents evaporate out of the casting solution until cellulose precipitates by forming a porous network (primary porous structure).

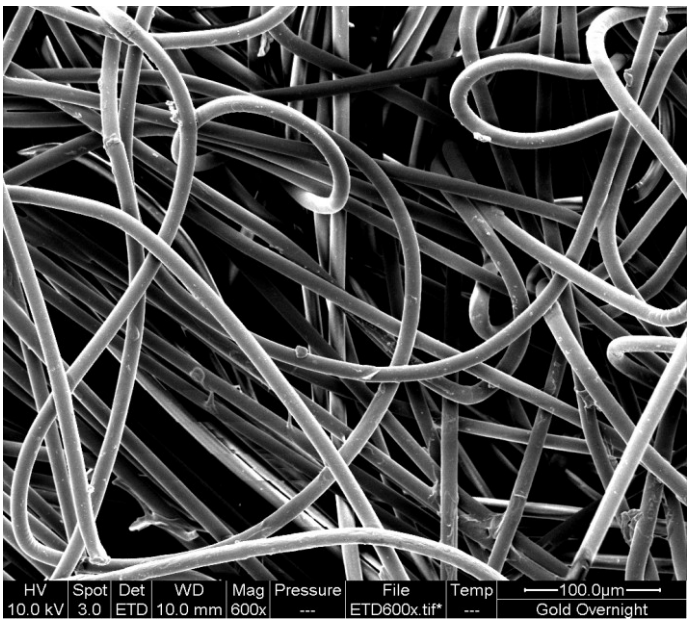

Fig. 3.1 SEM micrograph of polyester fleece used for the reinforcement of Sartobind® membranes (sputter coated with gold, ETD detector, magnification – 600x). Average pore diameter is 100-200 µm.

This phase inversion leads to a syneresis and therefore newly formed pores are filled with the remaining casting solution. Due to precipitation, the cellulose concentration in the casting solution drastically decreased. Further evaporation removes the solvents out of the pores and the remaining cellulose precipitates by forming a secondary finer porous structure.

In regard to this process description, the aim of this evaporative casting process may be considered as the refining of the fleece porosity over two steps. Porosity refining is necessary for the achievement of a high future adsorption area. According to this process description, a homogeneous membrane structure may only be achieved when the following conditions are fulfilled:

- The primary porosity is homogeneously distributed.
- The secondary porosity is formed homogenously inside of the primary structure.

The anion exchange functionality of Q-Sartobind® membranes is performed by a polymeric impregnation. This process step occurs after the evaporative casting and resulting structural changes could not be observed with SEM or X-ray microtomography.

It is common practice in membrane technology to differentiate gas side and conveyor side of a membrane. The gas side corresponds to the interface between casting solution and gaseous phase during the evaporative casting. The conveyor side is the lower side of the membrane, which is in contact with the conveyor during the process.

Fig. 3.2 shows micrographs of the gas side of a Q-Sartobind® membrane. Polyester fleece, primary and secondary porosities can be clearly recognized. The primary porosity appears to be homogeneously distributed and a heterogeneous repartition of the secondary porosity is observed in terms of strong fluctuations of pore diameters (from approx. 1 to 20 µm). Pores may be consequently classified in two classes: large and small depending on their diameter scale. Liquid flow would preferentially take place through the large pores.

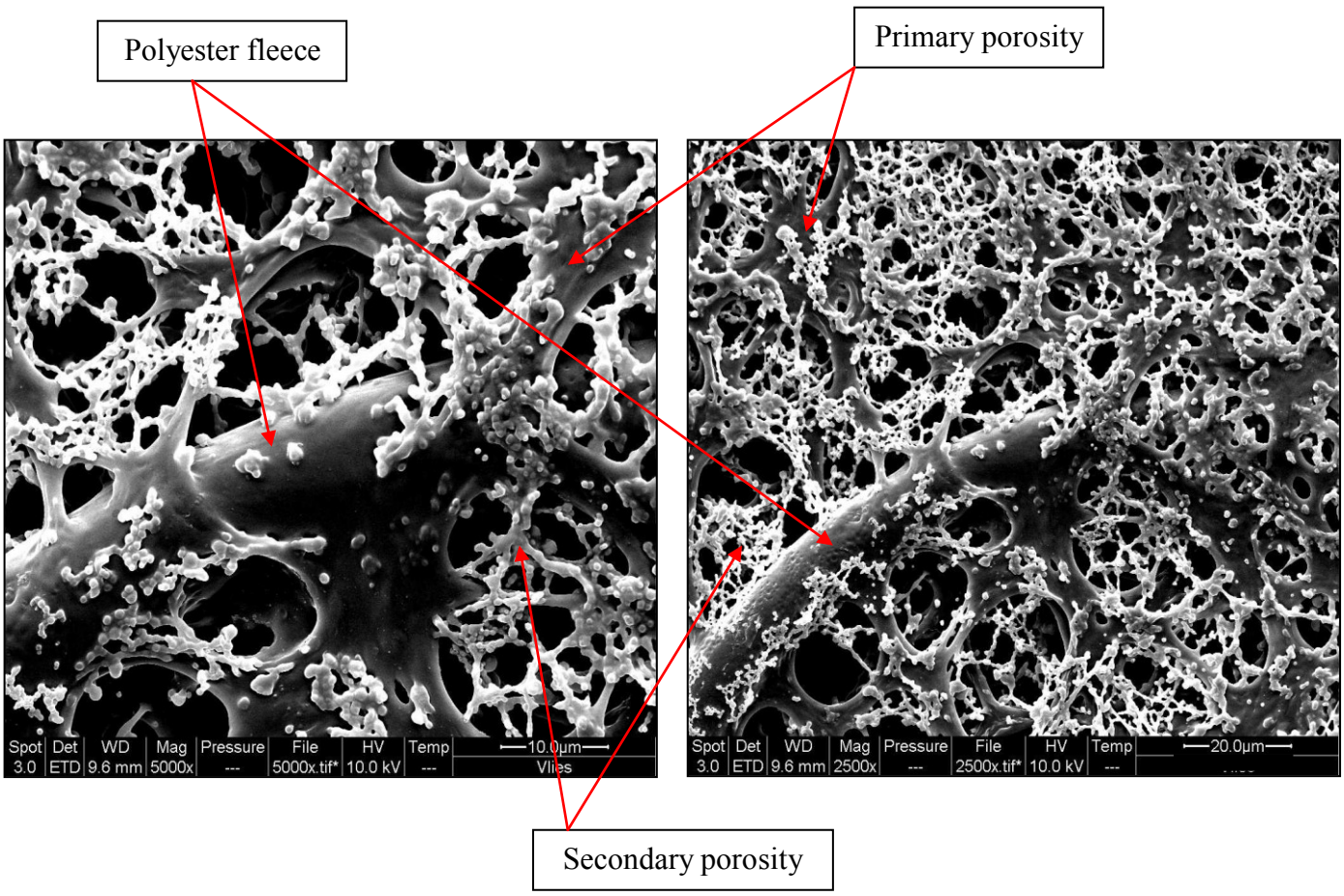

Fig. 3.2 SEM micrograph of Sartobind®Q membrane (sputter coated with gold, ETD detector, magnification – magnification: (A) - 5000x, (B) – 2500x).

Cross-sectional micrographs of Sartobind®Q membrane (Fig. 3.3) show an expected composite membrane structure with two structurally distinct layers. The upper part (gas side) of the membrane consists of an approx. 50 µm thick cellulose layer with a relative fine porosity. This can be considered as the active layer of the membrane, where adsorption mainly occurs and where the highest flow resistance is expected. The lower part of the membrane (approx. 200 µm) mostly corresponds to the polyester fleece partially filled with cellulose. This layer is characterized by a relative coarse porosity and mainly has a mechanical stabilizing function. Along the membrane depth, pores may be also classified in two size classes: large and small.

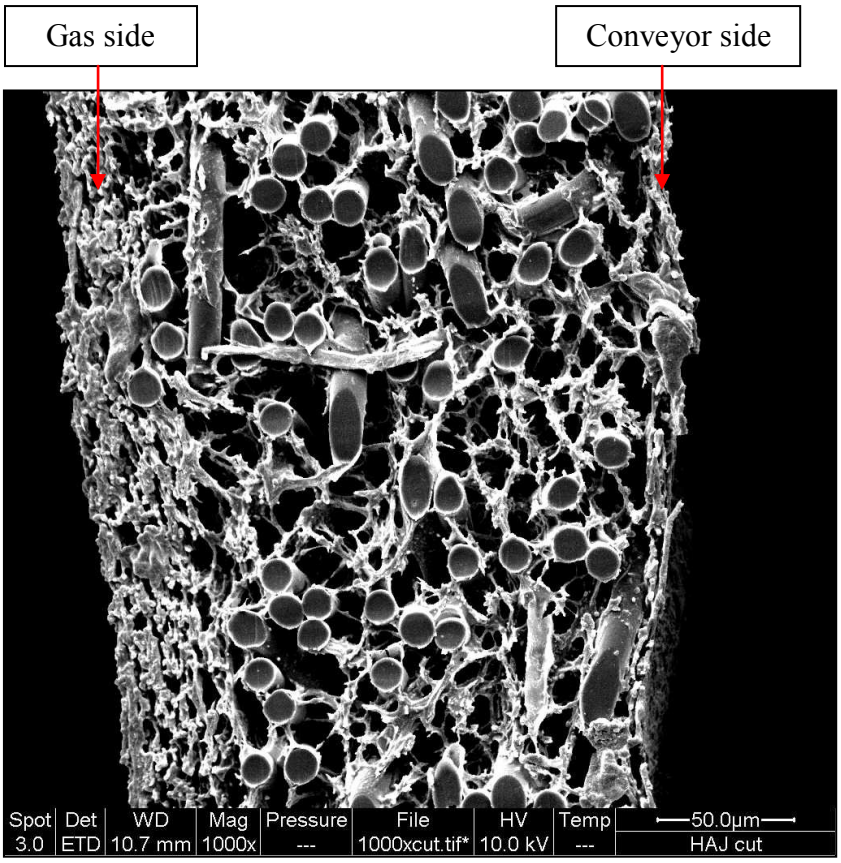

Fig. 3.3 SEM cross sectional micrograph of Q-Sartobind® membrane (Sputter coated with gold, ETD detector, magnification – 1000x)

3.4.1.2 Investigation using X-ray microtomography

While SEM investigations require the achievement of cut using e.g. microtomes, X-ray tomography enables the fully three dimensional visualization of porous samples without affecting the sample integrity. Fig. 3.4 shows radiographs obtained by X-ray microtomography at different depths, where zero depth corresponds to the gas side of the membrane. Considering a top-down analysis, a progressive deterioration of the porous homogeneity is observed. At zero depth, primary and secondary porosities can be recognized and seem both to be homogeneously distributed resulting in an apparent homogeneous pore scale. In the middle of the above mentioned active membrane layer (Depth = 32 µm), the radiograph reveals first signs of heterogeneity. At this depth, polyester fibers and pores with a higher diameter scale become visible. Near of the interface between active layer and polyester fleece (Depth = 52 µm), a very heterogeneous and wide pore size distribution appears. Approximately one half of this membrane cross section is covered by a fine porosity and the other half by a much coarser porosity. At depths lower than 50 µm, one can clearly recognize the network of polyester fibers. Despite the coarse porosity of this network, extreme fluctuation of pore diameter scale cannot be observed.

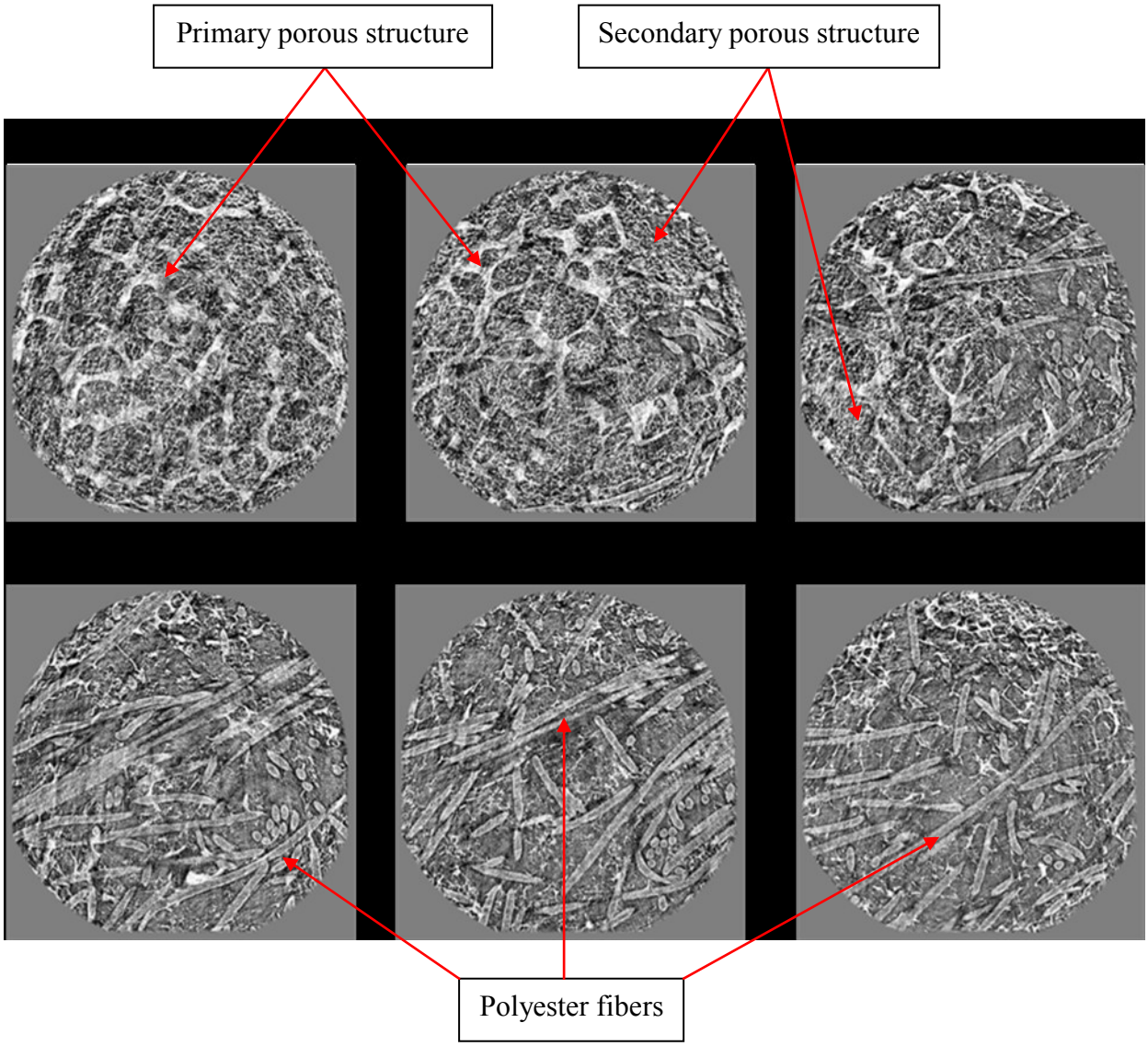

Fig. 3.4 Radiographs of Q-Sartobind® (with water saturated) membranes at different depths using X-ray microtomography (carried on the ID 19 beamline at the ESRF, Grenoble, France), X-ray energy: 15 keV, pixel size: 0.56µm. Zero depth corresponds to the gas side of the membrane.

Fig. 3.5 shows the cross sectional structure of a Q-Sartobind® membrane at different lengths. The composite structure of the membrane can be recognized and X-ray images are similar to SEM micrographs shown in Fig. 3.3. Structural variations along the membrane length are visible and the proportion of the active layer seems to be constant.

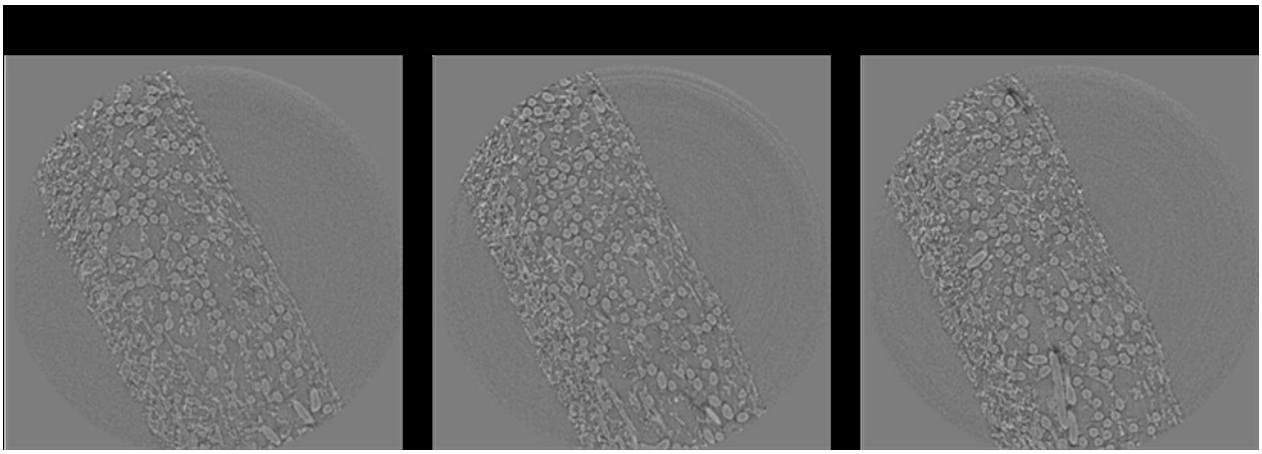

Fig. 3.5 Radiographs of Q-Sartobind® membranes (with water saturated) at different lengths using X-ray microtomography (carried on the ID 19 beamline at the ESRF, Grenoble, France), X-ray energy: 15 keV, pixel size: 0.56µm

3.4.2 Investigation of membrane swelling

Performing SEM in ESEM mode (Environmental Scanning Electron Microscopy) enables imaging at different water partial pressures. It is so possible to decrease the membrane water content of a saturated membrane by lowering the water partial pressure inside of the specimen chamber. When water has been fully removed out of the pores (Fig. 3.6), a slightly constriction of the membrane structure is observed by further drying. This swelling of the polymeric structure does not seem to affect the porous organization of the membrane.

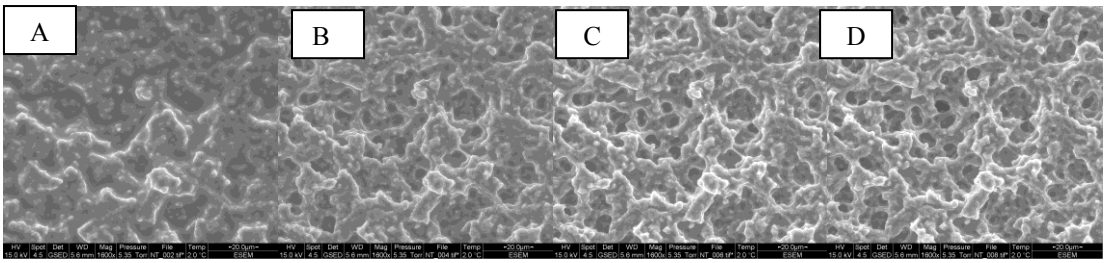

Fig. 3.6 SEM micrographs of Q-Sartobind® membrane (GSED detector, ESEM mode, magnification – 1600x) during drying, water pressure has been progressively reduced from A to D.

3.4.3 Adsorption behavior of Q-Sartobind® membranes

3.4.3.1 Adsorption of monoclonal conjugates on Q-Sartobind® membranes

Beside diffusion and convection, mass transport in adsorptive membranes is also affected by adsorption phenomena. In this regard, an accurate adsorption model is necessary in order to complete the prediction ability of the future CFD simulations. The first step of the presented approach was the localization of the adsorption sites in Q-Sartobind® membranes and the evaluation of their interactions with proteins. Therefore, the adsorption at saturation concentration of monoclonal conjugates has been imaged via LFD (Large Field Detector) coupled SEM. Monoclonal conjugates (40 nm nanoparticles) have been used to facilitate the visualization of protein adsorption and so reduce the necessary magnification.

The binding of conjugates resulted from electrical interactions between the negatively charged antibodies at the set pH value with the anion-exchange membrane and was so comparable with the adsorption mechanism of proteins. Previous investigations under non-binding pH values have shown the absence of unspecific adsorption of monoclonal conjugate on Q-Sartobind® membranes. Adsorbed conjugates were mainly visualized on the secondary porous structure. The upper micrograph (Fig. 3.7) shows the structure of a pore where adsorption could be observed. Monoclonal conjugates seem to be adsorbed homogeneously by building a well ordered monolayer.

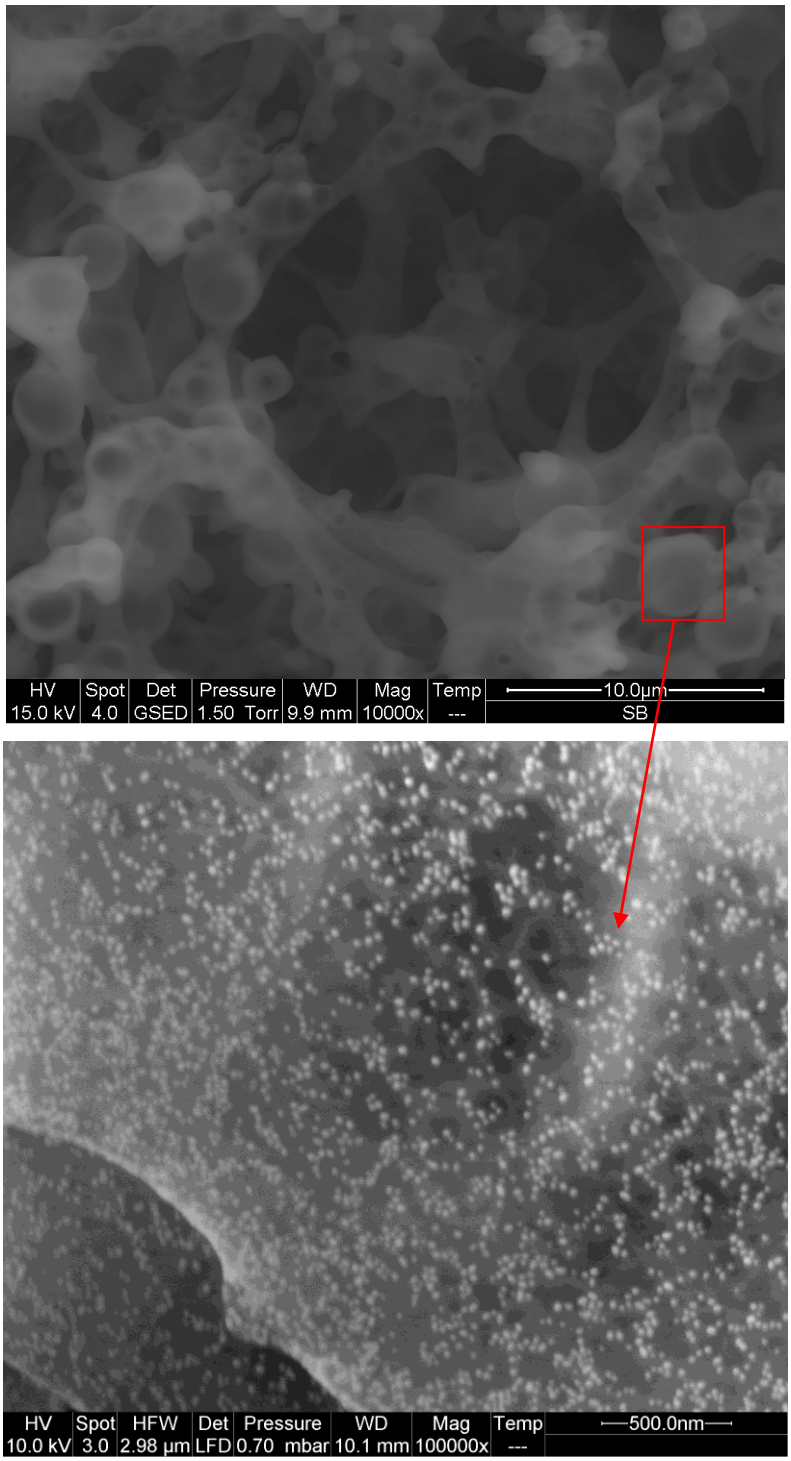

Fig. 3.7 SEM micrographs of Sartobind®Q membrane using a LFD detector, magnification – magnification: (A) – 10 000x, (B) – 100 000x. The adsorption of monoclonal conjugates (diameter 40 nm) may be observed in B.

3.4.3.2 Measurement of adsorption isotherms

Additionally, adsorption isotherms of Q-Sartobind® membranes have measured with BSA and benzoic acid. These measurements have been then fitted using the analytical formulation of the Langmuir adsorption isotherm. The Langmuir adsorption model is a well established model for the description of solute adsorption in chromatography (Gebauer, 1996). The curve fittings obtained (Fig. 3.8) are in good agreement with the measurements.

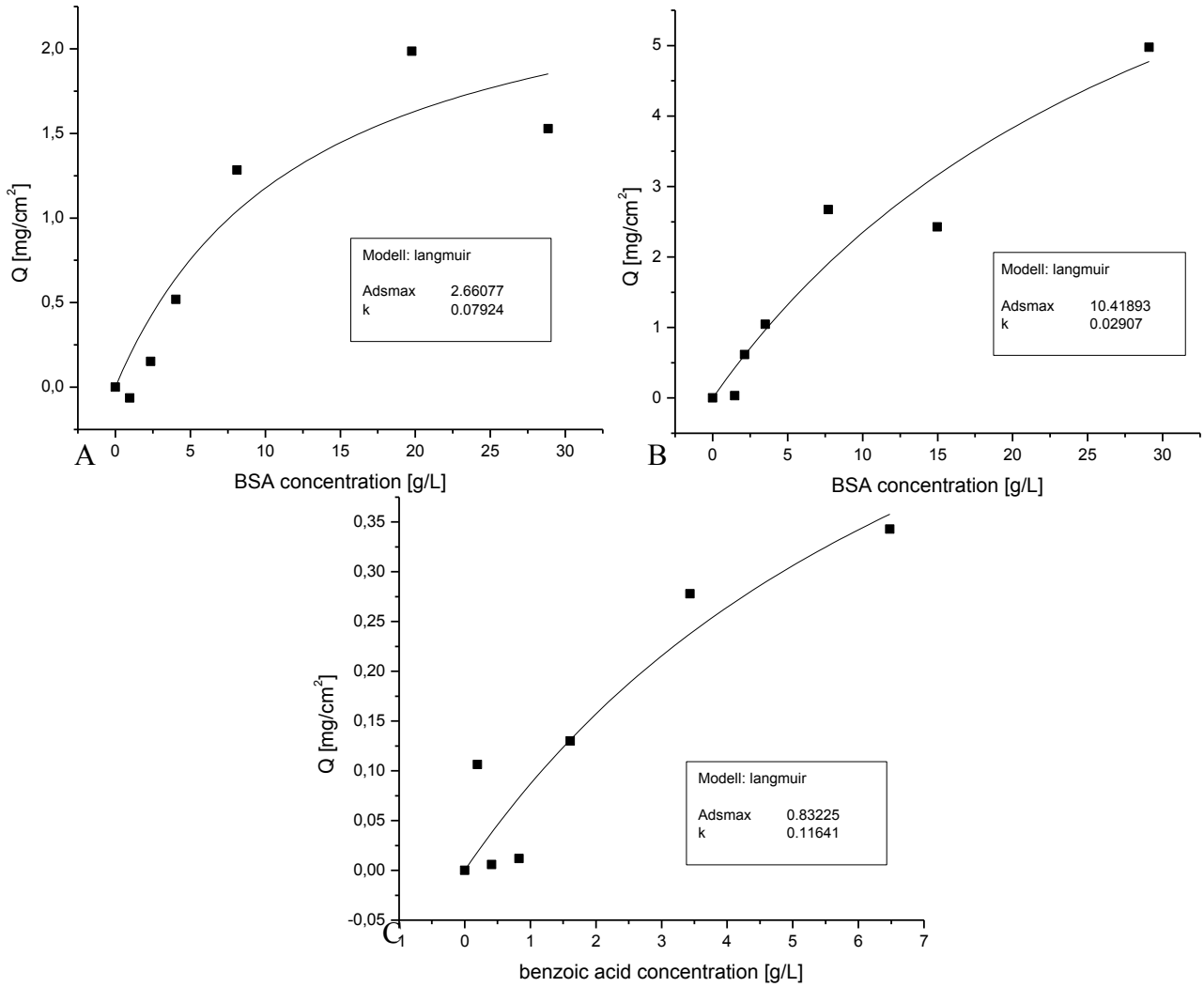

Fig. 3.8 Adsorption isotherms for BSA in 20 mM potassium phosphate buffer, IS 175 mM, pH 7.2 (A), BSA in 30 mM sodium acetate buffer, IS 50 mM, pH 5.2 (B) and benzoic acid in 200 mM sodium acetate buffer, IS 82 mM, pH 4.5 (C). Continuous lines correspond to fittings performed with Langmuir adsorption model.

According to the Langmuir equation, at low concentration the concentration C becomes negligible compared to the Langmuir constant Q_{max} and adsorption isotherms become nearly linear. Fig. 3.9 shows the linear fitting of adsorption measurements at lower concentration ranges. Maximum values of the plotted concentration ranges correspond to the tracer concentrations injected during the experiments described in the previous chapter. Therefore, adsorption isotherms can be assumed to be linear at the investigated concentration range. This assumption considerably simplifies the implementation of adsorption mechanisms in the future CFD model.

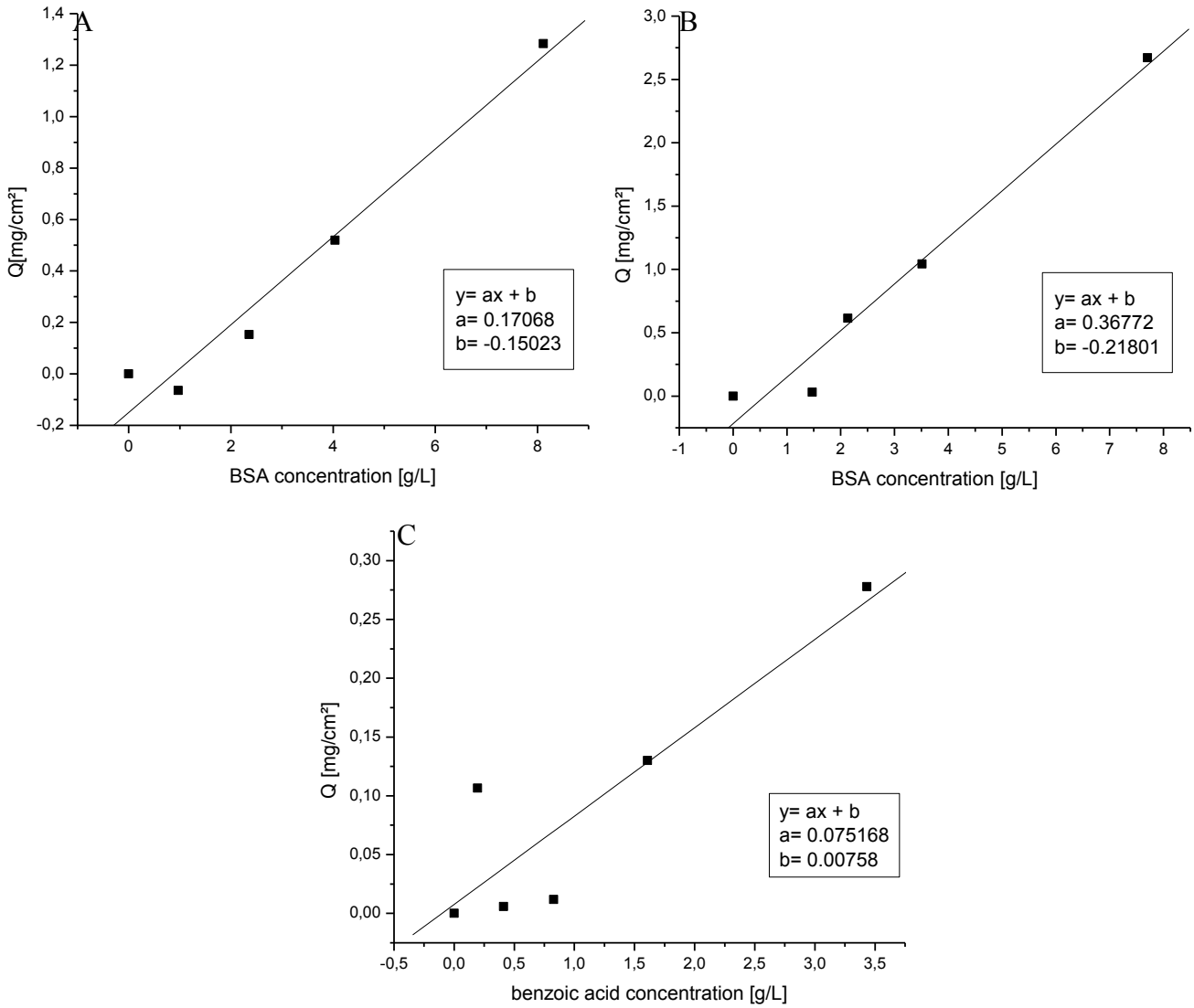

Fig. 3.9 Adsorption isotherms for BSA in 20 mM potassium phosphate buffer, IS 175 mM, pH 7.2 (A), BSA in 30 mM sodium acetate buffer, IS 50 mM pH 5.2 (B) and benzoic acid in 200 mM sodium acetate buffer, IS 82 mM, pH 4.5 (C), Continuous lines correspond to linear fittings.

3.5 Conclusions

SEM and X-ray microtomography have been shown to be very beneficial tools in getting a better understanding of the composite structure of Q-Sartobind® membranes, which consist of an active layer (approx. 20% of total membrane thickness) and a supporting layer (80% of total thickness).

The real imaged membrane structure did not really fit to the theoretical representation of adsorptive membranes (with homogeneous pore scale). High contrasts in pore scales have been observed inside of the active layer, which could strongly affect mass transport phenomena occurring in the membrane. The pore size distribution appears to be bimodal within the active layer consisting of a fine and a coarse porosity. This bimodal distribution has to be considered by the chosen transport model. A conceivable candidate is the dual porosity also called dual region model developed by Coats and Smith (1964) and modified by van Genuchten et al. (1989). According to this model, the porous medium is characterized by the coexistence of a mobile region and an immobile region. In this case the mobile region would represent the coarse porosity. There, solute transport results from:

- Diffusive and convective mass transport and
- Mass exchange with the immobile region.

The immobile region would represent the fine porosity and is characterized by the absence of any neither convection nor diffusion. Therefore, solute transport only results from the mass exchange within the mobile region.

Such a model would describe the preferential flow through large pores and their interaction with small pores (dead end zones). In terms of residence time distribution, solute transport in a dual porosity medium is characterized by early breakthrough resulting from rapid advective transport in the mobile region and tailing resulting from the slow diffusive mass transfer between the mobile and immobile regions (Neville et al., 2000). Such phenomena have been observed in Q-Sartobind® Membrane Adsorber Systems and discussed in the previous chapter.

Due to the superposition of two continua in a porous medium, this model also allows to consider the heterogeneous distribution of the adsorption sites inside of the membrane. Adsorption sites have been mostly identified in the secondary porous structure. The measurement of adsorption isotherms has shown that linear adsorption isotherms can be assumed for the range of tracer concentration used during the experiments presented in chapter 2.

3.6 References

Barbe S, Boller E, Faber R, Thom V, Scheper T. 2007. The use of X-ray microtomography for the characterization of macroporous membranes. JA SF2M, Ecole des mines de Saint Etienne (France), 30.05-01.06.2007.

Coats KH, Smith BD. 1964. Dead-end pore volume and dispersion in porous media. SPE J. 4: 73–84.

Culligan KA, Wildenschild D., Christensen BSB, Gray WG, Rivers ML, Tompson AFB. 2004. Interfacial area measurements for unsaturated flow through a porous medium. Water Res. 40.

Gebauer KH. 1996. Stofftransport und Kinetik in der Protein-Chromatographie am Beispiel neuer Membran-Adsorbentien. Fortschritt-Bericht-VDI Nr. 147, Reihe 17

Langmuir I. 1918. The adsorption of gases on plane surfaces of glass, mica and platinum. J.Am.Chem.Soc. 40: 1361-1403.

Neville CJ, Ibaraki M, Sudicky E. 2000. Solute transport with multiprocess nonequilibrium: a semi-analytical approach. Journal of Contaminant Hydrology 44: 141:159.

Norde W. 1986. Adsorption of proteins from solution at the solid-liquid interface. Adv. Colloid Interface Sci. 25: 267-340.

van Genuchten MT, Wagenet RJ. 1989. Two-site/two-region models for pesticide transport and degradation: Theoretical development and analytical solutions. Soil Sci. Soc. Am. J., 53(5): 1303-1310

Wildenschild D, Hopmans JW, Vaz CMP, Rivers ML, Rikard D, Christensen BSB. 2002. Using X-ray computed tomography in hydrology: systems, resolutions and limitations. J. Hydrol. 267: 285-297.

Wildenschild D, Hopmans JW, Rivers ML, Kent AJR. 2005. Quantitative Analysis of Flow Processes in Sand Using Synchrotron-Based X-ray Microtomography. Vadose Zone Journal 4:112-126.

4 Analysis of tracer transport in Q-Sartobind® membranes

4.1 Objectives

This chapter aims to evaluate the applicability of different transport models to describe the transport of passive scalars (in this case, tracer concentration) in Q- Sartobind® membranes. These models should not only properly describe the transport phenomena occurring in such membranes but also be implementable in a CFD code. CFD is based on continuum mechanics which consider changes in fluids at a macroscopic scale. In this regard, a robust one-dimensional numerical approach using averaged macroscopic models has been developed.

Because of its simplicity and its robustness, the CDE (Convection-Dispersion-Equation) model, which describes "normal" or "Gaussian" dispersion, is commonly used for the mathematical formulation of transport phenomena occurring in porous media and has been therefore chosen as a possible candidate. This model is only valid if the dispersion process is a combination of a large number of uncorrelated steps and is not valid if large size flow heterogeneities are present or if the medium contains dead volumes. Due to observed high contrasts in pore scale and the presumed existence of dead end pores in Q-Sartobind® membranes (chapter 3), the dual porosity model has been suggested as a second possible candidate.

The present chapter deals with the comparison of the capabilities of CDE and dual porosity models to fit RTD's measured with Q-Sartobind® membranes. Additionally, dispersion parameters (CDE and dual porosity model) have been determined which can be used as input parameters for further CFD implementations. In the frame of these investigations, following steps have been performed.

- An experimental setup with optimized flow distribution has been developed and enabled the measurement of dispersion curves with Q-Sartobind® membrane stacks and the further determination of dispersion parameters using the one-dimensional formulations of the above mentioned transport models.

- An optimization algorithm has been implemented in MATLAB, which allowed the fitting of RTD's with CDE and dual porosity models. Furthermore, this algorithm

enabled the estimation of dispersion parameters by eliminating extra membrane dispersion sources.

- RTD's obtained by injecting adsorptive (benzoic acid) and non adsorptive (BSA and acetone) tracers at different flow rates have been fitted with CDE and dual porosity models and the corresponding dispersion parameters have been determined.
- Fitting accuracies of CDE and dual porosity models have been compared in terms of residuals. Finally, the influence of the superficial velocity on dispersion parameters has been discussed

4.2 Theoretical background

4.2.1 Convection Dispersion Equation (CDE)

In porous media, the convection-dispersion equation (CDE) for one-dimensional transport of reactive solutes in porous media, that are subject to adsorption is written as

$$\frac{\partial}{\partial t}\left(\theta \cdot c_r + \rho_b \cdot s\right) = \frac{\partial}{\partial x}\left(\theta \cdot D \cdot \frac{\partial c_r}{\partial x} - v_x \cdot c_r\right)$$

where c_r is the volume averaged or resident concentration of the liquid, s is the concentration of the adsorbed phase, D is the dispersion coefficient, θ is the volumetric water content or porosity, v_x is the superficial flow velocity, ρ_b is the bulk density, x is the distance and t is the time.

Solute adsorption by the solid phase is described with a linear isotherm as

$$s = K_d \cdot c_r$$

where K_d is an empirical distribution constant. The CDE model is a so called equilibrium deterministic model, in which the porous medium consists of a set of channel or pores with the same diameter scale. Its formulation is very close to the formulation of the convection-diffusion equation. Mass transport in adsorptive membranes has been mainly predicted using this model (Gebauer, 1996).

4.2.2 Dual porosity model

In more complex porous media, a physical non equilibrium may occur as a result of a heterogeneous flow regime. This equilibrium is often modeled by using a dual porosity (two regions) type formulation (Toride et al., 1999). The medium contains two distinct mobile (flowing) and immobile (stagnant) liquid regions (Coats and Smith, 1964, van Genuchten and Wierenga, 1976). Mass transfer between the two regions is modeled as a first order process.

For an accurate mathematical description of mass transport phenomena occurring in such porous media, mass balances in both regions have to be formulated and lead to the following system of partial differential equations (one dimensional, van Genuchten and Wagenet, 1989)

$$\begin{cases} (\theta_m + f \cdot \rho_b \cdot K_d) \cdot \dfrac{\partial c_m}{\partial t} = \theta_m \cdot D_m \cdot \dfrac{\partial^2 c_m}{\partial x^2} - v_x \cdot \dfrac{\partial c_m}{\partial x} - \alpha \cdot (c_m - c_{im}) \\ [\theta_{im\cdot} + (1-f) \cdot \rho_b \cdot K_d] \cdot \dfrac{\partial c_{im}}{\partial t} = \alpha \cdot (c_m - c_{im}) \end{cases}$$

where the subscripts *m* and *im* refer to the mobile and immobile regions, respectively, f represents the fraction of adsorption sites that equilibrates with the mobile liquid phase and α is a first-order mass transfer coefficient governing the rate of solute exchange between the mobile an immobile regions. Note that θ, the total porosity, is equal to $\theta_m + \theta_{im}$. According to this model, neither convection nor diffusion exists in the immobile region and the dispersion coefficient always refers to the mobile region. Solute adsorption by the solid phase is also described with a linear isotherm.

4.3 Materials and methods

4.3.1 Chemicals

If not indicated otherwise all chemical reagents were obtained from Merck (Darmstadt, Germany).

4.3.2 Sample preparation

Membrane layers were prepared and sealed in so called membrane-containing-pucks. These consisted out of 30 circular pieces (diameter 25 mm) of membrane stacked upon each other. In addition, two pieces of polypropylene fleece were added on both sides of the membrane stacks to ensure homogeneous flow distribution. The stacked membranes were pressed between two symmetric Plexiglas forms (Fig. 4.1) and the outer part has been injection-moulded with silicon. Silicon hardening was achieved by incubation at 60°C for one hour.

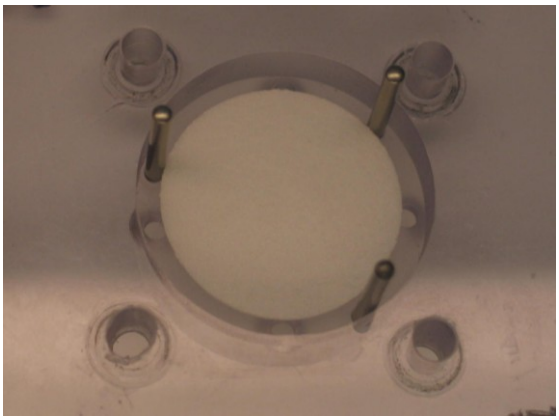

Fig. 4.1 Plexiglas form for membrane puck preparation. Three sticks were used for homogenous stacking of membranes with 25mm in diameter. Sequentially another Plexiglas form is connected using the four outer screw threads. Then silicone is injected through the four holes seen on the bottom of the outer concentric slot.

Q-Sartobind® Membranes (porosity = 0.72), used to prepare these pucks were taken from the same production charge as the membranes, which have been packed in the Membrane Adsorber modules described in chapter 2. Standard distributor plates (from MA 75 units, Sartorius-Stedim Biotech GmbH, Germany, Göttingen) have been filled with epoxy resin and newly milled in order to distribute the solute equally over the membrane surface (Fig. 4.2). After successful membrane stacking and silicon injection, distributor plates were added on both sides of the pucks, which could be connected to the FPLC capillaries. Homogeneity of

flow distribution was checked using an anionic dye (Ponceau S), which was injected through the membrane binding to cationic functional.

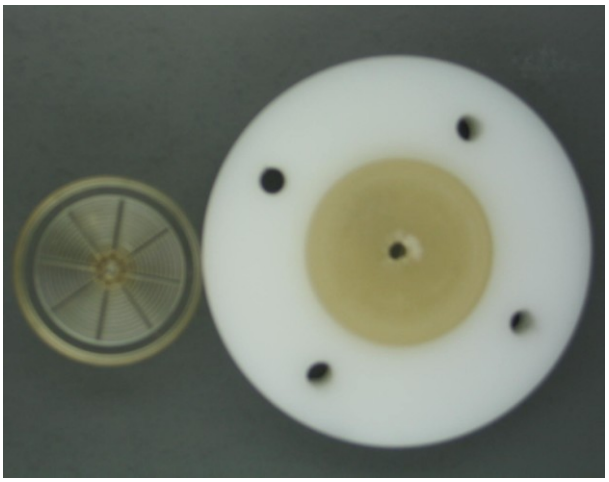

Fig. 4.2 Flow distributor plates and plastic housing. The left standard distributor plate (from MA 75 units) was first filled with epoxy resin, newly milled and then placed in a plastic housing (right side). Solute flow occurred through the middle orifice of the distributor plate.

Fig. 4.3 Final experimental unit. A membrane containing puck sealed with silicone and distributors attached on both sides. They are inserted in a plastic housing and fixed with screws.

For sealing the whole unit, pucks and distributors were pressed in a plastic housing (Fig. 4.3). In order to measure extra membrane dispersion, separate pucks only containing 4 layers of polypropylene fleece, so called non-membrane-containing-pucks, were prepared.

4.3.3 Dispersion measurement

Measurements were obtained with fast protein liquid chromatography (FPLC) measuring UV absorption (280nm). The applied equipment was the Äkta Explorer 100 system (GE Healthcare Bio-Sciences AB, Uppsala Sweden).

Tracer pulses were injected via a 400µl injection loop and output signals were monitored and recorded. As tracers, 5% acetone in 30 mM sodium acetate buffer (IS 50 mM, pH 5.2), BSA (10 g/L) in 200 mM sodium acetate buffer (IS 82 mM, pH 4.5) and benzoic acid (3.2 g/L) in 200 mM sodium acetate buffer (IS 82 mM, pH 4.5) were used. For each tracer, total dispersion of 9 membrane containing pucks was measured two times at following flow rates: 0.5, 1.0, 2.0, 4.0, 8.0, 16.0 and 24 mL/min.

Extra membrane dispersion of two non-membrane-containing-pucks was measured for each tracer and at each flow rate. Sources for extra membrane dispersion were:

- Sample valve
- Capillaries
- Fittings
- UV detector
- Flow distributors
- Fleece layers

4.3.4 Estimation of strictly membrane related dispersion parameters

Membrane dispersion signals may be interpreted as the response function obtained by the deconvolution of extra membrane dispersion signals out of total dispersion signals. In a first approach, usual deconvolution methods e.g. Laplace transformation, Fourier transformation and multi-dimensional arrays formulation have been performed leading to poor quality response functions.

A second approach had to be envisaged where total dispersion signals ($D_{total}(t)$, measured) have been interpreted as the convolution between extra membrane dispersion signals (D_{extra}

(t), measured) and the analytical one-dimensional solution of the corresponding model (CDE or dual porosity, hereafter referred to as $C_f(t)$).

$$D_{total}(t) = \int_0^t C_f(\tau) \cdot D_{extra}(t-\tau) \cdot d\tau$$

The estimation of dispersion parameters has been performed by minimizing the following objective function *O(x,t)*:

$$O(x,t) = \left| \sum_t \left(D_{total}(t) - \int_0^t C_f(x,\tau) \cdot D_{extra}(t-\tau) \cdot d\tau \right) \right|^2$$

Where *t* represents the time and *x* is the solution vector containing the dispersion parameters, which had to be optimized during the minimization process. This minimization has been performed using the large scale algorithm of the MATLAB's optimization Tool Box. Jacobians were not calculated analytically but approximated by finite difference.

For the CDE model, the following one-dimensional analytical solution (Toride et al., 1999) has been implemented in the corresponding objective function:

$$C_f(T) = \sqrt{\frac{R \cdot Pe \cdot Z}{4 \cdot \pi \cdot T^3}} \cdot \exp\left[-\frac{Pe \cdot (R \cdot Z - T)^2}{4 \cdot R \cdot T} \right]$$

With

$$T = \frac{v \cdot t}{L}$$

L: average pore size (5 µm) as the characteristic length for the porous medium

$$Pe = \frac{v \cdot L}{D}$$

$$Z = \frac{x}{L}, x = 0.8 \text{ cm}$$

$$R = 1 + \frac{\rho_b \cdot K_d}{\theta}$$

In this case, the solution vector *x* consisted of the following dispersion parameters:

$$x = |v, D, R|$$

For non-adsorbing-tracers (acetone and BSA), the retardation factor *R* was set to 1 and only the two remaining parameters were optimized. For adsorbing tracer (benzoic acid), *v* has been constrained by the minimal and maximal optimal values obtained with non adsorbing tracers.

For the dual porosity model, the following one-dimensional analytical solution (Toride et al., 1999) has been implemented in the corresponding objective function:

$$C_f(T) = \Gamma_1^N(T) \cdot \exp\left(-\frac{\omega \cdot T}{\beta \cdot R}\right) + \frac{\omega}{R} \cdot \int_0^T \sqrt{\frac{\tau}{\beta \cdot (1-\beta) \cdot (T-\tau)}} \cdot \Gamma_1^N(\tau, T) \cdot H_1 \cdot d\tau$$

Where the fully developed form was,

$$C_f(T) = \frac{Z}{T} \cdot \sqrt{\frac{\beta \cdot R \cdot Pe}{4 \cdot \pi \cdot T}} \cdot \exp\left[-\frac{Pe \cdot (\beta \cdot R \cdot Z - T)^2}{4 \cdot \beta \cdot R \cdot T}\right] \cdot \exp\left(-\frac{\omega \cdot T}{\beta \cdot R}\right) + \frac{\omega}{R} \cdot \int_0^T \sqrt{\frac{\tau}{\beta \cdot (1-\beta) \cdot (T-\tau)}} \cdot \frac{Z}{\tau}$$
$$\cdot \sqrt{\frac{\beta \cdot R \cdot Pe}{4 \cdot \pi \cdot \tau}} \cdot \exp\left[-\frac{Pe \cdot (\beta \cdot R \cdot Z - \tau)^2}{4 \cdot \beta \cdot R \cdot \tau}\right] \cdot \exp\left[-\frac{\omega \cdot \tau}{\beta \cdot R} - \frac{\omega \cdot (T-\tau)}{(1-\beta) \cdot R}\right] \cdot I_1\left[\frac{2 \cdot \omega}{R} \cdot \sqrt{\frac{(T-\tau) \cdot \tau}{(1-\beta) \cdot \beta}}\right] \cdot d\tau$$

With

I_1: first order modified Bessel function

$$T = \frac{v \cdot t}{L}$$

L: average pore size (5 µm) as the characteristic length for the porous medium

$$Pe = \frac{v \cdot L}{D}$$

$$Z = \frac{x}{L}, x = 0.8 \text{ cm}$$

$$\beta = \frac{\theta_m + f \cdot \rho_b \cdot K_d}{\theta + \rho_b \cdot K_d}$$

$$R = 1 + \frac{\rho_b \cdot K_d}{\theta}$$

$$\omega = \frac{\alpha \cdot L}{\theta \cdot v}$$

This analytical solution contains an additional convolution which has been calculated numerically for every time step via an explicit Euler method. In this case, the solution vector x consisted of the following dispersion parameters:

$$x = |v, D, R, \beta, \alpha|$$

For non-adsorbing-tracers (acetone and BSA), the retardation factor R was set to 1 and only the four remaining parameters were optimized. For adsorbing tracer (benzoic acid), v was constrained by the minimal and maximal optimal values obtained with non adsorbing tracers.

4.4 Results and discussion

4.4.1 Assumptions

In a three dimensional approach, dispersion is described by a dispersion tensor (diagonal 3 x 3 matrix). Within the frame of these experiments, considerable efforts were devoted to the achievement of a homogeneous flow distribution over the membrane surface. In this regard, polypropylene fleece layers were added on both sides of the membrane stacks and standard distributor plates (from MA 75 units) were filled with epoxy resin and newly milled. As above mentioned, homogeneous flow distribution has been checked using an anionic dye (Ponceau S).

Therefore, it was assumed that transverse concentration gradients were negligible and dispersion mainly occurred in the longitudinal direction. This assumption justified the use of one-dimensional transport models for the determination of dispersion parameters inside of Q-Sartobind® membranes. Considering a main flow in x-direction, only the x-component of the dispersion tensor, hereafter referred to as dispersion coefficient, was determined. Analytical solutions were available for one dimensional models (CDE and dual porosity models) and were therefore of great benefit for curve fittings and parameter estimation.

The numerical approach presented in this chapter is a one dimensional macroscopic approach. This means that local microscopic variables have been replaced by a macroscopic average defined on a representative elementary volume and membrane stacks have been considered as a porous body characterized by a single set of dispersion parameters. The contributions of microscopic structural properties of membrane stacks, such as the periodicity of the composite structure and the interstitial spaces, to the dispersion have been averaged on the elementary volumes.

4.4.2 Dispersion of non adsorptive tracers

Non-adsorptive tracers with different diffusion coefficients and molecular weights, acetone as a low molecular weight compound (56 g/mol, D_{diff}: $1.3 \cdot 10^{-9}$ m²/s) and BSA as a protein (large polymer of amino acids, approx. 66000 g/mol, D_{diff}: $5.9 \cdot 10^{-11}$ m²/s), have been used in this work. Dispersion measurements obtained with both tracers have been fitted with CDE and dual porosity models. Measurement conditions have been taken from the investigations performed in chapter 2.

The developed fitting algorithm worked successfully and high quality fits have been obtained with both transport models. All residuals determined in the frame of this investigation were lower than 10^{-5}. The major advantage of this algorithm is the simultaneous elimination of extra membrane dispersion sources via convolution and estimation of strictly membrane-related dispersion parameters. For non-adsorbing-tracers, CDE and dual porosity models were implemented as a two parameters model (v, D) and as a four parameters model (v, D, α, β), respectively.

The ratio between residuals achieved with CDE and dual porosity fits was used to describe the relative accuracy of the dual porosity model compared to the CDE model. The orders of magnitude of the accuracies achieved with both models were similar. All investigated flow rates showed higher fit accuracies when the dual porosity model was used (Fig. 4.5). A maximum has been observed at 16mL/min.

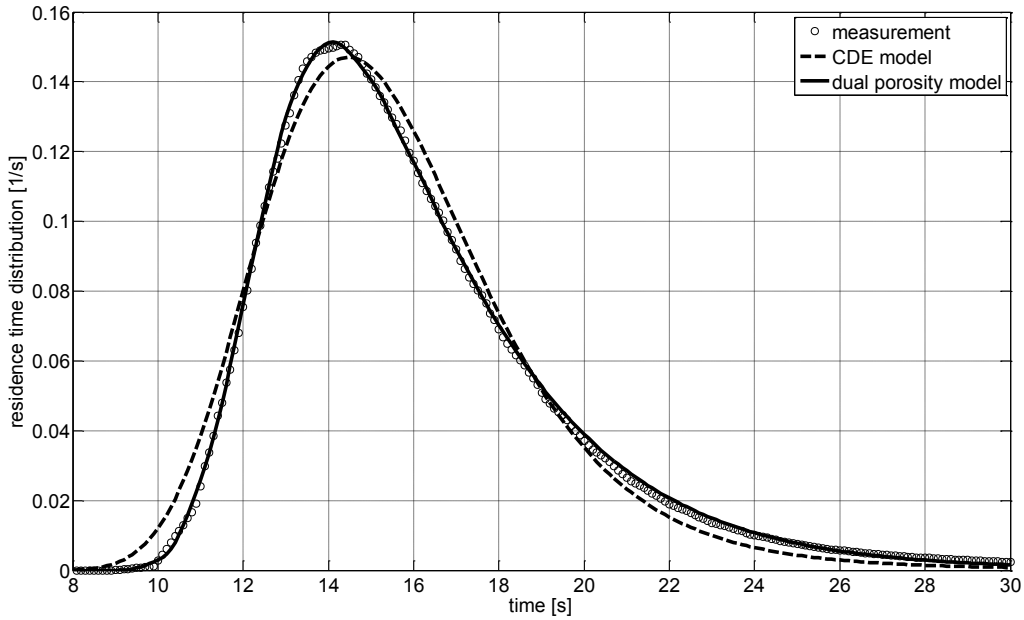

Fig. 4.4 Residence time distribution measured with a membrane-containing-puck (diameter 25 mm, 30 layers, Q-Sartobind®). Tracer was BSA (10 g/L) in 200 mM sodium acetate buffer (IS 82 mM, pH 4.5), flow rate: 16 mL/min. Continuous line shows the fitting obtained with the dual porosity model and discontinuous line shows the fitting obtained with the CDE (convection-Dispersion Equation). Extra membrane sources have been eliminated during the fitting procedure

At this critical flow rate, the CDE model still gave an acceptable fitting but failed to perfectly fit early breakthrough and peak tailing (Fig. 4.4) while the curve given by the dual porosity model nearly overlapped with dispersion measurements. According to this observation, these "non-Gaussian" anomalies could result from a solute transport limitation between mobile and immobile regions. The existence of concentration gradients between both regions would explain the preferential convective solute transport through the mobile region (early breakthrough) and the solute release from the immobile region into the mobile region (peak tailing).

A dependency of the impact of these "non Gaussian" anomalies on the flow rate was observed and might be related to a diminishing time of solute exchange between both regions with increasing flow rates. At increasing subcritical flow rates, decreasing exchange times would lead to higher magnitudes of concentration gradients between the two regions. This would explain the growing relative accuracies of the dual porosity model reflecting a more distinct "dual porosity behaviour". At flow rates higher than the critical value, despite high magnitudes of concentration gradients, low exchange times would progressively reduce the probability for solute molecules to penetrate the immobile region. Consequently, at high flow rates, solute transport would increasingly take place in the mobile region and explain the less pronounced "dual porosity behaviour" which was observed.

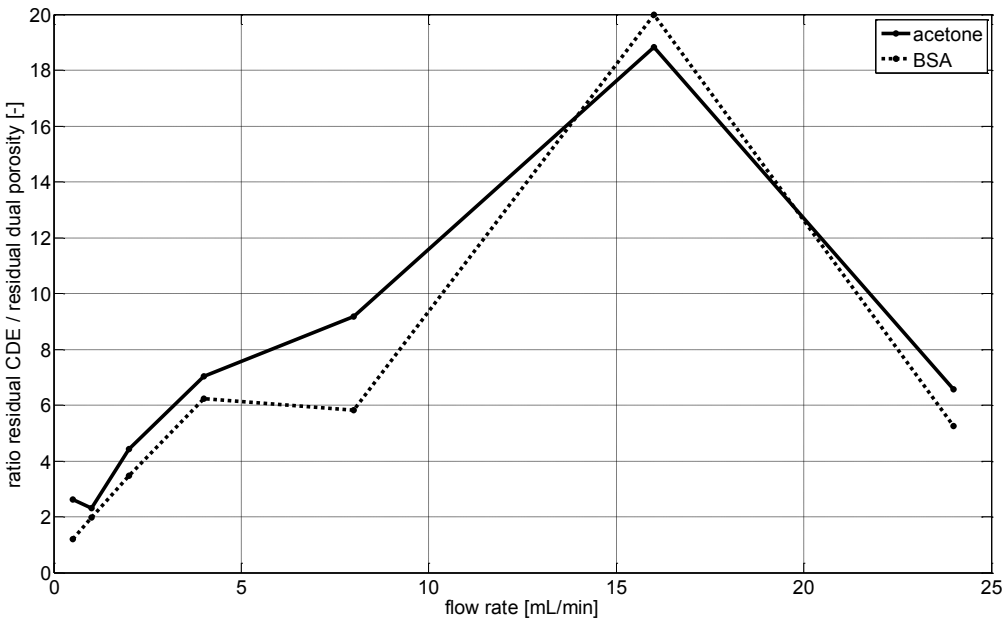

Fig. 4.5 Ratio between residuals achieved by fitting dispersion curves with CDE and dual porosity models as functions of the flow rate. The ratio was used to describe the relative accuracy of the dual porosity model compared to the CDE model. Dispersion measurements have been performed in membrane-containing-pucks (diameter 25 mm, 30 layers, Q-Sartobind®). Tracers were acetone 30 mM sodium acetate buffer (IS 50 mM, pH 5.2) and BSA (10 g/L) in 200 mM sodium acetate buffer (IS 82 mM, pH 4.5).

The superficial velocities have been estimated by fitting dispersion curves with the CDE as well as with the dual porosity model and their orders of magnitude were consistent with calculated hydrodynamic residence times. The superficial velocity strongly contributed to the fitting flexibility allowing the models to adjust times of modelled RTD's with times of measured RTD's and to balance the relative contribution of the convective term to total

dispersion. Fig. 4.6 and 4.7 show the estimated superficial velocities as functions of the set flow rate using CDE and dual porosity models for acetone and BSA.

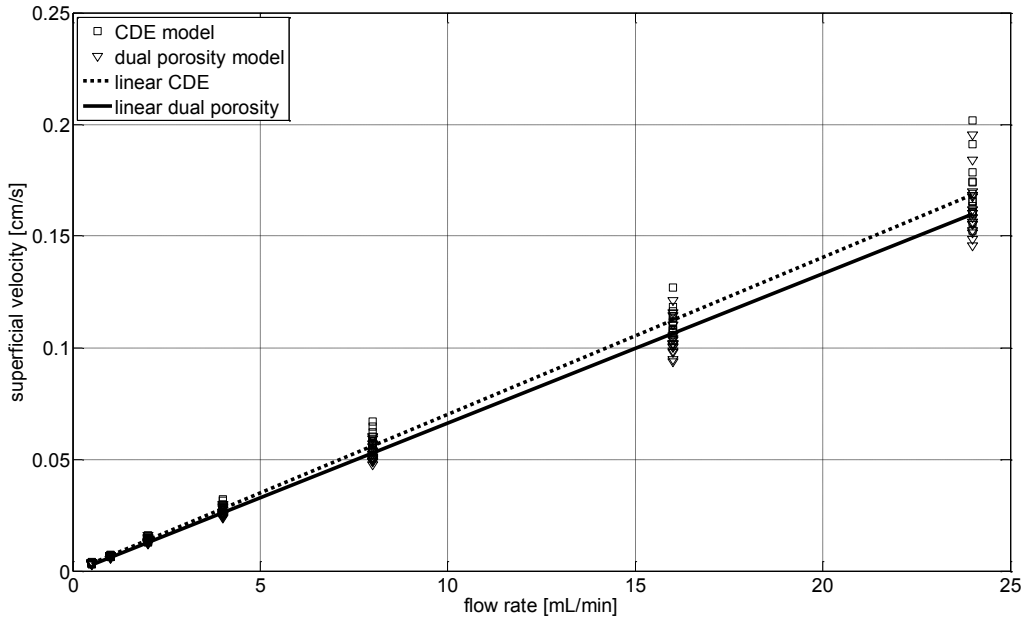

Fig. 4.6 Superficial velocities estimated by fitting dispersion curves with CDE and dual porosity models as a function of the set flow rate. Dispersion measurements have been performed membrane containing pucks (diameter 25 mm, 30 layers, Q-Sartobind®). Tracer was acetone 30 mM sodium acetate buffer (IS 50 mM, pH 5.2).

For both tracers, superficial velocities estimated by fitting measurements with the CDE model were slightly higher (approx. 7%) than the corresponding values given by the dual porosity model. Estimated superficial velocities resulting from dispersion curves measured with BSA, as a high molecular tracer, were considerably higher (approx. 20 %) than the velocities obtained by injecting the low molecular weight tracer acetone. This observation might be explained by a size exclusion effect and is further discussed in 4.5.

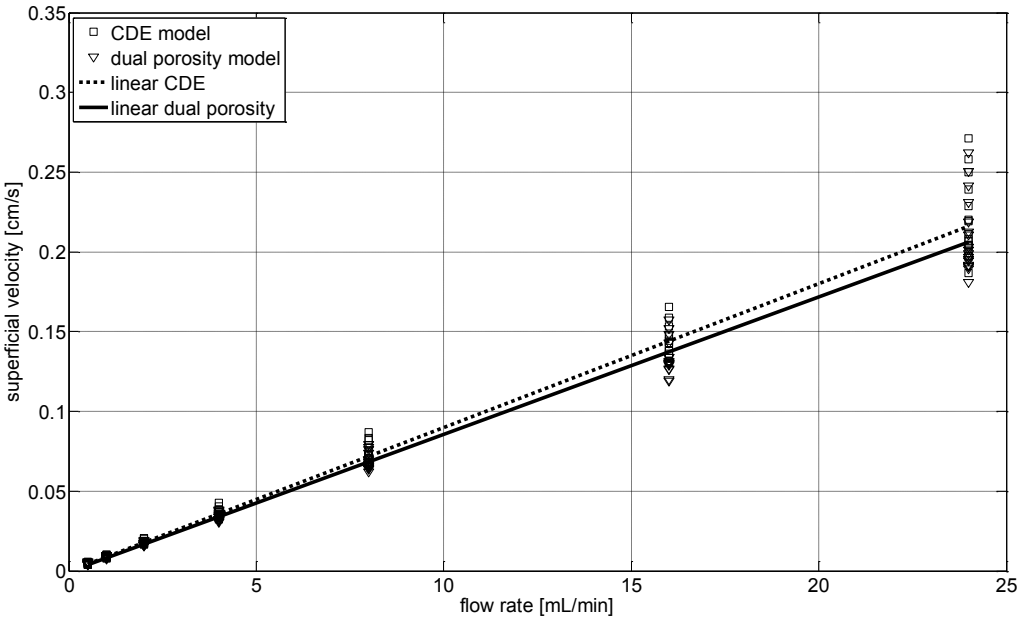

Fig. 4.7 Superficial velocities estimated by fitting dispersion curves with CDE and dual porosity models as a function of the set flow rate. Dispersion measurements have been performed membrane containing pucks (diameter 25 mm, 30 layers, Q-Sartobind®). Tracer was BSA (10 g/L) in 200 mM sodium acetate buffer (IS 82 mM, pH 4.5).

No significant dependency of dispersion coefficients on the superficial velocity was found for fits performed with the dual porosity model and average values of D = $1.18 \cdot 10^{-8}$ m²/s for acetone and D = $2.48 \cdot 10^{-8}$ m²/s for BSA have been determined. A superficial flow velocity dependency of dispersion coefficients estimated according to the CDE model has been observed for both tracers (Fig. 4.8) and, compared to the dual porosity model, values were approx. 10-100 times higher (from $2.0 \cdot 10^{-7}$ to $2.0 \cdot 10^{-6}$ m²/s). In contrast to the CDE model, dispersion coefficients given by the dual porosity model were very close to the diffusion coefficients of the tracers (acetone $1.3 \cdot 10^{-9}$ m²/s, BSA $5.9 \cdot 10^{-11}$ m²/s, Gebauer, 1996).

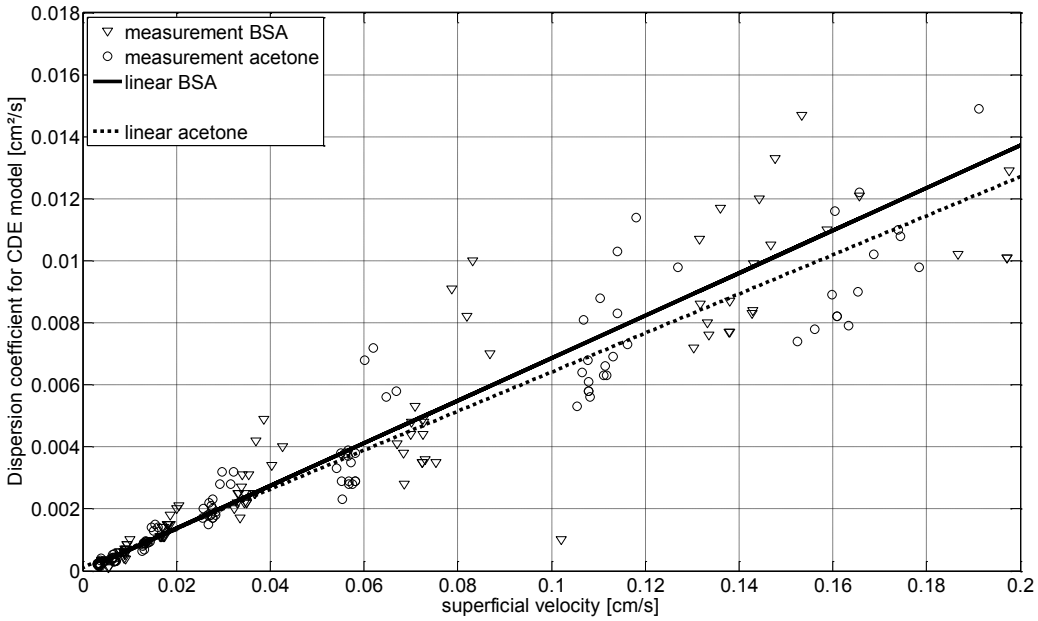

Fig. 4.8 Dispersion coefficients estimated by fitting dispersion curves with the CDE model as a function of the superficial velocity. Dispersion measurements have been performed membrane containing pucks (diameter 25 mm, 30 layers, Q-Sartobind®). Tracers were acetone 30 mM sodium acetate buffer (IS 50 mM, pH 5.2) and BSA (10 g/L) in 200 mM sodium acetate buffer (IS 82 mM, pH 4.5).

Additionally to the superficial velocity and the dispersion coefficient, the dual porosity gave a dimensionless variable for region partitioning β and the first order exchange coefficient between both regions α. Constant β –values were estimated over the investigated flow range and a porosity of 0.28 were found for the immobile region (θ_{im}) by injecting acetone as well as BSA. This represented a considerable proportion (approx. 39%) of the total porosity (0.72).

Fig. 4.9 shows nearly linear increases of the solute exchange coefficient with the superficial velocity for both tracers, where an approx. 20% steeper slope has been observed when acetone was used as a low molecular weight tracer. According to the dual porosity model, for a single diffusive exchange mechanism between both regions, mass exchange from the mobile into the immobile region may be formulated as follows.

$$\alpha \cdot (c_m - c_{im}) = \frac{D_{diff} \cdot A}{V_m \cdot dx}(c_m - c_{im})$$

Where A is the surface area of the interface between both regions, V_m is the volume of mobile region in the considered representative elementary volume, D_{diff} is the diffusion coefficient of

the corresponding tracer and *dx* is the distance between the locations where mobile and immobile concentrations are considered. According to this formulation, the exchange coefficient is not dependent on the superficial velocity and would have remained constant if solute transport between the two regions had exclusively been diffusive.

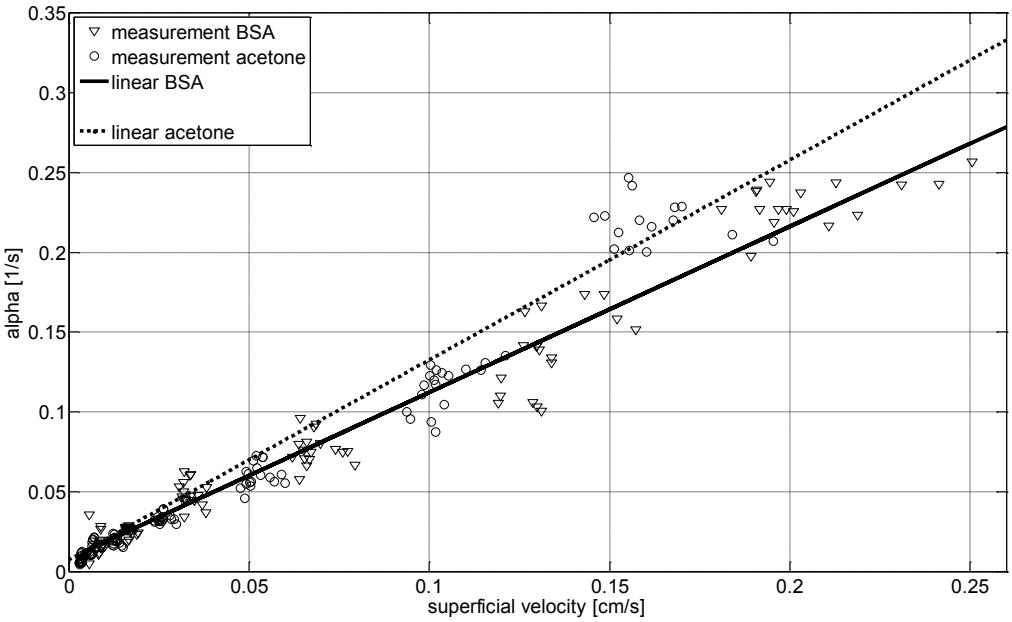

Fig. 4.9 First order exchange coefficient versus superficial velocity estimated by fitting dispersion curves with the dual porosity model as a function of the superficial velocity. Dispersion measurements have been performed membrane containing pucks (diameter 25 mm, 30 layers, Q-Sartobind®). Tracers were acetone 30 mM sodium acetate buffer (IS 50 mM, pH 5.2) and BSA (10 g/L) in 200 mM sodium acetate buffer (IS 82 mM, pH 4.5).

Another possibility is to consider the solute exchange between both regions to take place through a boundary layer, which thickness would decrease with the superficial velocity. In this case, the corresponding exchange coefficient may be written similarly to the above equation by substituting *dx* by the thickness of the boundary layer. According to the literature (Gebauer, 1996), the diffusion coefficients of BSA is approximately 50 times lower than diffusion coefficient of acetone. In this case, the magnitude of differences between the exchange coefficients estimated with BSA and acetone should have been much higher than 20 %. According to these observations, solute transport between the two regions was probably caused by multiple mechanisms (diffusive, dispersive and convective), where convective transport may have the major contribution.

4.4.3 Dispersion of adsorptive tracer

Benzoic acid has been used as an adsorbing tracer and measurement conditions have been taken from the investigations performed in chapter 2. In this case, CDE and dual porosity models were implemented as a three parameter model (v, D, R) and as a five parameter model (v, D, α, β, R), respectively. It has been shown in the previous chapter that, in the range of tracer concentrations used in this work, the adsorption of benzoic acid on Q-Sartobind® membranes was following a linear adsorption isotherm. This allowed the use of the above mentioned one-dimensional analytical solutions, where adsorption was modeled via a retardation factor R.

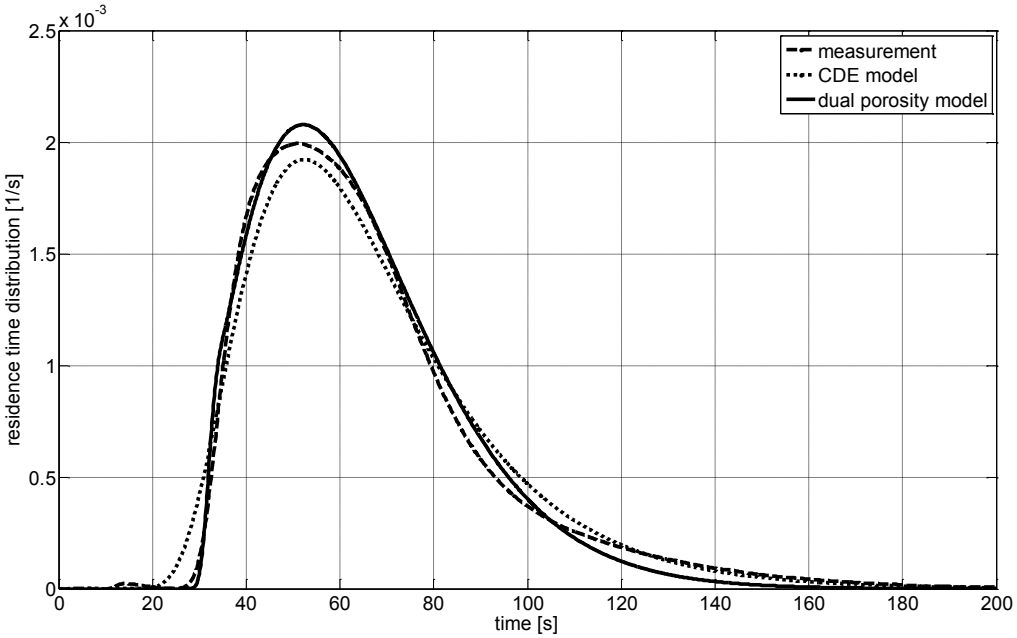

Fig. 4.10 Residence time distribution measured with a membrane containing puck (diameter 25 mm, 30 layers, Q-Sartobind®). Tracer was benzoic acid (3.2 g/L) in 200 mM sodium acetate buffer (IS 82 mM, pH 4.5), flow rate: 16 mL/min. Continuous line shows the fitting obtained with the dual porosity model and dotted line shows the fitting obtained with the CDE (convection-Dispersion Equation). Extra membrane sources have been eliminated during the fitting procedure.

In contrast to the results obtained with non adsorptive tracers, less accurate but still satisfying fitting accuracies (residuals lower than 10^{-4}) have been achieved (Fig. 4.10). Fittings accuracies given by both models had the same order of magnitude with exception of very low flow rates, where a maximum relative accuracy has been found (1 mL/min) for the dual porosity model (Fig. 4.11). Non Gaussian anomalies could not be clearly observed even at flow rates corresponding to the above mentioned maximum relative accuracy. As already mentioned in Chapter 2, under binding conditions, the adsorption equilibrium appeared to have the major contribution to the total dispersion.

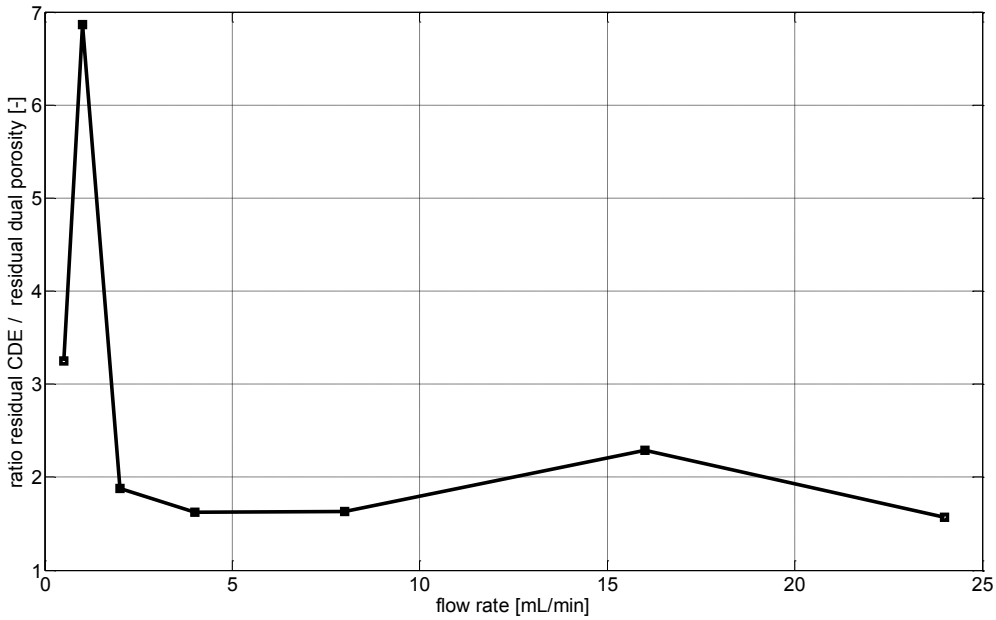

Fig. 4.11 Ratio between residuals achieved by fitting residence time distributions with CDE and dual porosity models as functions of the flow rate. This ratio was used to describe the relative accuracy of the dual porosity model compared to the CDE model. Dispersion measurements have been performed with membrane containing pucks (diameter 25 mm, 30 layers, Q-Sartobind®). Tracer was benzoic acid (3.2 g/L) in 200 mM sodium acetate buffer (IS 82 mM, pH 4.5).

Similarly to the investigation under non-binding conditions, no significant variations of dispersion coefficient with the superficial velocity were observed analyzing fits performed according to the dual porosity model. An average value of $1.9 \cdot 10^{-9}$ m²/s has been determined, which is also very close to the diffusion coefficient of benzoic acid ($9.4 \cdot 10^{-9}$, Deng et al., 2005). A linear increase of the dispersion coefficient with the superficial velocity was observed for fittings performed with the CDE model (Fig. 4.12) and estimated values were approximately 500-1000 times higher than the corresponding diffusion coefficient.

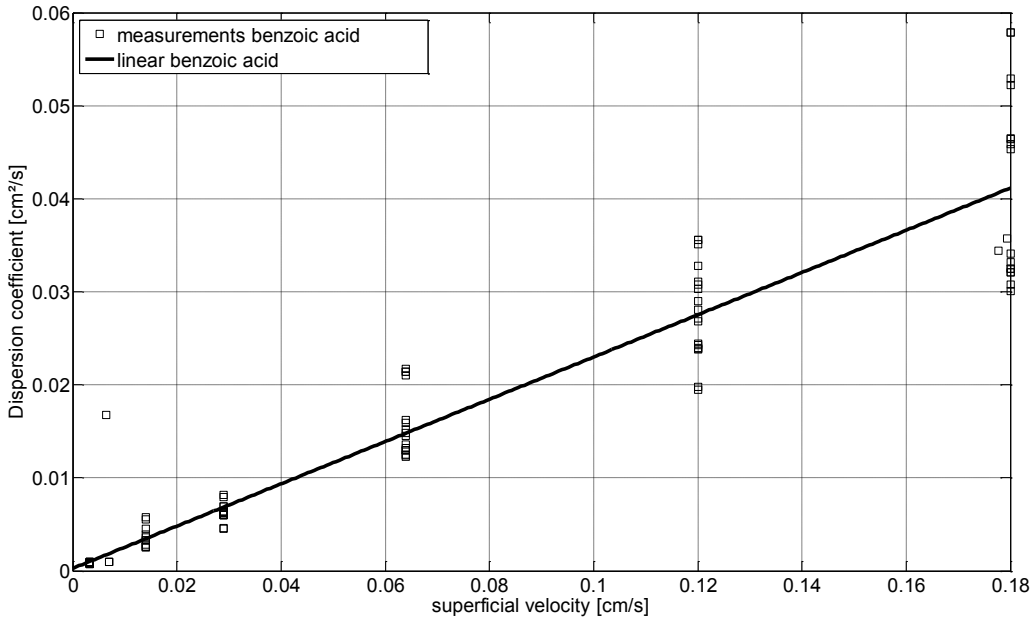

Fig. 4.12 Dispersion coefficients estimated by fitting dispersion curves with the CDE model as a function of the superficial velocity. Dispersion measurements have been performed in membrane-containing-pucks (diameter 25 mm, 30 layers, Q-Sartobind®). Tracer was benzoic acid (3.2 g/L) in 200 mM sodium acetate buffer (IS 82 mM, pH 4.5).

Distribution coefficient for linear adsorption distribution K_d have been calculated from the corresponding estimated retardation factors. They did not vary with the superficial velocity and both models gave similar average values (5.9 m³/kg for the CDE model and 6.0 m³/kg for the dual porosity model). A linear increase of exchange coefficients with the superficial velocity has been also observed (Fig. 4.13) and estimated values were approximately three times higher than the ones estimated by injecting non adsorptive tracers. Due to the superposition of two continua in a porous medium, the dual porosity model also allows considering the heterogeneous distribution of the adsorption sites inside of Q-Sartobind® membranes and only 38% of the adsorption sites were found in the mobile region.

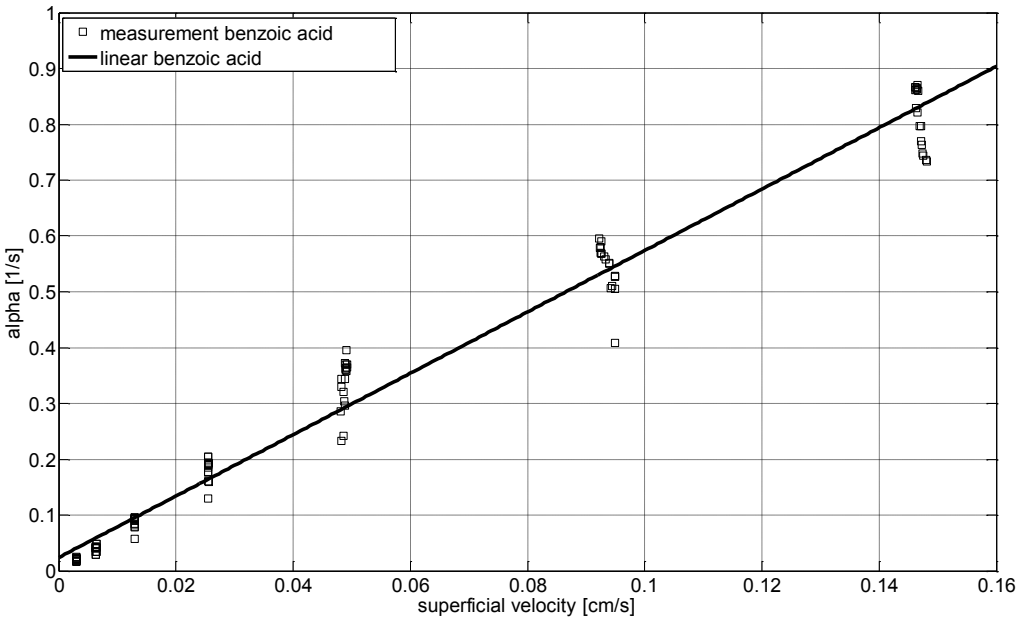

Fig. 4.13 First order exchange coefficient versus superficial velocity estimated by fitting dispersion curves with the dual porosity model. Dispersion measurements have been performed with membrane containing pucks (diameter 25 mm, 30 layers, Q-Sartobind®). Tracer was benzoic acid (3.2 g/L) in 200 mM sodium acetate buffer (IS 82 mM, pH 4.5).

4.5 Conclusions

CDE and dual porosity model give quite different representations of the transport phenomena occurring in Q-Sartobind® membranes. According to the parameters estimated using the CDE model, the membrane might be considered as a porous medium consisting of pores with similar diameter scales in which all dispersion sources may be merged in a single dispersion coefficient. The latter results from the combination of a large number of uncorrelated steps which can be:

- Velocity variations in pores due to shear flow dispersion
- Multi-channeling
- Tortuosity differences
- Adsorption equilibrium

The magnitude of the above mentioned dispersion coefficient increases with the superficial velocity and is much higher than the corresponding diffusion coefficient.

In contrast to the CDE model, flow non equilibrium is taken into account by the dual porosity model and convective solute exchange from the mobile region into the immobile region was found. Consequently, the representation of the Q-Sartobind® membrane as a porous medium consisting of a mobile and an immobile region has to be corrected. Representing such a membrane by two coexisting mobile regions characterized by two different classes of pore diameter scale and two different flow regimes seems to be more consistent with the estimations given by the dual porosity model. Such a bimodal distribution of pore diameter has been observed for Q-Sartobind® membranes using imaging methods in chapter 3. According to this model, flow predominantly takes place in the high pore diameter scale region which corresponds to approximately 60% of the total porosity. Solute dispersion in this region appears to be mostly caused by molecular diffusion. The low pore diameter scale region corresponds to approximately 40% of the total porosity and flow magnitude there is low compared to the high pore diameter scale region. Despite of the higher proportion of porosity occupied by the high pore diameter scale region, only 38% of the adsorption sites were found in this region. This distribution of adsorption sites between both regions might be related to a higher specific surface area in the low pore diameter scale region.

CDE and dual porosity models both enabled the satisfying fitting of measured dispersion curves using adsorptive as well as non-adsorptive tracers. Allowing the superficial velocity to be a fitting parameter was, on the one hand, necessary for the achievement of accurate fittings. On the other hand, this made the models very flexible and higher superficial velocities were estimated when injecting the high molecular weight tracer BSA. This inconsistency between both tracers may be caused by a size exclusion effect. It is indeed conceivable that BSA, due to its higher hydrodynamic diameter, may not access fine porous zones of Q-Sartobind®membranes. Such zones have been clearly identified and discussed in chapter 3. Furthermore, the CDE model systematically gave slightly higher superficial velocities than the dual porosity model. It is consequently not yet possible to know which model describes the reality best, and both models should be considered for the implementation of tracer transport in the CFD model. This implementation was the object of the next and last chapter of this thesis.

4.6 References

Abramowitz M, Stegun IA, Handbook of Mathematical Functions (Dover Publishing Co., New york)

Bear J. 1972. Dynamics of Fluids in Porous Media (Elsevier, New York)

Carnahan B, Luther HA, Wilkes JO. 1969. Applied Numerical Methods (John Wiley & Sons, Inc, New York)

Charlaix E, Hulin JP, Plona TJ. 1987. Experimental study of tracer dispersion in sintered glass porous materials of variable compaction. Phys. Fluids 30 (6) 1690-1698

Coats KH, Smith BD. 1964. Dead-end pore volume and dispersion in porous media. SPE J. 4: 73–84.

Deng Y, Fan Y. 2005. The Effects of Recirculation Flows on Mass transfer from the arterial Wall to Flowing blood. From Proceeding (485) Biomechanics

D'Onofrio A, Freytes VM, Rosen M, Allain C, Hulin JP. 2002. Echo tracer dispersion in flows of polymer solutions through porous media : A tool for detecting weak permeability heterogeities ?. Eur. Phys. J. E 7 : 251-259

Gebauer KH. 1996. Stofftransport und Kinetik in der Protein-Chromatographie am Beispiel neuer Membran-Adsorbentien. Fortschritt-Bericht-VDI Nr. 147, Reihe 17

Neville CJ, Ibaraki M, Sudicky E. 2000. Solute transport with multiprocess nonequilibrium: a semi-analytical approach. Journal of Contaminant Hydrology 44: 141:159

Paterson A, d'Onofrio A, Allain C, Hulin JP, Rosen M, Gauthier C. 1996. Tracer Dispersion in a Polymer Solution Flowing Through a Double Porosity Medium. J. Phys. II France 6: 1639-1654

Raymond ST, Breedveld V. 2005. Microrheological detection of protein unfolding. Phys. Rev. E 72.041914

Taylor SG. 1953. Dispersion of soluble matter in solvent flowing slowly through a tube. Proc. Roy. Soc. A 216: 186:203

Taylor SG. 1954. Conditions under which dispersion of a solute in a stream of solvent can be used to measure molecular diffusion. Proc. Roy. Soc. A 217: 473:477

Toride N, Leij FJ, van Genuchten MT. 1999. The CXTFIT Code for Estimating Transport Parameters from Laboratory or Field Tracer Experiments Version 2.1. Research Report No. 137. U.S. Salinity Laboratory Agricultural Research Service, U.S. Department of Agriculture. Riverside, California

van Genuchten MT, Wagenet RJ. 1989. Two-site/two-region models for pesticide transport and degradation: Theoretical development and analytical solutions. Soil Sci. Soc. Am. J., 53(5): 1303-1310

5 Fluid dynamics in Q-Sartobind® Membrane Adsorber Systems using CFD

5.1 Objectives

This last chapter demonstrates how flow fields, pressure fields and RTD's of adsorptive and non-adsorptive tracers in a Q-Sartobind® Membrane Adsorber System might be predicted using CFD. It also shows how these predictions may be used to detect eventual flow heterogeneities and estimate the quality of the flow distribution in such devices.

Transport models for passive scalars in porous media are not implemented in most commercial and open source CFD codes. It was therefore necessary to use an open source CFD code (Code_Saturne) and to modify the implementation of transport of passive scalars in its source code. Thanks to the chosen macroscopic numerical approach for the mathematical formulation of tracer transport in Q-Sartobind® membranes, CDE and dual porosity models have been easily implemented in the core of Code_Saturne. In the frame of these implementations, dispersion and adsorption parameters as well as their velocity dependence acquired in chapter 4 were used as input parameters.

Predicted RTD's obtained for non-adsorptive tracers have been compared with the experimental results presented in chapter 2 in order to evaluate the accuracy of the performed CFD simulations. The additional aim of these comparisons was to find out which transport model (CDE or dual porosity) is more appropriate for a certain type of tracer.

5.2 Theoretical Background

5.2.1 Computational Fluid Dynamics (CFD)

Computational Fluid Dynamics enables to solve fluid flow problems by solving the corresponding governing equations on one or more processors. Due to considerable developments in the last two decades, modern CFD codes are now able to solve a wide range of problems from simple laminar flows to very complicated multi-phase flows, including heat exchange and/or chemical reaction. CFD simulations are continuously gaining in accuracy which leads to the progressive establishment of CFD as an engineering tool.

The Continuity and Navier-Stokes equations are coupled partial differential equations and constitute the governing equations of fluid dynamics. Analytical solutions can only be formulated for simple problems, which are not of much practical interest. The numerical methods used for CFD require a partition of the computational domain into a finite number of subdomains, also called computation cells. This set of cells is called a mesh and the corresponding process is called meshing. A certain variation of the dependent variables over each cell has to be assumed. This, together with the boundary conditions lead to a system of N algebraic equations with N unknowns for each dependent variable, N representing the number of cells.

The Finite Volume Method (FVM) is the more common discretisation practice used in the CFD community. In this case, the discretisation is performed using the integral formulation of the conservation laws which are then discretised on the computational domain. Linear variation of the dependent variables between the cells is assumed. The Finite Volume Method allows the use of different types of mesh, where cells can be of arbitrary topology consisting of general polyhedral volumes. The FVM practice is conservative and the quantities like momentum, mass, energy remain conserved during the calculation process (Juretic, 2004). A detailed description of CFD methods and algorithms would exceed the scope of this thesis. Versteeg and Malalasekera (2007) gave a very good introduction to the Finite Volume Method. Advanced CFD methods and algorithms may be found in Ferziger and Peric (2002).

5.2.2 Code_Saturne®

Code_Saturne® is EDF's general purpose computational fluid dynamics software and consists of approx. 500 000 lines in Fortran, C and Python. Developed since 1997 at EDF R&D, it is based on a co-located Finite Volume approach. It is therefore possible to use meshes with any different cell types (tetrahedral, hexahedral, prismatic, pyramidal, polyhedral...) and any type of grid (unstructured, block structured, hybrid, conforming or with hanging nodes...).

Its basic capabilities enable the simulation of either incompressible or expandable flows with or without heat transfer and turbulence (mixing length, 2-equation models, v2f, Reynolds stress models, Large Eddy Simulations...). Dedicated modules are available for specific physics such as radiative heat transfer, combustion (gas, coal, heavy fuel oil), magneto-hydro

dynamics, compressible flows, two-phase flows. Parallel code coupling can be performed using the FVM library (EDF's "Finite Volume Mesh" library, under LPGL licence).

EDF makes Code_Saturne available as an open source software under the General Public Licence GPL since march 2007. It is portable on Linux PCs and UNIX platforms (no Windows versions are available).

5.3 Case setup and model implementation

5.3.1 Geometry and meshing

The 3D-geometry (Fig. 5.1) of the Sartobind® Membrane Adsorber System (bed height 3cm, bed thickness 4 mm) has been built from 2D technical drawing using the open source CAD software Salome-Meca® 2008 (provided by EDF, France, Paris). For meshing purposes, the software PATRAN® (MSC Software, USA) has been used and the geometry has been divided in the three following parts:

- Inlet distributor
- Central core
- Outlet distributor

Inlet and outlet distributors have been meshed with tetrahedral cells. Because of the high pressure gradients occurring in cells corresponding to the porous medium, it was necessary to mesh the central core with hexahedral cells. The three parts have been connected by the pre-processor of Code_Saturne® 1.3.2 (ecs) via arbitrary interfaces. The final mesh may be seen on Fig. 5.6. The open source visualization software PARAVIEW® (Kitware, USA, New York) has been used for post-processing. This software enables the visualization of tetrahedral and hexahedral cells. During the creation of arbitrary interfaces, complex polyhedral cells occurred which have been properly used by Code_Saturne® 1.3.2 for the computation. These cells could not be post-processed by PARAVIEW® and it was therefore necessary to disable the output of such cells for post-processing purposes inside of the Code_Saturne® 1.3.2 core (usini1.F).

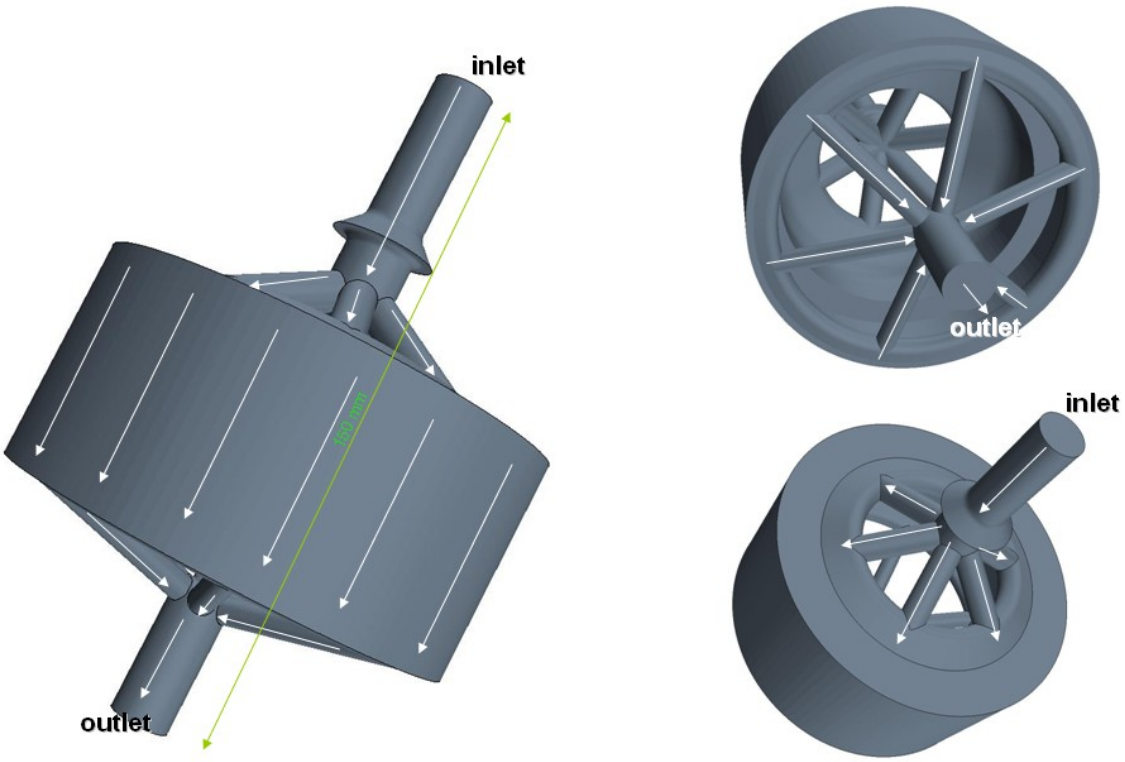

Fig. 5.1 3D geometry of a Sartobind® Membrane Adsorber System (bed height 3cm, bed thickness 4 mm). The geometry has been built with the open source software Salome-Meca® 2008 (provided by EDF, France, Paris).

5.3.2 Calculation of flow field and pressure field

The 3D-geometry exhibits internal symmetry and the full geometry were not necessary for the computation. The calculation has been therefore performed on one sixth of the total geometry (Fig. 5.2) using 4 processors (2 x intel xeon dual core (2x3.2 GHz)). Lateral sides have been defined as symmetry boundary faces (symmetry condition). Zero flux condition for pressure and Dirichlet conditions for all other variables have been implemented at the inlet. Because injection of tracers always occurred under stationary flow conditions with fully developed flow, a parabolic velocity profile has been implemented at the inlet (flow rate was 0.68 L/min). Dirichlet condition for pressure and zero flux conditions for all other variables have been implemented at the outlet. Remaining boundary faces have defined as no slipping walls (wall law).

The flow resistance of the porous medium has been implemented as a head loss in form of a diagonal resistance tensor using the subroutine uskpdc.F. The k-ω model has been used for turbulence computation.

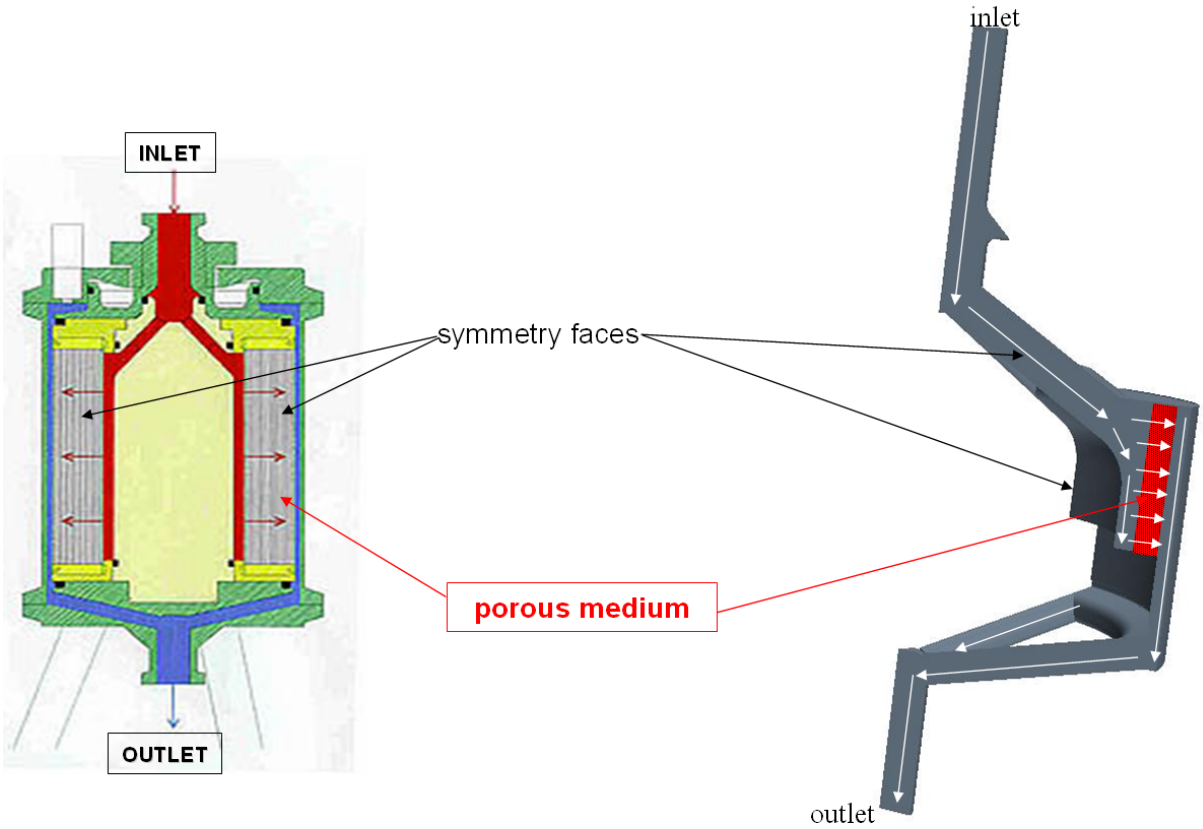

Fig. 5.2 Descriptive drawing of the geometry used for CFD computations. One sixth of the geometry has been used and lateral sides have defined as symmetry boundary faces.

5.3.3 Calculation of residence time distributions

Pressure fields and flow fields have been frozen during the computation of concentration fields. This reduced the number of variables to solve and only tracer concentrations were calculated. A Dirac pulse of tracer has been implemented at the inlet and the transient calculations have been performed with a time step of 0.01s using 4 processors (2 x intel xeon dual core (2x3.2 GHz)). Average tracer concentrations at the outlet have been calculated at the end of every time step (in the user subroutine usproj.F) and written in a corresponding file so that the resulting residence time distributions could have been plotted.

5.3.4 Implementation of the CDE model

The 3D-Convection-Dispersion equation may be written as follows:

$$\Theta \cdot \frac{\partial c}{\partial t} = \nabla\left(\Theta \cdot D_{Disp} \cdot \nabla c\right) - v \cdot \nabla c$$

The effect of the porosity (0.72) on the transient term for tracer concentrations has been implemented by modifying the source subroutine covofi.F.

Dispersion has not been implemented as a tensor but as a velocity dependent scalar dispersion coefficient (in the user subroutine usphyv.F). Consequently, it has been assumed that the three diagonal elements of the dispersion tensor had the same magnitude. A linear dependency of the dispersion coefficient on the flow velocity has been implemented according to the measurements described in chapter 4. The effect of the porosity on the dispersion coefficient has been taken into account during this implementation. Outside of the porous medium, transport of tracer concentration has been implemented via Convection-Diffusion using the diffusion coefficient of the corresponding tracers.

The variable v in the above mentioned equation corresponds to the superficial velocity. In this study, the effect of the porosity on the convective term has not been taken into account and linear velocities have been used. This did not affect the mass balance of tracer because mass fluxes remained the same when using total surface areas of cell faces.

Considering tracer adsorption, the CDE may be rewritten as follows:

$$\left(\Theta + \rho_b \cdot K_d\right) \cdot \frac{\partial c}{\partial t} = \nabla\left(\Theta \cdot D_{Disp} \cdot \nabla c\right) - v \cdot \nabla c$$

For the computation of tracer concentrations under adsorptive conditions, a new formulation of the transient term has been performed in the source subroutine covofi.F using the adsorption parameters determined in chapter 4.

5.3.5 Implementation of the dual porosity model

Outside of the porous medium, transport of tracer concentration has been implemented via Convection-Diffusion using the diffusion coefficients of the corresponding tracers. The key concept of the implementation of the dual porosity model was to define tracer concentrations in the different regions as two distinct user scalars c_m (concentration in the mobile region) and c_{im} (concentration in the immobile region). 3D-mass balance in dual porosity systems is described by the following system of partial differential equations:

$$\begin{cases} \Theta_m \cdot \dfrac{\partial c_m}{\partial t} = \nabla(\Theta_m \cdot D_{Disp,m} \cdot \nabla c_m) - v \cdot \nabla c_m - \alpha \cdot (c_m - c_{im}) \\ \Theta_{im} \cdot \dfrac{\partial c_{im}}{\partial t} = \alpha \cdot (c_m - c_{im}) \end{cases}$$

The upper part of this system formulates the mass balance of tracer in the mobile region and the corresponding concentration is subject to dispersion, convection and exchange with the immobile region. Transient, dispersive and convective terms have been implemented similarly to the above described method for the CDE model. Considering an integration over a finite volume, the exchange with the immobile region has been implemented as an explicit $S_{m,t}$ source term via the user subroutine ustssc.F as follows:

$$S_{m,t} = \alpha \cdot \left(c_{m,t-1} - c_{im,t-1}\right) \cdot \beta \cdot \theta \cdot V_{Cell}$$

Tracer concentrations of mobile and immobile regions have been initialized to zero. V_{cell} is the volume of the considered cell and α has been implemented as a velocity dependent first order exchange coefficient using the linear dependency determined in chapter 4.

The lower part of the above system of partial differential equations describes the mass balance of tracer in the immobile region. The concentration in this region is a particular user scalar which is neither diffused nor convected. In order to consider these features the corresponding variables IDIFF and ICONV have been set to zero for this user scalar in the source subroutine iniini.F. The value of c_{im} has been calculated at the end of every time step by integrating the corresponding differential equation via an explicit Euler method in the user subroutine usproj.F.

Considering tracer adsorption, the 3D-mass balance has to be reformulated in the following way:

$$\begin{cases} \left(\Theta_m + f\rho_b K_d\right) \cdot \dfrac{\partial c_m}{\partial t} = \nabla(\Theta_m \cdot D_{Disp,m} \cdot \nabla c_m) - v \cdot \nabla c_m - \alpha \cdot (c_m - c_{im}) \\ \left[\Theta_{im} + \left(1 - f\right)\rho_b K_d\right] \cdot \dfrac{\partial c_{im}}{\partial t} = \alpha \cdot (c_m - c_{im}) \end{cases}$$

For this purpose, a new implementation of the transient term (in the source subroutine covofi.F) has been performed using the adsorption parameters determined in chapter 4. The integral for the calculation of c_{im} under adsorptive conditions has been reformulated (in the user subroutine usproj.F) and also solved via an explicit Euler method.

5.4 Results and discussion

5.4.1 Comparison between model predictions and measurements

In order to estimate the accuracy of the predictions given by the different CFD simulations and to know which transport model (CDE or dual porosity) is more appropriate for a certain type of tracer, predicted and measured RTD's were compared. During the measurements (presented in Chapter 2), tracer concentrations were measured at the inlet (input signal) as well as at the outlet (output signal) of the investigated Membrane Adsorber System. RTD's obtained from CFD simulations resulted from a Dirac pulse and had to be convoluted with the above mentioned input signals in order to be comparable with the measured RTD's. This convolution has been performed using MATLAB.

Fig. 5.3 and Fig. 5.4 show the comparison between measured (from Chapter 2) and predicted RTD's (after convolution using measured input signals) for a low molecular weight tracer (acetone, Fig. 5.3) and a high molecular weight tracer (BSA, Fig. 5.4). The ranges of residence times obtained from measurements and calculations appear to be defined by very similar extreme values.

However, CFD predictions using CDE and dual porosity models also considerably differ from each other. In case of a low molecular weight compound, the prediction of the CFD simulation using the CDE model fails to describe the occurring early breakthrough. Using the dual porosity model enables the prediction of this early breakthrough and the calculated RTD is in good agreement with the measurement.

In case of a high molecular weight tracer, the opposite situation is observed and a very accurate prediction of the corresponding RTD is obtained by the CFD simulation using the CDE model. The prediction obtained using the dual porosity model does not fit with the measurement and fails to describe the "Gaussian" behaviour of the measured RTD.

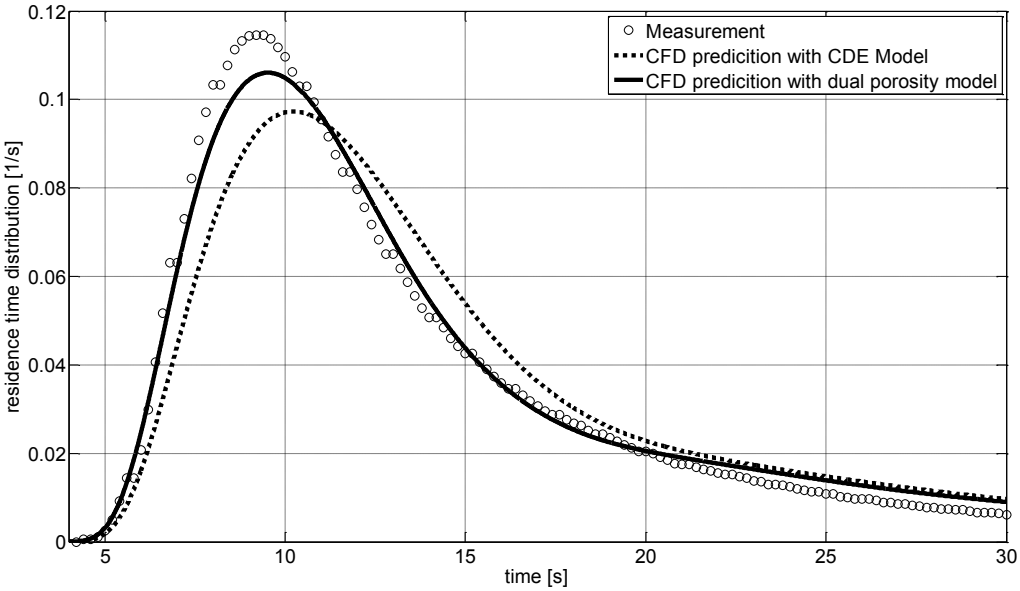

Fig. 5.3 Comparison between measured and predicted residence time distributions of acetone in a Q-Sartobind® Membrane Adsorber System (bed height 3cm, bed thickness 4 mm). Predicted curves were obtained via CFD calculations using Code_Saturne (EDF, France, Paris). Buffer was 30 mM sodium acetate (IS 50 mM, pH 5.2) and flow rate was set to 0.68 L/min.

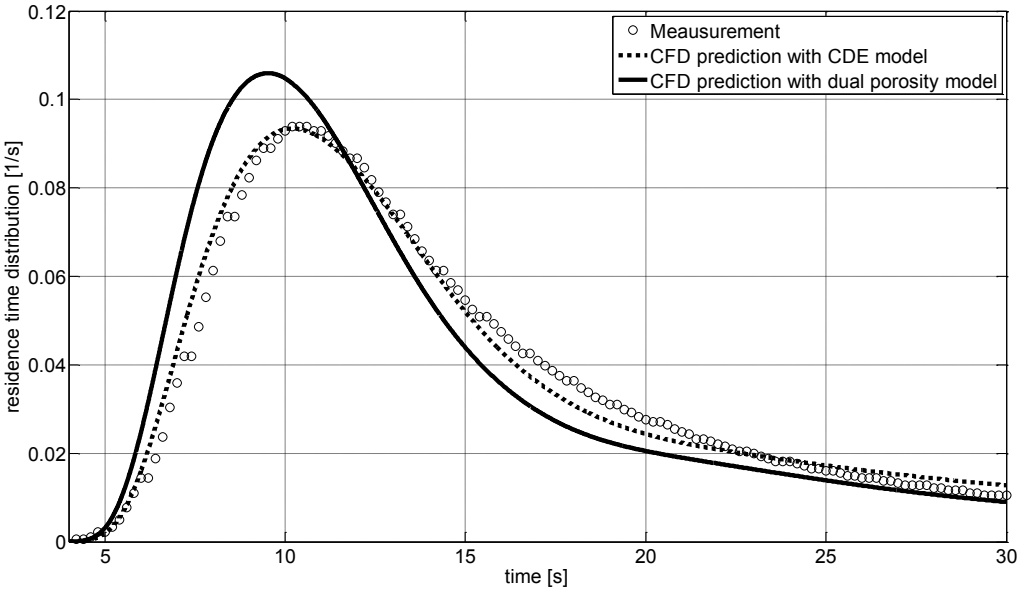

Fig. 5.4 Comparison between measured and predicted residence time distributions of bovine serum albumin (BSA) under non adsorptive conditions in a Q-Sartobind® Membrane Adsorber System (bed height 3cm, bed thickness 4 mm). Predicted curves were obtained via CFD calculations using Code_Saturne (EDF, France, Paris). Buffer was 200 mM sodium acetate (IS 82 mM, pH 4.5) and flow rate was set to 0.68 L/min.

The RTD's resulting from CFD predictions for an adsorptive tracer (benzoic acid) are shown on Fig. 5.5. CFD simulations seem to successfully describe the qualitative retardation of adsorptive tracers. Lower peak maxima can be observed and result from the contribution of the adsorption equilibrium to the total dispersion. The simulation using CDE and dual porosity models give very different predictions where RTD's predicted by the dual porosity model are much narrower than RTD's predicted by the CDE model. A comparison between measurements and calculated RTD's for benzoic acid could not be performed because the RTD's of benzoic acid have been measured at a different flow rate than the one implemented in the presented CFD simulations.

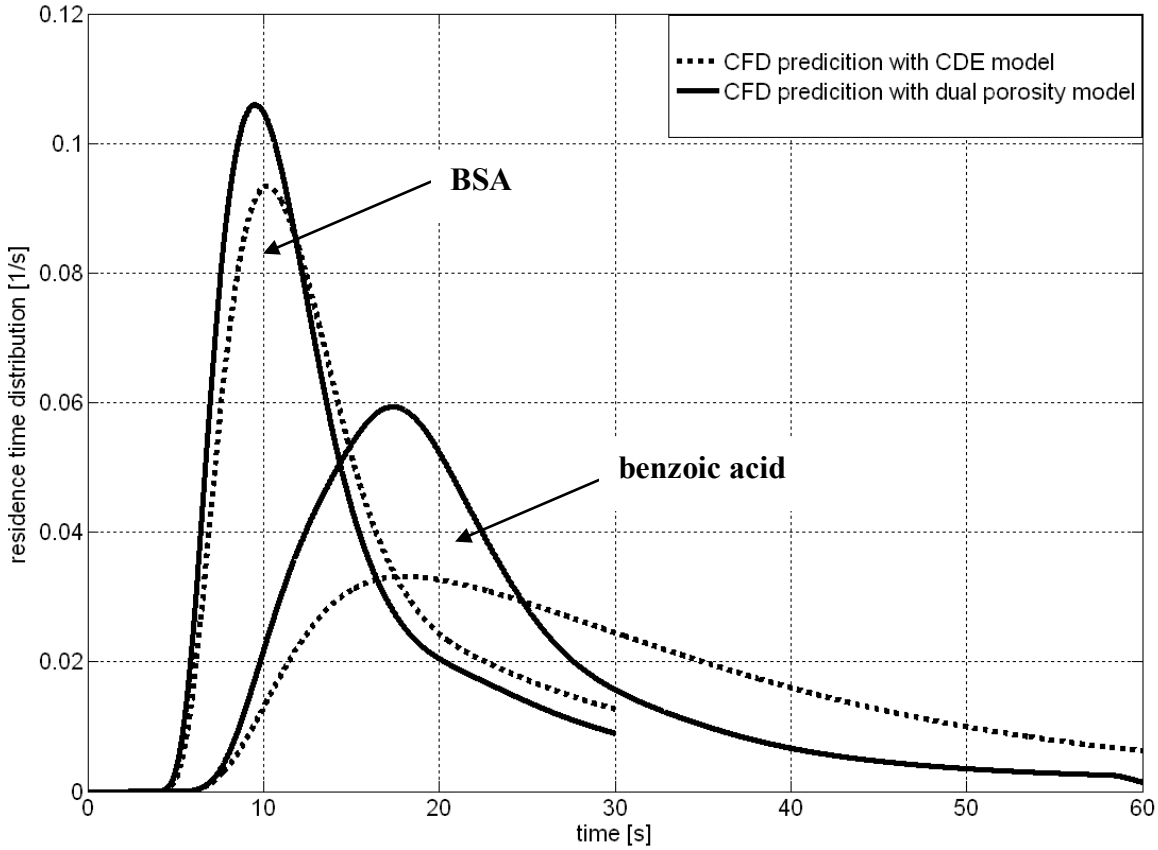

Fig. 5.5 Comparison between predicted residence time distributions of bovine serum albumin (BSA) under non adsorptive conditions and benzoic acid under adsorptive conditions in a Q-Sartobind® Membrane Adsorber System (bed height 3cm, bed thickness 4 mm) using CDE and dual porosity models. Predicted curves were obtained via CFD calculations using Code_Saturne (EDF, France, Paris). Flow rate was set to 0.68 L/min.

5.4.2 Pressure and flow fields

The really good agreements between measurements and CFD predictions for non-adsorptive tracers can be considered as a "validation" of the implemented CFD models (using CDE for BSA and dual porosity for acetone). This allows the analysis of the predicted pressure and flow fields inside of the investigated Q-Sartobind® Membrane Adsorber System (Fig. 5.6).

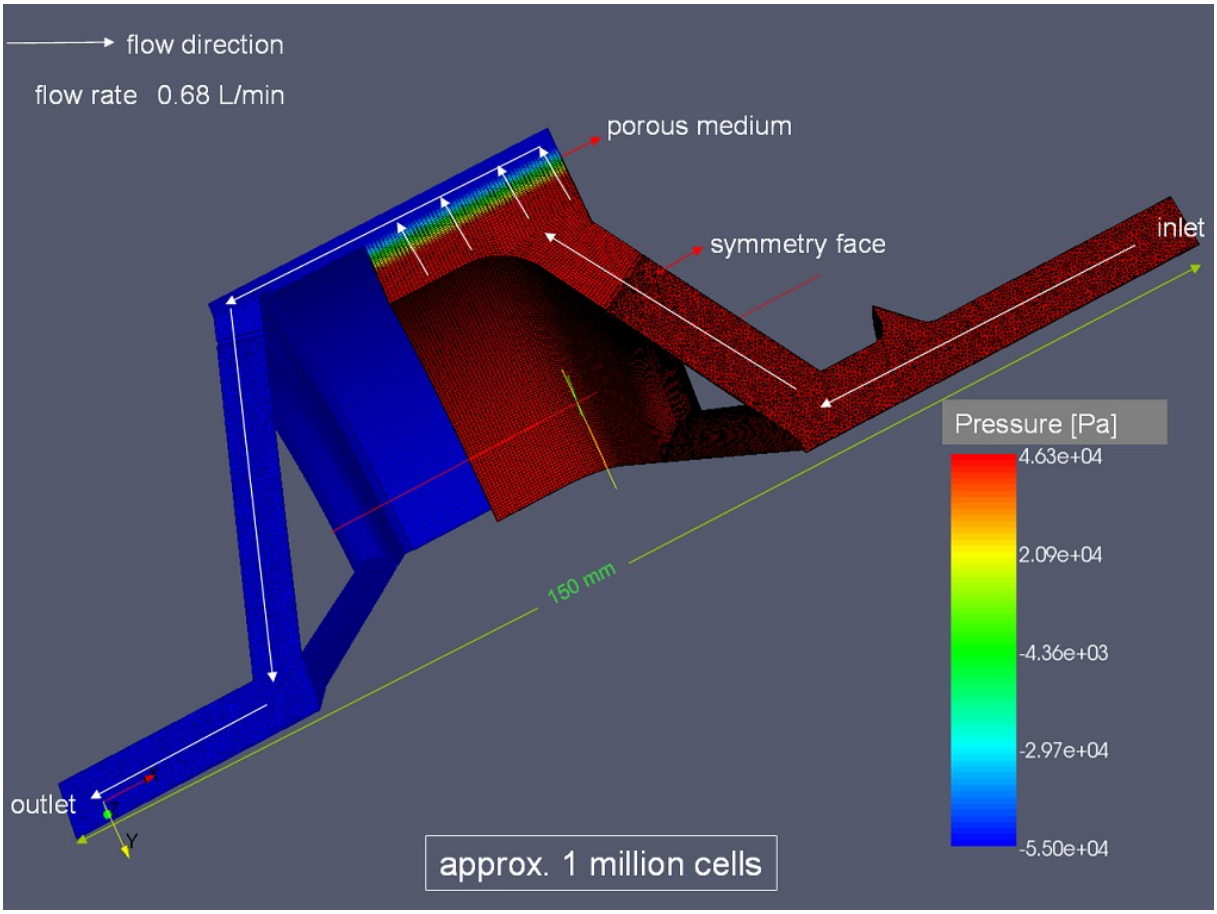

Fig. 5.6 Mesh and predicted pressure field inside of a Q-Sartobind® Membrane Adsorber System (bed height 3cm, bed thickness 4 mm). Flow rate was set to 0.68 L/min and CFD calculation has been performed with Code_Saturne (EDF, France, Paris).

It appears that the porous medium is mostly responsible for the total pressure drop through the device. This observation fits with the aim which has been followed by Nußbaumer during the conception of these Membrane Adsorber Systems. In his work, he calculated the width of internal and external channels in such a way that their pressure drops were negligible compared to the pressure drop of the porous medium. A pressure drop of 1.13 was predicted by the CFD model which is very close to the pressure drop of 1 bar set during measurements.

The predicted field of velocity magnitude may be observed on Fig. 5.7 and enables the detection of flow imperfections. The sharp flow deflections strongly affect the flow homogeneity which has to be conserved and controlled in such chromatographical devices. Furthermore an expected dead zone was observed in the inlet distributor which corresponds to a transition between the inlet plate and the tubing.

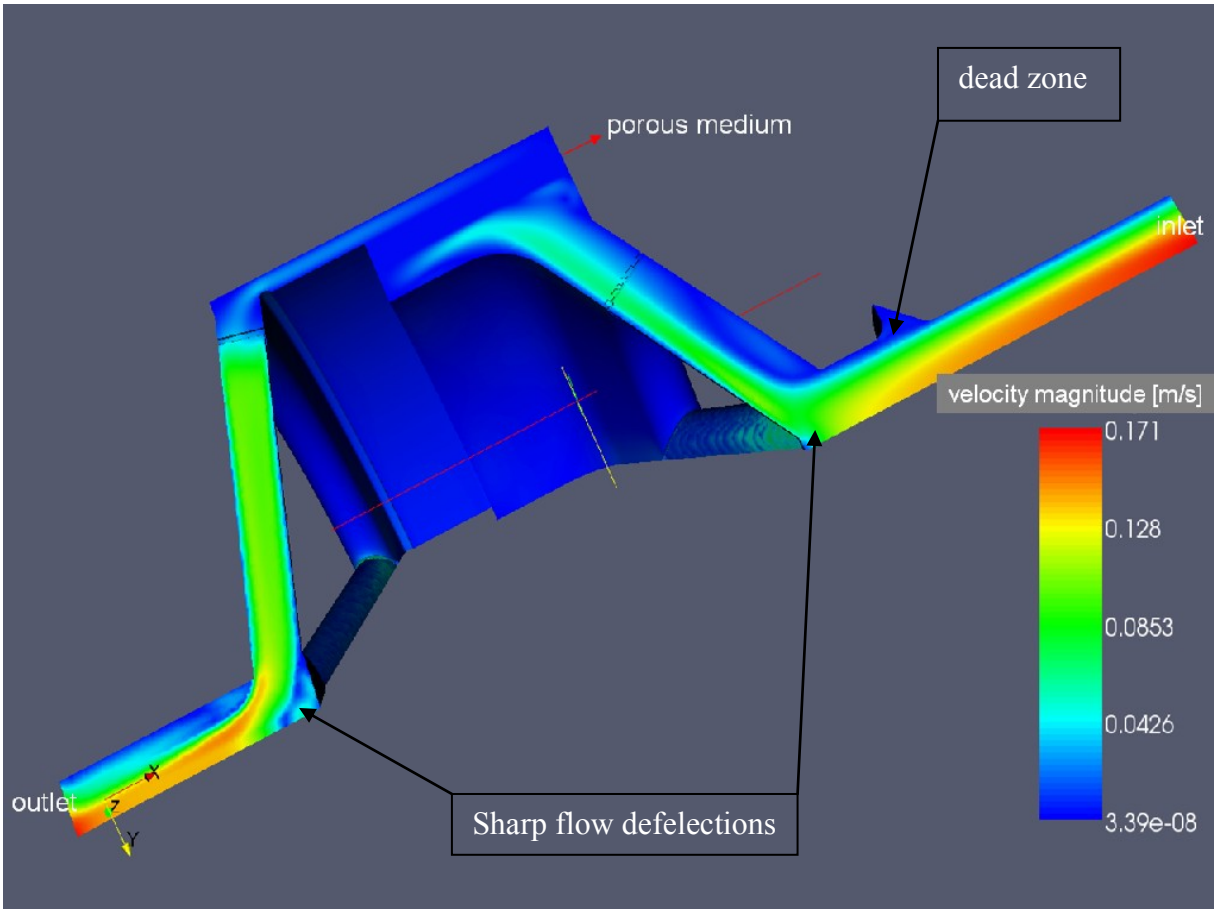

Fig. 5.7 Predicted field of velocity magnitude inside of a Q-Sartobind® Membrane Adsorber System (bed height 3cm, bed thickness 4 mm). Flow rate was set to 0.68 L/min and CFD calculation has been performed with Code_Saturne (EDF, France, Paris).

Due to a higher flow surface area, the velocity strongly decreases inside the porous medium and the flow in the internal channel does not appear to be homogeneously distributed over the height of the porous medium. Plotting the flow field in term of velocity vectors helps to estimate the quality of flow distribution in the internal channel (Fig. 5.8). A swirling in this channel creates mixing zone which existence has been suggested and discussed in chapter 2.

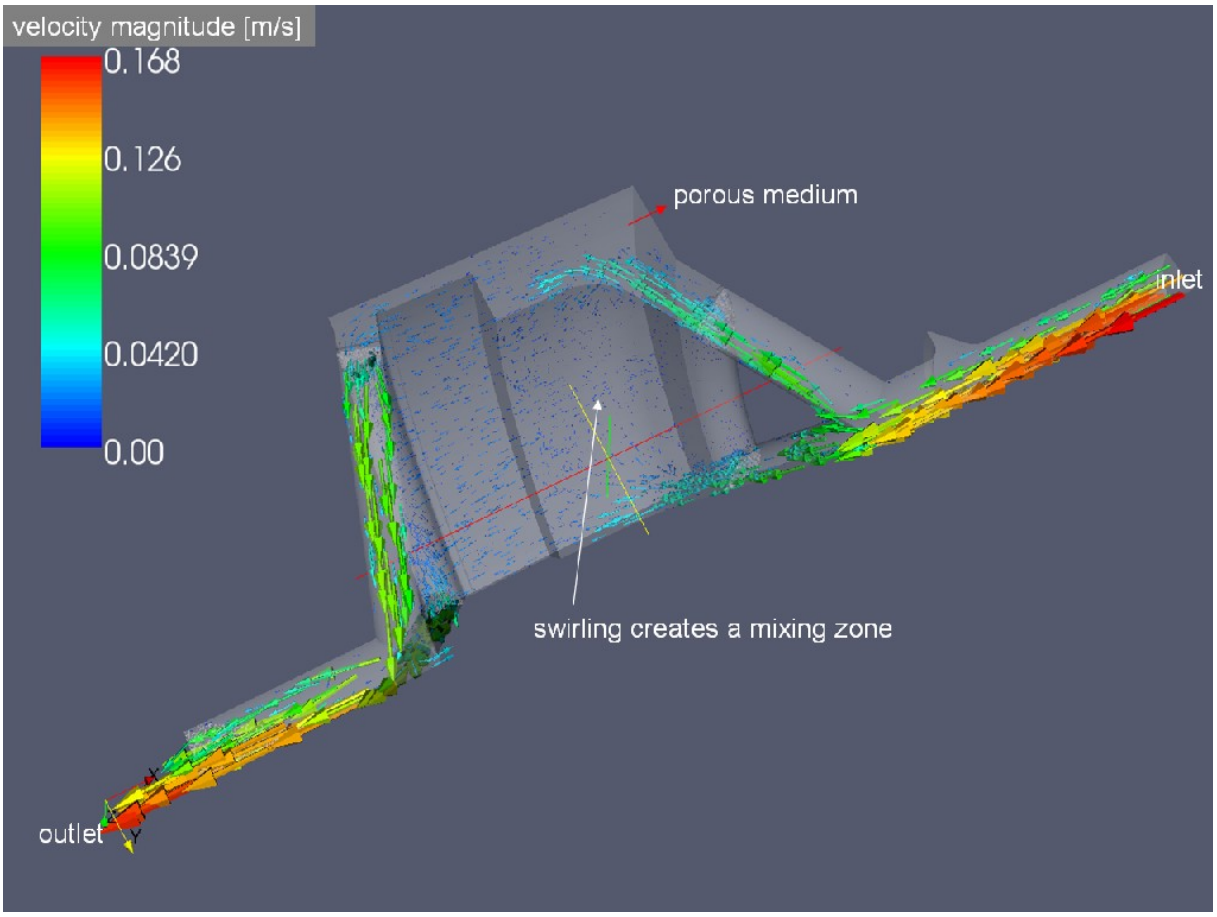

Fig. 5.8 Predicted flow field inside of a Q-Sartobind® Membrane Adsorber System (bed height 3cm, bed thickness 4 mm). Flow rate was set to 0.68 L/min and CFD calculation has been performed with Code_Saturne (EDF, France, Paris).

5.4.3 Concentration field

The visualisation tool PARAVIEW allows performing cuts of geometry. This can be very helpful for a more precise analysis of the tracer transport within the porous medium. Fig. 5.9 shows predicted fields of acetone concentration for different times (top: 1.2 s, bottom: 2.4s) in such cuts. Tracer molecules appear to be transported much earlier into the membrane parts close to the tubes of the inlet distributor. This heterogeneous distribution was expectable and can be related to the heterogeneous flow field observed on Fig. 5.8. Considering an adsorptive protein, this behaviour would lead to an early breakthrough, where membrane parts close to the distributor tubing would be saturated before parts which are at the middle between two tubes of the inlet distributor.

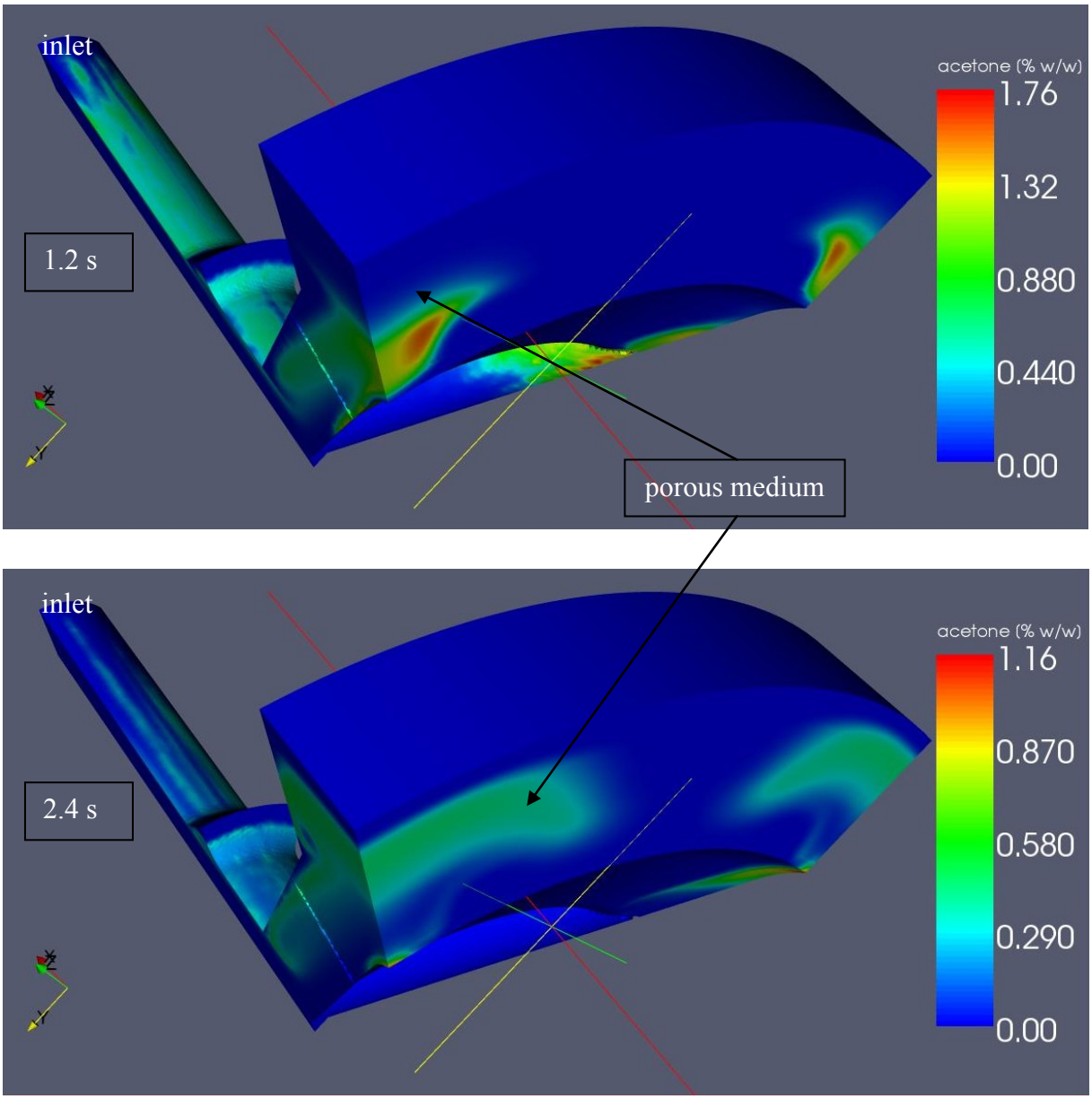

Fig. 5.9 Predicted fields of acetone concentration for different times (top 1.2 s, bottom 2.4s) inside of a Q-Sartobind® Membrane Adsorber System (bed height 3cm, bed thickness 4 mm). A Dirac pulse of acetone (5 % w/w) has been implemented at the inlet. Geometries correspond to cuts. Flow rate was set to 0.68 L/min and CFD calculation has been performed with Code_Saturne (EDF, France, Paris).

5.5 Conclusions

The use of a macroscopic numerical approach for the implementation of tracer transport in Q-Sartobind® membranes in a CFD code based on FVM enabled successful simulations that accurately predict residence time distributions of low and high molecular weight tracers. Additionally, this work has demonstrated that Code_Saturne is applicable for industrial cases.

The comparison between measured and predicted RTD's has shown, on the one hand, that the transport of low molecular weight tracers e.g. acetone or metabolites in Q- Sartobind® membranes might be modelled using the dual porosity model. On the other hand, high molecular weight tracers e.g. BSA or others proteins should be implemented according to the CDE model. Low molecular weight tracers seem to be small enough to significantly diffuse into the fine porosity and high molecular weight tracers seem to be excluded by the fine porosity. This observation is consistent with the higher superficial velocity estimated for BSA and the size exclusion effect suggested in the previous chapter.

Furthermore, CFD has been revealed to be a very helpful tool for the design of module housings and the estimation of the quality of flow distribution through the membrane. This estimation revealed the existence of flow imperfections due to sharp flow deflections and dead zones.

The experimental and numerical methods presented in this work constitute a very promising opportunity for the prediction of residence time distributions and breakthrough curves in Q-Sartobind® Membrane Adsorber Systems. Nevertheless, the robustness of this approach has to be further tested by comparing its results with measurements using different types of modules and different types of tracers.

5.6 References

Archambeau F, Méchitoua N, Sakiz M. 2004. Code_Saturne: a finite volume code for the computation of turbulent incompressible flows-industrial applications. Int. J. on Finite Volumes.

Barbe S, Kneer A, Wirtz M, Scheper T. 2008. Predicition of mass transport phenomena in Membrane Adsorber Systems (MAS) using a dual porosity model. Code_Saturne user conference 2008, 01.12-02.12.2008, R&D EDF Paris (France).

Barbe S, Kneer A, Wirtz M, Scheper T. 2009. Fluid dynamics in Membrane Adsorber Systems, DECHEMA Arbeitsausschuss für Membrantechnik. 15.01.2009, DECHEMA HAUS, Frankfurt am Main (Germany).

Ferziger JH, Peric M. 2002. Computational Methods for Fluid Dynamics (Springer-Verlag Berlin Heidelberg).

Ghosh R, Wong T. 2006. Effect of module design on the efficiency of membrane chromatographic separation processes. Journal of Membrane Science, Volume 281, issues 1-2, 532-540.

Juretic F. 2004. Error Analysis in Finite Volume CFD. PhD thesis. Imperial College, University of London.

Machado RL, Figueredo A, Carneiro DGP, Castiho LR, Nedronho RA. 2007. CFD-Aided Design of Hollow Fibre Modules for Integrated Mammalian Cell retention and Product Purification in Cell Technology for Cell Products (book) (Springer Netherlands)

Rhie CM, Chow WL. 1982. A Numerical Study of a Turbulent Flow past an Isolated Airfoil with Training Edge Separation. *AIAA paper*, 82-0998.

Rutherford A. 1989. Vectors, Tensors and the Basic Equations of Fluid Mechanics (Dover Publications, INC., New York).

Versteeg HK, Malalasekera W. 2007. An Introduction to Computational Fluid Dynamics, The Finite Volume Method (Pearson , Prentice Hall).

6 Summary and perspectives

The four steps presented in this thesis progressively lead to the successful development of a CFD model for the prediction of RTD's in Q-Sartobind® Membrane Adsorber Systems. Starting from the observation of measured RTD's, the detection of non-Gaussian anomalies suggested the existence of dead end pores within the membrane and highlighted the necessity of an investigation of the membrane structure using imaging methods.

This investigation enabled the formulation of a phenomenological approach explaining the non Gaussian shape of the measured RTD's. According to this approach, CDE and dual porosity models were proposed as conceivable candidates for the computation of solute transport in Q-Sartobind® Membranes. They are macroscopic transport models and therefore well implementable in a CFD Code. They both appeared to properly fit RTD's measured with stacked membrane sheets (Pucks). The corresponding fitting method was based on a convolution coupled optimization method, which simultaneously removed extra membrane dispersion effects and estimated the transport parameters by using the one-dimensional analytical solution of the investigated model.

Finally, the three-dimensional forms of these models have been implemented in the open source CFD code Code_Saturne. In this frame, the three-dimensional geometry of a 30 mm high Q-Sartobind® Membrane Adsorber System has been generated and meshed. The comparison between measured and predicted RTD's confirmed the prediction of pressure and flow fields as well as solute transport for low and molecular weight compounds.

The robustness of the presented model has to be further investigated especially for higher systems, where the heterogeneity of the membrane structure increasingly affects the behaviour of RTD's. It is therefore expectable that this additional dispersion effect has to be taken into account by e.g. implementing height dependant permeability. Due to the analogy between solute transport and heat transfer, this model may used for the prediction of heat transfer in porous media like metallic foams.

List of publications

Reports, Reprints und Abstracts of conferences/journals:

Barbe, S.; Wilhelm, P.; Müller, U.; „Nichtthermische Entkeimungseffekte bei der Sattdampfbehandlung von Oberflächen“, Summary. Proceedings GDL-Kongress Lebensmitteltechnologie 2001, Berlin, 8.-10.11.2001, GDL e.V., Bonn, (Germany) (ISDN 3-931678-04-0)

Müller, U.; Wilhelm, P.; Barbe St.; „ Schonende Sattdampfentkeimung von pflanzlichen Materialien mit dem Lemgoer Sattdampfentkeimungsverfahren“, Reprint GDL-Symposium „Aktuelle Aspekte der Technologie von Kräutern und Gewürzen II“, Gießen, 23.-25.09.2002, GDL e.V., Bonn (Germany)

Müller U. Wilhelm P., Lilie M., Barbe St.; „Mechanichal decontamination effects during a steam treatment of foods“, Reprint International Congress on Engineering and Food (ICEF), Montpelier (France), 8.-11.-03.2004

Wilhelm P., Lilie M., Barbe S., U. Müller; „ Mild steam decontamination of drugs and other plant material using mechanical effects“. Reprint “International Meeting on Pharmaceutics, Biopharmaceutics and Pharmaceutical Technology”, Nürnberg (Germany), 15.-17.03.2004

Danneel H.J., “Entwicklung eines Verfahrens zur Gewinnung der Aminosäure L-Methionin aus Pressrückständen der Paranussölproduktion“. Final report aFuE Fördervorhaben, 14.12.2005

Barbe S. “Design of membrane chromatography systems for large scale applications“, Reprint Network Young Membrains 2006 (NYM8), Institute of Membrane Technology Rende (Italy), 21.-23.09.2006

Barbe S., Boller E., Faber R., Thom V., Scheper T. “The Use of X-Ray Microtomography for the Characterization of Macroporous Membranes”Reprint Journée annuelle de la Socété Française de Métallurgie et de Matériaux, Ecole Nationale Supérieure des Mines de Saint Etienne (France), 30-31.05-01.06.2007

Conferences and posters:

Barbe, S; Wilhelm, P.; Müller, U.; „Nichtthermische Entkeimungseffekte bei der Sattdampfbehandlung von Oberflächen“, Poster GDL-Kongress Lebensmitteltechnologie 2001, Berlin (Germany), 8.-10.11.2001

Müller, U.; Wilhelm, P.; Barbe St.; Lehre G.; „Vorstellung eines Sichtzellenautoklaven zur Untersuchung der Entkeimung mit Dampf“ VDI-GVC-Fachausschuss Lebensmittelverfahrenstechnik, Jena (Germany), 6.-8.03.02

Wilhelm P.; Barbe, St.; Müller, U.; „Untersuchung nichtthermischer Entkeimungseffekte bei der Sattdampfbehandlung von Modelloberflachen mit den Beispielen B. subtilis und L. plantarum“ VDI-GVC-Fachausschuss Lebensmittelverfahrenstechnik, Weimar (Germany), 6.-8.03.2002

Wilhelm, P.; Müller, U.; Barbe, St.; „Mechanische Wirkungen beim Lemgoer Sattdampfentkeimungsverfahren“, InnoFood 2002 (Hochschule Anhalt), Bernburg (Germany), 18./19.09.2002

Müller, U.; Wilhelm, P.; Barbe, St.; „Schonende Entkeimung mit dem Lemgoer Entkeimungsverfahren“, GDL-Symposium „Aktuelle Aspekte der Technologie von Kräutern und Gewürzen II“, Gießen (Germany), 23.-25.09.2002

Wilhelm, P.; Müller, U.; Barbe, St.; Lilie M.; “Mechanical Components in the Decontamination of B. subtilis and L. plantarum on various surfaces – A Progress Report”, Institute of Food Research, Norwich (UK), 14.11.2003

Barbe S, Zeilfelder K, Danneel H J “L-methionine and L-cysteine from brazil nut as functional ingredients in food and food related products”, Arbeitskreis Funktionelle Lebensmittel, Food Processing Initiative NRW, IHK Bielefeld (Gremany), 06.2003

Wilhelm, P.; Müller, U.; Barbe, St.; Lilie M.; „ Mechanische Effekte bei der Sattdampfentkeimung von B. subtilis ind L. plantarum auf verschiedenen Oberflächen“; Lemgoer Nachmittag zu Entkeimungsfragen, FH Lippe und Höxter, Lemgo (Germany), 12.12.2003

Müller, U.; Wilhelm, P; Lilie M.; Barbe, St.; „Mechanical decontamination effects during steam treatment of foods“, Poster international Congress on Engineering and Food (ICEF 9), Montpelier (France), 8.-11.03.2004

Wilhelm, P.; Lilie M.; Barbe, S.; Müller, U.; „Mild steam decontamination of drugs and other plant material using mechanical effects“, conference “International Meeting on Pharmaceutics, Biopharmaceutics and Pharmaceutical Technology”, Nürnberg (Germany), 158.-17.03.2004

Danneel H.J.; Barbe S., Zeilfelder K. „Gewinnung der Aminosäure L-Methionin aus Pressrückständen der Paranussölproduktion“, conference DECHEMA/GVC-Gemeinschaftsausschuss „Extraktion“, Aachen (Germany), 01.04.2004

Barbe S „Präparative Gewinnung eines methioninreichen Proteins aus Paranusspressrückstände“ Ergebnissevorstellung der Kompetenzplattform „Lebensmittelqualität und –sicherheit“, University of applied sciences, Lemgo (Germany), 02. 04.2004

Barbe S. “Design of membrane chromatography systems for large scale applications“, conference Network Young Membrains 2006 (NYM8), Institute of Membrane Technology Rende (Italy), 21.-23.09.2006

Barbe S., Nussbaumer D., Demmer W., Weiß A., Faber R., Scheper T. “Presentation of a tandem-Sartobind pilot plant as an approach for large scale membrane chromatography” Euromembrane 2006, Giardini Naxos Taormina (Italy), 24.-28.09.2006

Barbe S., Boller E., Faber R., Thom V., Scheper T. “The Use of X-Ray Microtomography for the Characterization of Macroporous Membranes” Journée annuelle de la Socété Française de Métallurgie et de Matériaux, Ecole Nationale Supérieure des Mines de Saint Etienne (France), 30-31.05-01.06.2007

S. Barbe, A. Kneer, M. Wirtz, T. Scheper "Prediction of mass transport phenomena in Membrane Adsorber Systems (MAS) using a dual porosity model" oral presentation at the code_saturne user conference 2008, R&D EDF Paris (France), 01.12–02.12.2008

S. Barbe, A. Kneer, M. Wirtz, T. Scheper "Fluid dynamics in Membrane Adsorber Systems" oral presentation DECHEMA Arbeitsausschuss für Membrantechnik, DECHEMA HAUS Frankfurt am Main (Germany), 15.01.2009

Article

Stephan Barbe, Dietmar Nussbaumer, Wolfgang Demmer, Abdul Weiss, Rene Faber, Thomas Scheper "Presentation of a Tandem–Sartobind pilot plant as an approach for large scale membrane chromatography". Desalination 200 (2006) 480-482

Curriculum vitae

Stéphan Barbe

geboren am 11.11.1976 in Dieuze (Frankreich)

Studium

Juni 1996	Bacalauréat général (Abitur), Fachrichtung Naturwissenschaft (*Bac S – scientifique*), Lycée Mangin in Sarrebourg (Frankreich)
1996-1997	Medizinstudium (2 Semester), Faculté de médecine, Université Henry Poincaré, Nancy (Frankreich)
1997-1999	Diplôme Universitaire de Technologie Génie Biologique (DUT), Institut Universitaire de Technologie (IUT) Brabois, Université Henri Poincaré, Nancy (Frankreich)
März-Juli 1999	DUT-Abschlussarbeit „Chemische Entkeimung von Förderflüssigkeiten und Abwasser“ (auf Französisch), Fa. SOFREB Custines (Frankreich)
2000-2002	Studium an der Fachhochschule Lippe und Höxter, Fachbereich „Lebensmitteltechnologie“, Schwerpunkt „Biotechnologie“
Sept. 2001- Mai 2002	Diplomarbeit „Nicht thermische Entkeimung mit Dampf und Überprüfung der Druckerniedrigungsgeschwindigkeit als Ursache für die Wirkung“ (auf Deutsch) unter der Leitung von Prof. Dr. Müller, Labor für Verfahrenstechnik, Fachhochschule Lippe und Höxter, Lemgo
2003-2005	Chemiestudium an der Universität Hannover zur Erlangung der Promotionszulassung des Instituts für Technische Chemie (TCI)
Sept. 2005	Promotionszulassung des Instituts für Technische Chemie (TCI) der Universität Hannover
Sept. 2005- Sept.2009	Anfertigung der Dissertation „Fluid Dynamics in Membranadsorber Systems“ (auf Englisch). Die Arbeit wurde von Prof. Dr. Thomas Scheper (Institut für Technische Chemie, Universität Hannover) betreut.

Berufliche Erfahrung

Aug.-Dez. 1999	Mitarbeiter bei der Fa. SOFREB in Custines (Frankreich). „Inbetriebnahme einer Mikrofiltrations- und Umkehrosmoseanlage für Abwasser“
2001-2005	Betreuung des Biochemie Praktikums und entsprechender Seminare unter der Leitung von Prof. Dr. Danneel. Zentrales Chemie-Labor der FH Lippe und Höxter, Lemgo
Juni 2002-Aug. 2005	Wissenschaftlicher Mitarbeiter bei FH Lippe und Höxter unter der Leitung von Prof. Dr. Danneel. Zentrales Chemie-Labor der FH Lippe und Höxter, Lemgo. “Gewinnung der Aminosäure L-Methionin aus Pressrückständen der Paranussölproduktion“ aFuE-Projekt.
Sept. 2005-Sept. 2008	Doktorand, Sartorius-Stedim Biotech GmbH, Abteilung „Membranadsorber“, Göttingen
Seit Sept. 2008	Wissenschaftlicher Mitarbeiter, Modellierungsgruppe, Sartorius-Stedim Biotech GmbH, Göttingen

---

Auszeichnungen

Dezember 2001	DAAD-Preis

Spezielle Kenntnisse

- Computational Fluid Dynamics (CFD): Code_Saturne, Comet, Star-CCM+, StarCD, CFD-ACE+, Patran, Cubit und Paraview
- Programmiersprachen: Fortran, C und C++
- Numerische Software: Matlab, Scilab, Simulink und Scicos
- Linux

Sprachen

Deutsch, Französisch und Englisch fließend (schriftlich und mündlich)